11171

NATIONAL LIBRARY
OTTAWA

CANADA

BIBLIOTHÈQUE NATIONALE
OTTAWA

NAME OF AUTHOR..VENKATACHARY SRINIVASAN.....

TITLE OF THESIS..ELASTOHYDRODYNAMIC LUBRICATION IN ROLLING AND SLIDING CONTACTS.....

.....

UNIVERSITY....UNIVERSITY OF ALBERTA.....

DEGREE FOR WHICH THESIS WAS PRESENTED...Ph. D.....

YEAR THIS DEGREE GRANTED...1972.....

Permission is hereby granted to THE NATIONAL LIBRARY OF CANADA to microfilm this thesis and to lend or sell copies of the film.

The author reserves other publication rights, and neither the thesis nor extensive extracts from it may be printed or otherwise reproduced without the author's written permission.

(Signed)..V. Srinivasan.....

PERMANENT ADDRESS:

Reader in Mech Engg
M.R. Engg College, Jaipur
India

DATED..25 May.....19 72

NL-91 (10-68)

THE UNIVERSITY OF ALBERTA

ELASTOHYDRODYNAMIC LUBRICATION IN ROLLING AND SLIDING CONTACTS

BY

VENKATACHARY SRINIVASAN

A THESIS

SUBMITTED TO THE FACULTY OF GRADUATE STUDIES AND RESEARCH

IN PARTIAL FULFILMENT OF THE REQUIREMENTS FOR THE DEGREE

OF

DOCTOR OF PHILOSOPHY

DEPARTMENT OF MECHANICAL ENGINEERING

EDMONTON, ALBERTA

SPRING, 1972

THE UNIVERSITY OF ALBERTA

FACULTY OF GRADUATE STUDIES AND RESEARCH

The undersigned certify that they have read, and recommend to the Faculty of Graduate Studies and Research, for acceptance, a thesis entitled "ELASTOHYDRODYNAMIC LUBRICATION IN ROLLING AND SLIDING CONTACTS" submitted by VENKATACHARY SRINIVASAN in partial fulfilment of the requirements for the degree of Doctor of Philosophy.

.....
Supervisor

.....

.....

.....

.....

.....

.....
External Examiner

Date 25th May 1972

ABSTRACT

The thermal elastohydrodynamic problem of contacts subjected to rolling and sliding is investigated. The governing continuity and momentum equations have been combined to yield a modified form of the Reynolds equation. The viscosity and density of the lubricant are assumed functions of temperature and pressure. The coupled equations of elasticity, Reynolds and energy equations for the fluid and the energy equations of the solids are solved iteratively for values of the non-dimensional speed parameter $\frac{\mu_s \bar{U}}{ER}$ ranging from 10^{-12} to 10^{-10} and for slip ratios ranging between 0 to 0.25. The numerical scheme solves the 'isothermal' problem first and the results are used as an input to the thermal problem. Comparison with other theoretical solutions and experimental results show that the results of film thickness obtained in the present work correlate more favourably with experimental work. The temperature distribution in the lubricant, the surface temperature of solids and the tractive forces are also given. The agreement between the calculated and the experimental values on drag force available in literature is moderately good.

ACKNOWLEDGEMENTS

The author wishes to express his deep appreciation to Dr. C. M. Rodkiewicz for his guidance and supervision of this study. He was patient, accessible and was a source of constant encouragement.

Dr. C. Dayson of the Lubrication Division, National Research Council of Canada, was associated with this study from an early stage. The author wishes to thank him earnestly for his guidance and interest.

Dr. J. Pounder of the Department of Mathematics and Dr. J. Tartar of the Department of Computing Science were willing and cooperative at various stages of this study. Their help is gratefully acknowledged.

Several members of the Department of Mechanical Engineering were consulted during the study. Particular thanks are extended to Dr. M. Charles (France), Dr. D. Dale and Dr. G. Faulkner.

The financial support in the form of assistantships from the University of Alberta and research grants from the National Research Council of Canada are thankfully acknowledged.

The author is highly indebted to his wife, Jalaja, for her extreme patience and understanding during these long years.

Thanks are also extended to Mrs. E. Bell for her excellent typing of the thesis.

TABLE OF CONTENTS

TABLE OF CONTENTS (cont'd)

TABLE OF CONTENTS (cont'd)

LIST OF FIGURES

LIST OF FIGURES (cont'd)

LIST OF SYMBOLS

English

a	semi-Hertzian width, defined by equation (2.27)
a_1	defined in equation (4.4)
a_{n_1}	defined in equation (4.10)
a_{n_3}	defined in equation (4.12)
A	integration constant, defined by equation (2.9)
A'	lower limit of integration in equation (2.26)
b_1	defined in equation (4.5)
b_n	defined in equation (4.11)
B	integration constant, defined by equation (2.6)
B'	upper limit of integration in equation (2.26)
C_1	defined in equation (4.6)
C_p	specific heat
C_A	coefficient for pressure in expression (2.32)
$\bar{C}_A$	$\frac{C_A W}{a}$
C_B	coefficient for pressure in expression (2.32)
$\bar{C}_B$	$\frac{C_B W}{a}$
d_m	defined in equation (4.7)
D_t	$\frac{1}{\rho_s} \frac{d\rho}{dT}$
$\bar{D}_t$	$D_t T_s$
E	a modified Eckert number $= U^2/C_p T_s$

LIST OF SYMBOLS (cont'd)

English

E_1	modulus of elasticity of lower solid
E_2	modulus of elasticity of upper solid
$\frac{1}{E'}$	$\frac{1}{\pi}\left[\frac{1-\sigma_1^2}{E_1}+\frac{1-\sigma_2^2}{E_2}\right]$
F	$\frac{2WL}{ah_0E'}$
G	$\frac{L^2}{2Rh_0}$
h	film thickness
$\bar{h}$	h/h_0
h_r	a reference thickness
h_{r_1}	a reference thickness for lower solid, equation (2.21)
h_{r_2}	a reference thickness for upper solid, equation (2.21)
$\bar{\bar{h}}$	$h - h_0$ defined by equation (2.30a) and 2.30b)
J	Joule's equivalent of heat
k	coefficient of thermal conductivity
L	Hertzian width - 2a
L_1	3L
LP	load parameter defined by equation (3.8)
M	$\frac{W}{C_p\rho_s T_s aJ}$

English

MP	materials parameter defined in equation (3.10)
p	pressure
$\bar{p}$	$\frac{pa}{W}$
Pr	Prandtl number = $\frac{C_p \mu_s}{k}$
Q	mass flow
R	$\frac{R_1 R_2}{R_1+R_2}$
R_1	radius of lower solid
R_2	radius of upper solid
Re	Reynolds number = $\frac{\rho_s UL}{\mu_s}$
Re^*	modified Reynolds number = Re h_0^2/L^2
RS_1	defined in equation (2.54a)
RS_2	defined in equation (2.54b)
SP	speed parameter defined in equation (3.9)
t_1	defined in equation (2.38d)
t_2	defined in equation (2.38e)
T	temperature
$\bar{T}$	T/T_s
$\bar{T}_j^r$	non-dimensional temperature at the j^{th} location at the r^{th} iteration
u	velocity along the film

English

$\bar{u}$	u/U
U	$U_1 + U_2$
U_1	velocity of the lower solid
U_2	velocity of the upper solid
$\bar{U}$	$\frac{U_1 + U_2}{2}$
W	load
x	coordinate along the film
$\bar{x}$	x/L
y	coordinate across the film
$\bar{y}$	y/h
$\bar{\bar{y}}_1$	y/h_{r_1}
$\bar{\bar{y}}_2$	y/h_{r_2}

Greek

α	pressure viscosity exponent
$\bar{\alpha}$	$\frac{\alpha W}{a}$
$\bar{\bar{\alpha}}$	defined in equation (2.35)
β	temperature viscosity exponent
$\bar{\beta}$	β/T_s
γ	pressure temperature viscosity exponent

Greek

$\bar{\gamma}$	$\frac{\gamma W}{aT_s}$
ε	coefficient of thermal expansivity
$\bar{\varepsilon}$	defined in equation (2.48)
ξ	auxiliary x coordinate
λ	defined in equation (2.42)
μ	viscosity
$\bar{\mu}$	$\frac{\mu}{\mu_s}$
μ_e	defined in equation (2.8a)
μ_e'	defined in equation (2.8b)
μ_e''	defined in equation (2.8c)
$\bar{\mu}_e$	defined in equation (2.38a)
$\bar{\mu}_e'$	defined in equation (2.38b)
μ_e''	defined in equation (2.38c)
υ	$\frac{2}{E'}\int_{-\infty}^{x^*} p(\xi) \ln \frac{x-\xi}{x_0-\xi}\, d\xi$
ρ	density
$\bar{\rho}$	ρ/ρ_s
$\bar{\bar{\rho}}$	defined in equation (2.10)
σ	Poisson's ratio
$\bar{\phi}$	$\bar{\alpha} + \bar{\gamma}$

Greek

ω	$\frac{2}{E'}$
ω_n	defined in equation (4.13)

Subscripts

s	evaluated at inlet conditions
1	refers to bottom solid
2	refers to top solid
o	evaluated at the line of centres

Superscripts

*	evaluated at the down-stream end $\bar{x} = 0.5$

CHAPTER I

INTRODUCTION AND REVIEW OF LITERATURE

1.1 Statement of the Elastohydrodynamic Problem

Elastohydrodynamic lubrication may be defined as the study of those situations where the elastic deformation of the bounding solids has a very significant role in the hydrodynamic lubrication. In most machines forces are transmitted from one component to another by means of large effective bearing areas. In several applications, as in gears, cams and roller bearings, the contact is limited to a point or line. The present study pertains to such situations and the geometry envisaged is that of two cylinders in contact along a generator.

In order to fully understand the problem it is necessary to consider the features of such contacts. The size of the Hertzian [1] zone of contact between two elastic solids is representative of the region of effective pressure generation in elastohydrodynamic contacts. This is of order 10^{-2} inches. The usual surface speeds are of order 10^{2} to 10^{3} inches per second. The maximum contact pressures are of order 10^{1} to 10^{2} tons per square inch. Film thicknesses are of order 10^{-5} inches.

The distinguishing feature of elastohydrodynamic lubrication is the elastic deformation of the solids. This is significant compared to the lubricant film thickness. The stress distribution determines the local shape of the elastic solids. This in turn determines the shape of the lubricant film. Thus, the isothermal elastohydrodynamic

problem calls for the simultaneous solution of the continuity and momentum equations for the fluid and elasticity equations for the solid.

The very high contact pressures have a marked influence on the properties of the lubricant. In particular, viscosity of the lubricant increases enormously at high pressures and the compressibility of the lubricant is also significant and cannot be ignored.

When the effect of temperature change is considered, the problem becomes extremely difficult and very little theoretical work has been done. If the opposing surfaces have nearly equal velocities, the problem can be idealised to be an isothermal problem. This has been the usual approach. If the velocities of the mating surfaces are widely different, viscous dissipation becomes important. Further, temperature changes have a significant influence on viscosity. Thus, the basic differential equations for a complete study of elastohydrodynamic lubrication are the continuity equation, the momentum equations, the energy equations for the fluid, the energy and elasticity equations for the solid and the equations of state for the lubricant. These equations are interdependent through the physical properties of the lubricant and solid. They are extremely complicated and several simplifying assumptions have to be made before a solution can be obtained.

Experimental work has revealed the effect of temperature upon film thickness to be little. One of the most important conclusions of elastohydrodynamic analysis and experiment up to date is that the viscosity of the lubricant in the vicinity of the inlet to the contact controls the film thickness within the contact. The inlet viscosity of the lubricant is determined mainly by the temperature of the surrounding

solids. This temperature is not sensitive to the heat generated in the fluid within the contact. Thus, film thickness can be calculated accurately by neglecting energy equations [2]. Then the effects of temperature can be analysed.

In the present study two rotating elastic cylinders with a thin lubricant film inbetween are subjected to a heavy load. Considering viscosity and density of the fluid as functions of temperature and pressure, and assuming the elastic properties of the solids in contact, the film thickness, the pressure and temperature distribution within the lubricant film and the temperature distribution in the solids are computed for different rolling and sliding velocities. The frictional forces are also calculated under these conditions.

1.2 Review of Relevant Literature

The initial interest in elastohydrodynamic lubrication was generated by the study of lubrication in gears. Martin [3] made a theoretical approach to the problem of lubrication of rigid cylinders. For an isoviscous incompressible lubricant he derived an expression of the form

$$\frac{h_o}{R} = 2.45\ \mu_s\ \frac{U_1 + U_2}{W} = 4.9\ \frac{U\mu_s}{W} \qquad \ldots\ldots \qquad (1.1)$$

Substituting representative values for viscosity, load and speed, it is found that the thicknesses are too small as compared to actual thicknesses.

Peppler [4] considered the elastic distortion problem assuming an isoviscous lubricant. He came to the conclusion that maximum oil pressure cannot exceed the maximum Hertzian pressures. This

conclusion is not true for high speeds. Meldahl [5] examined the effect of high pressure on film shape and pressure profile for an isoviscous lubricant. He derived expressions for the elastic displacement of a semi-infinite elastic solid subjected to an arbitrary surface loading. He tried to solve the elastic and the hydrodynamic equations together, using iterative methods. Convergence was poor and considerable computational effort was required for a single solution. Nevertheless, it was a move in the right direction.

Gatcombe [6] took into account the effect of pressure on viscosity. He used an exponential relation and solved the Reynolds equation. His calculated film thicknesses were higher than previous calculations. Hersey and Lowdenslager [7] employed a parabolic viscosity relationship and arrived at results similar to that of Gatcombe [6]. Cameron [8] and McEwen [9] employed a boundary condition assuming cavitational effects and improved upon the previous workers' approach. Block [10] gave a mathematical reasoning proving the existence of a minimum film thickness for lubricants obeying an exponential pressure viscosity law. Thus far it has been shown that elastic distortion and viscosity pressure effects could separately account for modest improvements in minimum film thickness predictions.

Grubin and Vinogradova [11] examined the combined effect of both elastic distortion and viscosity pressure effects. Grubin made a simplifying assumption that the solids adopt the form of dry contact. Pressure at entry to the high pressure zone was assumed very high. Under these assumptions Grubin calculated the separation of the solids within the Hertzian contact zone. This approach eliminated the need

of solving the elastic equations since the Hertzian form of dry contact was accepted. This assumption is particularly valid at high loads, where the hydrodynamic film thickness in the high pressure region is a small proportion of the local elastic displacement. The important contribution of this method was that an approximate formula for film thickness for highly loaded contacts could be derived whichwas 2 orders of magnitude greater than Martin's [3] expression. Grubin's [11] work further postulated the existence of a pressure spike at the outlet end of the Hertzian region.

The search for accurate formulae for pressure distribution and film shape has proved very interesting. Weber and Saalfeld [12] obtained a closed form solution to the elastohydrodynamic problem for constant and pressure dependent viscosity fluids. Their solutions are restricted to very small deformations. Their results indicate the change of film shape with load. Dowson and Higginson [13] developed an interesting numerical method to solve the isothermal elastohydrodynamic problem. They found the film shape corresponding to an initially assumed pressure distribution by solving the Reynolds equation. For the same pressure distribution the elastic film shape was determined by solving the elastic equation. The elastic film shape and the hydrodynamic film shapes were compared. If there was sufficiently close agreement, the pressure and film profiles were accepted. If not, the pressure curve was modified and the procedure repeated till there was acceptable agreement. The deficiency in the method was that the adjustment of the pressure curve had to be done manually and required experience and judgement. Further, the results did not reveal any

pressure spikes, which was due to the very low velocities for which the investigations were carried out. In a later paper Dowson and Higginson [14] investigated the effect of the material properties on the isothermal elastohydrodynamic situation. They found that an outlet pressure peak existed for realistic values of speeds and loads. The magnitude of the pressure peak varied very slightly with load but markedly with speed and material properties. The centre-line film thickness varied hardly with the load and was significantly related to the product of speed and inlet viscosity. Archard, Gair and Hirst [15] developed an iterative procedure for the isothermal elastohydrodynamic problem. The lubricant was assumed to be incompressible. Its viscosity was assumed to be dependent on pressure only. They divided the pressure region into four regions and employed the inverse hydrodynamic procedure. They verified the earlier predictions in a number of cases. The film thicknesses they calculated are uniformly higher than those of other workers and available experimental values. The method they developed is valuable in that the whole calculations can be carried out in a computer without the need for human intervention which was necessary in the methods adopted by Dowson et al. Archard and Kirk [16] examined the lubrication of point contacts and came to the conclusion that at heavy loads elastohydrodynamic theory had to be applied to achieve acceptable results. Dowson, Higginson and Whitaker [17] investigated the effects of speed on film thickness. They also took into account lubricant compressibility. Speed of rollers had significant effect on film thickness and the effect of compressibility of the lubricant on film thickness was little. Compressibility had an

effect on the pressure peak. Stephenson and Osterle [18] also came to similar conclusions. The numerical scheme adopted by these authors is however useful only for a narrow range of loads. Dowson and Whitaker [19] have also indicated easy methods to determine whether a particular problem is to be treated as a rigid cylinder or as an elastohydrodynamic problem. Herrebrugh [20] examined the isothermal problem from a mathematical viewpoint. For an isoviscous lubricant he combined the Reynolds and elasticity equations to yield a Fredholm equation of the second kind. For a number of loading conditions he has presented numerical solutions. In the range covered, he did not find pressure spikes in the pressure distribution, showing that spikes occur if the viscosity increases rapidly with pressure.

When temperature variation and its effect on viscosity and density of the lubricant is taken into account, the problem becomes much more difficult. This is indicated by the limited literature available on the subject. Cheng and Sternlicht [21] examined the problem of thermal elastohydrodynamic lubrication of rolling and sliding cylinders. They made an assumption of an average effective viscosity across the film thickness. Instead of hunting for the spike position, they fixed the location of the pressure spike and their numerical procedure was to find the corresponding rolling velocity. Their important conclusions were that:

(a) Pressure peak existed near the downstream end of the film for all heavily loaded cases and position of the spike was dependent upon rolling velocity;

(b) Temperature did not reduce the pressure peak but increased it slightly;

(c) Temperature had a moderate influence on film thickness.

The compressible work term used by these authors was in error as was pointed out by Dowson [22] in his discussion of the paper. In a subsequent paper Cheng [23] removed the restriction of average viscosity across the film. His form of Reynolds equation has been found to be in error by this author. His important conclusions were:

(a) The position of the peak is strongly influenced by speed, load and inlet viscosity;

(b) No significant difference existed between isothermal film profiles and thermal film profiles for various ratios of slip;

(c) The frictional force was strongly influenced by the temperature rise.

Dowson and Whitaker [24] have presented results for various sliding velocities, keeping the rolling velocity constant. In their numerical solution, the property expressions of the lubricant are not differentiated or integrated. This necessitates finding thermal coefficients in order to use the modified Reynolds equation. Their main conclusions are:

(a) The effect of temperature on the film thickness is negligible;

(b) Sliding speed has little effect on the film thickness;

(c) Height of the pressure spike is reduced by sliding and its location moves towards the centre of the Hertzian zone. The spike becomes more gentle and rounded.

One important common feature of the solutions offered by the foregoing three references [21, 23, 24] is that all these assumed a surface temperature equation of the solids as a boundary condition on

temperature for the fluid. The temperature distributions within the solids were not investigated. When it is realised that experimental measurements of temperature have necessarily to be done beneath the surface, the temperature distribution in the solids assumes importance. Shear stress is significantly dependent on temperature.

O'Donoghue and Cameron [25] correlated all available data on friction between hardened steel discs and it is possible to see the effect of solid temperature on friction. In another paper these authors [26] investigated the mechanism of scuffing between gears. They came to the conclusion that scuffing takes place when the surface attained the transition temperature of the particular metal-oil-metal combination. If this temperature is reached then scuffing will ensue (even if the surfaces are fully lubricated) due to chance contacts.

Blok [27], Carslaw and Jaeger [28], Jaeger [29], have studied the theoretical problem of a moving heat source of constant strength. It is usual in elastohydrodynamic studies to consider the source strength over the Hertzian width as constant. The question of partition of heat between two bodies has been studied by Allen [30] and Cameron, Gordon and Symm [31]. These authors took as their system a source of uniform strength and put in the condition that at all points in the zone of contact the surface temperatures of the solids must be equal. They have derived expressions for temperatures in terms of the source strength. Francis [32] has derived an analytic expression for the interfacial temperature in a sliding circular Hertzian contact, where one surface was stationary and the other moving. He has introduced the method of the harmonic mean for matching the interfacial temperature.

It has been suggested that the non-newtonian behaviour of the lubricant might influence the film thickness in elastohydrodynamic contacts. Cheng and Orcutt [33] considered a visco-elastic model of Maxwell and found that the shape of the pressure profile obtained was closer to the experimental results. Milne [34], Tanner [35] and Bell [36] have come to the conclusion that the load capacity of a Maxwell fluid was less than that of a Newtonian fluid. Bell [37] derived a formula for film thickness for a Ree-Eyring fluid. Chow and Saibel [38] analysed the isothermal problem of a heavily loaded line contact of rollers in the presence of a Maxwell lubricant. They have found that the non-Newtonian effect had the tendency to flatten the contact region. The load capacity was reduced. The shape of the pressure curve did not vary significantly. The existence of a spike was found as in the case of newtonian fluids.

A number of experimental investigations have been made for the problem under study. A brief review of these is presented to indicate the extent of the correlation between available experimental results and theoretical findings. Merrit [39] was the first to design and build a disc machine which simulated gear tooth contact conditions. His measurement of the coefficient of friction under various sliding conditions presented valuable design data. Lane and Hughes [40] studied the oil film formation between gear teeth using electrical resistance method. They found that under sliding conditions film thickness was less than under pure rolling conditions. Crook [41] investigated the possibility of a quantitative evaluation of the film thickness by a knowledge of the specific resistance of the oil. He found that even

very small quantities of moisture vitiated the results considerably. El Sisi and Shawki [42] tried to overcome the effect of moisture by adding 4 per cent sodium petroleum sulphonate. But since they used rather heavy currents, their results were one order of magnitude higher. Leach and Kelley [43] have used electrical resistance methods across the contact zone to identify lubricant failure point and the effect of deposit forming additives. They have come to the conclusion that the load capacity of a lubricant varies inversely with reference to specimen temperature and that lubricant failure for any lubricant-material combination occurred at a constant critical temperature. This temperature did not depend on the range of load, sliding or rolling velocities or film thickness. Tallian, Chik, Huttenlocher, Kamenshine, Sibley and Sindlinger [44] have found that there is a good order of magnitude agreement between measured and theoretical values of film thickness. Significant wear occurred only in regions where the film was interrupted. All the experimental investigations using resistance method have qualitatively confirmed predictions of the elastohydrodynamic theory.

Sibley and Orcutt [45] devised a method which consisted of directing a mono-chromatic beam of X-rays tangentially at the contact of the lubricated discs. The amount of the X-ray beam passing through the gap was measured by a Geiger counter and was used to determine film thickness. The wave length of the X-rays was so chosen that the lubricants were quite readily penetrated but the steel surfaces absorbed the beam entirely. The elastohydrodynamic theory fitted the experimantal results well up to an oil film thickness of 10^{-5} inches. At lower thicknesses (the lowest thickness measured was 3½ micro-inches) it

deviated twenty per cent below theoretical. The authors attributed this deviation to the non-Newtonian behaviour of the lubricant at high shear rates. The X-ray method relies on the direct transmission of X-rays through the contact which limits it to discs.

Measurement of the electrical capacity between two surfaces separated by an oil film has been found to give good results. Crook [46] used a modified disc machine so that the oil coming from the contact zone remained on the surfaces and was carried under a flat plate. The capacitance between each plate and its disc was measured. The use of the subsidiary plate eliminated uncertainties of the geometry of the contact zone. From the capacitances the rate of oil flow was deduced and thus the thickness of the film could be calculated. The method is applicable for both rolling as well as rolling and sliding conditions. The important findings of these measurements were that film thickness at high loads varied little with load, less than proportionately with speed and greatly with the temperature of the surfaces. The temperature of the oil in the high pressure region had negligible influence on the film thickness. Crook thus came to the conclusion that film thickness is largely determined by the conditions on the entry side of the conjunction ahead of the region in which the viscous losses and heating of the oil became appreciable. In a second paper Crook [47] investigated the effect of viscosity and speed on film thickness. He found that the viscosity of greatest importance with respect to film thickness was the viscosity of the oil at the surface temperature of the discs. It was also found to depend upon the mean peripheral speed of the discs. This was found to be valid even when sliding conditions

prevailed. In a third paper Crook [48] found that under sliding conditions conduction to the solid surfaces to be the important mechanism of dissipation of heat. He has also developed expressions for frictional traction. In a fourth paper Crook [49] has described the measurement of friction in disc machines. He found that rolling traction was independent of load and was proportional to the thickness of the film. Sliding traction was dependent upon sliding speed. Friction was found to increase with sliding speed to a maximum and then full. The four papers [46, 47, 48, 49] have been described in some detail because they represent a landmark in the experimental investigation of elastohydrodynamic lubrication in line contacts. Dyson and Wilson [50] have investigated the effect of high slide/roll ratios on film thickness, using electrical capacitance method. They found that as the slide/roll ratio increased above a certain level, experimental values of the film thickness became greater than the values predicted by isothermal theory. They explain this on the principle that there is a temperature variation of oil across the film at the inlet zone and this becomes important at high sliding rates.

Kannel, Bell and Allen [51] have reported two different methods for measuring pressure distributions in rolling contact. The first method was to use an X-ray technique and pressures were inferred from observed deformations of the discs. The second method used a strip of manganin as a pressure transducer to measure pressures in the contact. The important feature of the measured profiles were that they did not show the pressure spike predicted by theory. The authors themselves have posed the question whether lack of accuracy could have been

a cause of the absence of pressure spike. Qualitatively the pressure profiles have agreed with the theoretical predictions. Kannel [52] refined the manganin pressure transducer technique so that pressures could be measured between steel discs. The measured pressures showed general trends similar to those predicted by theory. For heavily loaded rolling-contact conditions, a slight pressure spike has been reported. Longfeld [53] used oil pressure tappings to measure directly the pressure in the contact. Facilities were available enabling measurements of pressure over the entire contact area. At greater loads, rudimentary peaks were observed on the downstream end of the contact. Orcutt [54] has reported a detailed experimental study of the conditions occurring in the conjunctive region of two lubricated cylindrical discs which roll or roll and slide on their peripheral surfaces. Platinum transducers were used to measure temperature. Capacitance method was adopted to measure film thickness. Manganin pressure transducers measured the pressure. Experimental pressure results indicated that significant pressures were not generated until about two Hertzian contact zone half widths ahead of the line of centres. Experimental pressure profiles were more rounded without the sharp pressure peak which may be due to the rheological effects. The measured value of the film thicknesses was about 60 to 70 per cent of theoretical values. The shapes of the deformation profiles differ from the calculated profiles which are flatter than the measured ones. The measured temperature rise is less than the calculated values. However, these measurements indicate qualitative agreement with theoretical results.

Optical interference technique has been used for the measurement of film thicknesses. The advantage of this method is that the measurement is made at the actual contact and that it is independent of external calibration. The difficulties are two-fold. Firstly, most transparent materials such as glass have refractive indices very close to that of normal lubricants. Secondly, glass is a bad bearing material. If perspex or some other plastic is used then the modulus of elasticity and yield stress are small so that the pressures generated are too low for the pressure-viscosity effect to occur. Cameron and Gohar [55] employed glass with a high refractive index which enabled the colours of the fringes to be photographed. The opposing surface was a one inch steel ball. The pressures were high enough to get an elastohydrodynamic lubrication. The experimental results gave the exit constriction predicted by theory. Very recently, Westlake and Cameron [56] have used optical elastohydrodynamic techniques for testing a wide range of lubricants. The pressure viscosity coefficients agree well with those determined in conventional high pressure viscometers. The effect of aging on the oil could be studied. Sanborn and Winer [57] have used the optical interference technique for the study of the rheological effects in sliding elastohydrodynamic contacts. They used a steel sphere and synthetic sapphire in their apparatus. Film thickness profile was not affected by rapid application of the load. These authors also measured the temperature at the inlet and it was found that there was only a very slight increase in temperature after a long time which affected the film thickness only slightly. In a companion paper Sanborn and Winer [58] have described traction measurements. The traction values obtained

were primarily a function of the sliding velocity. Large variations in fluid composition and inlet viscosity had little influence on the traction force. Rapid application of the normal load also had negligible effect on the traction force.

1.3. Approach to the Thermal Elastohydrodynamic Problem

Combining the continuity and the momentum equations for a compressible fluid, a modified form of Reynolds equation has been derived in Chapter II. The energy equations for the fluid and solids have also been detailed. The elastic equation and the applicable Hertzian formulae have been listed in Chapter II. The problem under study was solved in two steps. The first step was to idealise the problem so that the fluid properties were dependent on pressure only. This is usually known in the technical literature as the 'isothermal' problem. The manner in which the coupled elastic and Reynolds equations have been solved has been shown in detail in Chapter III. This step yielded the pressure distribution and film thickness.

Using the well documented assumption that the film thickness was not sensitive to the temperature of the lubricant in the high pressure region, the second step was to devise an iterative numerical procedure which took into account the variation of the fluid properties with reference to temperature as well. An implicit finite difference technique has been developed to solve the energy equations of solid-fluid-solid together. These numerical procedures are the subject matter of Chapter IV.

The solution to the momentum and energy equations enable the

calculation of shear stress and the tractive forces. The pertinent expressions have been listed in Chapter IV. Results for different values of rolling velocity for a constant load and variable slip ratios have been displayed. The rolling velocities varied from 30 inches per second (slow) to 400 inches per second (moderately high). Discussion of these results and conclusions thereof form the subject content of Chapter V.

While some of the assumptions have been indicated at the appropriate places, it has been considered pertinent to list the general assumptions usually made in the derivation of governing equations. This is done in the next article.

1.4. General Assumptions

For the contacts under consideration in the present study, the loads are transmitted through lubricant films of very short length. For this reason the undeformed solids can be adequately represented by cylinders in the region of the contact zone. Following Dowson and Higginson [59] it is possible to replace the two cylinders by a geometrically equivalent cylinder near a plane.

The following assumptions are made in the development of the governing equations.

1. Body forces are neglected.
2. Pressure is constant across the film.
3. Inertia forces are neglected.
4. Curvature effects are small and can be neglected.
5. The length of the contact region is orders of magnitude smaller

than the radii of the rollers. Thus, surface deformation of the rollers can be approximated by those of semi-infinite solids subjected to the same normal load. Elastic deformations due to surface shear is neglected.

6. Viscosity is a function of pressure and temperature only and not dependent on shear rate.
7. Side leakage is neglected.
8. There is no slip at the boundaries.
9. Flow is considered laminar.
10. The thickness of the lubricant film is orders of magnitude smaller than the length of the contact.
11. The problem is two-dimensional and steady-state has been reached.

CHAPTER II

FLOW GOVERNING EQUATIONS

2.1. Modified Reynolds Equation

One of the major assumptions in the two-dimensional Reynolds equation, commonly used, is that viscosity is constant throughout the thickness of the film. Cheng and Sternlicht [21] improved their solution by using an amended form of the Reynolds equation where an 'effective' viscosity of the lubricant considered constant across the film was used. Cheng [23] derived a modified Reynolds equation which removed the assumption of the 'effective' viscosity. Unfortunately, certain errors have occurred in Cheng's analysis and these seem to have been left unnoticed so far. In this article, the thermal form of the Reynolds equation is derived and compared with Cheng's [23] expression. To facilitate direct comparison, Cheng's notation has been adopted.

Neglecting inertia, the momentum equation is

$$\frac{dp}{dx} = \frac{\partial}{\partial y}\left(\mu \frac{\partial u}{\partial y}\right) \tag{2.1}$$

The boundary conditions are

$$u(x,o) = U_1 \qquad u(x,h) = U_2 \tag{2.2}$$

$$p(-\infty) = p(x^*) = 0 = \frac{dp}{dx}(x^*) \tag{2.3}$$

Integrating equation (2.1) once with respect to y

$$\frac{\partial u}{\partial y} = \frac{dp}{dx}\frac{y}{\mu} + \frac{A(x)}{\mu} \tag{2.4}$$

Integrating equation (2.4) once again with respect to y

$$u = \frac{dp}{dx} \int_0^y \frac{y}{\mu}\, dy + A(x) \int_0^y \frac{1}{\mu}\, dy + B(x) \tag{2.5}$$

Using boundary condition $u(x,o) = U_1$ in equation (2.5) one obtains

$$B = U_1 \tag{2.6}$$

Using boundary condition $u(x,h) = U_2$ in equation (2.5) one obtains

$$U_2 = \frac{dp}{dx} \int_0^h \frac{y}{\mu}\, dy + A(x) \int_0^h \frac{1}{\mu}\, dy + U_1 \tag{2.7}$$

Following Cheng [23] we define

$$\frac{1}{\mu_e} = \frac{1}{h} \int_0^h \frac{1}{\mu}\, dy \tag{2.8a}$$

$$\frac{1}{\mu_e'} = \frac{2}{h^2} \int_0^h \frac{y}{\mu}\, dy \tag{2.8b}$$

$$\frac{1}{\mu_e''} = \frac{3}{h^3} \int_0^h \frac{y}{\mu}\, dy \tag{2.8c}$$

$$t_1 = 12 \left\{ \frac{\mu_e}{3\mu_e''} - \left(\frac{\mu_e}{2\mu_e'}\right)^2 \right\} \tag{2.8d}$$

$$t_2 = 1 + \frac{U_2 - U_1}{U_2 + U_1} \left\{ 1 - \frac{\mu_e}{\mu_e'} \right\} \tag{2.8e}$$

From (2.7)

$$A(x) = \frac{U_2 - U_1 - \frac{dp}{dx}\frac{h^2}{2\mu'_e}}{\frac{h}{\mu_e}} \tag{2.9}$$

We define an effective density $\bar{\bar{\rho}} = \bar{\bar{\rho}}(x)$ (2.10)

such that

$$\text{mass flow} = Q = \bar{\bar{\rho}} \int_0^h u\,dy \,^{\dagger} \tag{2.11}$$

Integrating by parts equation (2.11)

$$Q = \bar{\bar{\rho}} \{uy \Big|_0^h - \int_0^h y \frac{\partial u}{\partial y}\,dy\}$$

$$= \bar{\bar{\rho}} \{U_2 h - \frac{dp}{dx}\int_0^h \frac{y^2}{\mu}dy - A\int_0^h \frac{y}{\mu}\,dy\}$$

$$= \bar{\bar{\rho}} \{U_2 h - \frac{h^3}{3\mu''_e}\frac{dp}{dx} - \frac{h\mu_e}{2\mu''_e}(U_2 - U_1 - \frac{dp}{dx}\frac{h^2}{2\mu'_e})\}$$

$$= \bar{\bar{\rho}} \{U_2 h + \frac{dp}{dx}(\frac{h^3\mu_e}{4\mu'^2_e} - \frac{h^3}{3\mu''_e}) - \frac{h\mu_e}{2\mu'_e}(U_2 - U_1)\}$$

$$= \bar{\bar{\rho}} \{U_2 h - \frac{t_1 dp}{12dx}\frac{h^3}{\mu_e} - U_2 h + \frac{t_2 h}{2}(U_2 + U_1)\}$$

$$= \bar{\bar{\rho}} \{\frac{U_1+U_2}{2} h\, t_2 - \frac{1}{12}\frac{dp}{dx}\frac{h^3 t_1}{\mu_e}\} \tag{2.12}$$

---

† Dowson and Whitaker [24] ignored variation of density across the film thickness.

Following Cheng and Sternlicht [21] and Dowson and Whitaker [59] we adopt the boundary condition that

$$\text{at } x = x^* \quad p = \frac{dp}{dx} = 0$$

Let at $x = x^*$ $\bar{\bar{\rho}} = \bar{\bar{\rho}}^*$ and $h = h^*$

Then

$$Q\,\Big|_{x = x^*} = \bar{\bar{\rho}}^* \frac{U_1+U_2}{2} h^* t_2^* \tag{2.13}$$

Equating mass flow

$$\bar{\bar{\rho}}^* \left(\frac{U_1+U_2}{2} h^* t_2^*\right) = \bar{\bar{\rho}} \frac{U_1+U_2}{2} h\, t_2 - \frac{1}{12} \frac{dp}{dx} \frac{h^3 t_1}{\mu_e}$$

$$\frac{dp}{dx} = \frac{6\mu_e (U_1+U_2) \{t_2 - \frac{h^*\bar{\rho}^*}{h\bar{\rho}} t_2^*\}}{t_1 h^2} \tag{2.14}$$

The expression (2.14) is to be contrasted with Cheng's [23] expression which reads

$$\frac{dp}{dx} = \frac{6\mu_e (U_1+U_2)}{t_1 h^2} \{t_2 - \frac{h^*\rho^*}{h\rho}\} \tag{2.15}$$

This is true only if $t_2^* = 1$ and from equation (2.8e) it follows that for t_2^* to be equal to unity

$$\mu_e^* = \mu_e'^*$$

Thus, it seems to be tacitly assumed that the temperature at $x = x^*$ is constant. The validity of this assumption is certainly questionable.

However, it can be used to start an iterative process in the numerical procedure.

2.2. 'Isothermal' Expressions

The expressions for the case where lubricant properties are only pressure dependent can be easily deduced from equation (2.13). For the 'isothermal' case

$$\mu_e = \mu; \quad \mu_e' = \mu; \quad \mu_e'' = \mu; \quad t_1 = 1; \quad t_2 = 1$$

$$\frac{dp}{dx} = \frac{6\mu\ (U_1+U_2)\ \{1 - \frac{h^*\rho^*}{h\rho}\}}{h^2}$$

$$= \frac{6\mu\ (U_1+U_2)}{h^3}\ \{h - \frac{h^*\rho^*}{\rho}\} \tag{2.16}$$

2.3. Energy Equations for the Fluid and Solids

Following Dowson and Whitaker [24] the reduced form of energy equation for the fluid is

$$\rho C_p u \frac{\partial T}{\partial x} = \epsilon u T \frac{\partial p}{\partial x} + \mu \left(\frac{\partial u}{\partial y}\right)^2 + k \frac{\partial^2 T}{\partial y^2} \tag{2.17}$$

Boundary conditions are

$$T(-\infty, 0) = T_s \tag{2.18a}$$

$$k \frac{\partial T}{\partial y}\Big|_{y=0} = k_1 \frac{\partial T_1}{\partial y}\Big|_{y=0} \tag{2.18b}$$

$$k \frac{\partial T}{\partial y}\Big|_{y=h} = k_2 \frac{\partial T_2}{\partial y}\Big|_{y=h} \tag{2.18c}$$

The temperature distribution in the solids is governed by [60]

$$k_1 \left(\frac{\partial^2 T_1}{\partial x^2} + \frac{\partial^2 T_1}{\partial y^2}\right) = \rho_1 C_{p_1} U_1 \frac{\partial T_1}{\partial x} \tag{2.19}$$

$$k_2 \left(\frac{\partial^2 T_2}{\partial x^2} + \frac{\partial^2 T_2}{\partial y^2}\right) = \rho_2 C_{p_2} U_2 \frac{\partial T_2}{\partial x} \tag{2.20}$$

Non-dimensionalising the equations as shown below

$$\bar{T} = \frac{T}{T_s} \qquad \bar{x} = \frac{x}{L_1} \qquad \bar{y} = \frac{y}{h_r} \tag{2.21}$$

we obtain

$$\frac{h_r^2}{L_1^2} \frac{\partial^2 T_1}{\partial \bar{x}^2} + \frac{\partial^2 \bar{T}_1}{\partial \bar{y}^2} = \frac{h_r^2}{L_1} \frac{\rho_1 C_{p_1} U_1}{k_1} \frac{\partial \bar{T}_1}{\partial \bar{x}} \tag{2.22}$$

$$\frac{h_r^2}{L_1^2} \frac{\partial^2 \bar{T}_2}{\partial \bar{x}^2} + \frac{\partial^2 \bar{T}_2}{\partial \bar{y}^2} = \frac{h_r^2}{L_1} \frac{\rho_2 C_{p_2} U_2}{k_2} \frac{\partial \bar{T}_2}{\partial \bar{x}} \tag{2.23}$$

substituting (2.21) in (2.18a) yields

$$\frac{k}{k_1} = 0 \left|\frac{h}{h_r}\right|$$

usually $$\frac{k}{k_1} = \frac{1}{200}$$

$\frac{h}{L_1} = 0\,(10^{-3})$ in an elastohydrodynamic contact

hence

$$\frac{h_r^2}{L_1^2} = 0\ |(200 \times 10^{-3})^2| = 0\ |10^{-2}|$$

consequently in equations (2.19) and (2.20) we may neglect second order derivatives with respect to x and obtain

$$k_1 \frac{\partial^2 T_1}{\partial y^2} = \rho_1 C_{p_1} U_1 \frac{\partial T_1}{\partial x} \tag{2.24}$$

$$k_2 \frac{\partial^2 T_2}{\partial y^2} = \rho_2 C_{p_2} U_2 \frac{\partial T_2}{\partial x} \tag{2.25}$$

O'Donoghue and Cameron [26] have obtained very satisfactory correlations between experimentally obtained values of temperature and calculated values using relations similar to (2.24).

2.4. Elasticity Equation and Useful Hertzian Relations

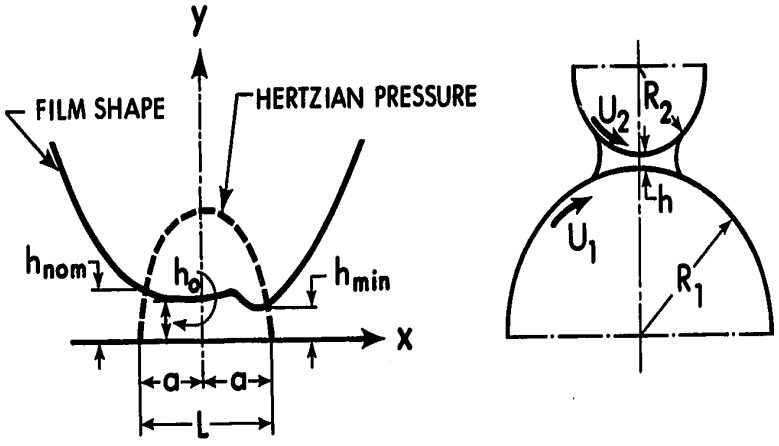

h_{nom} = NOMINAL FILM
h_o = CENTRAL FILM
h_{min} = MINIMUM FILM

FIGURE 1

Nomenclature of the Film Thicknesses

For the co-ordinate system shown in Fig. 1, the vertical displacement of a two-dimensional elastic half space under a distributed normal load $p(\xi)$ can be determined [61] from the following equation

$$h = h_0 + \frac{x^2}{2R} - \omega \int_A^B p(\xi) \ln \left| \frac{x-\xi}{x_0-\xi} \right| d\xi \tag{2.26}$$

For the following Hertzian relations [60]

$$a = \left\{ \left(\frac{1-\sigma_1^2}{E_1} + \frac{1-\sigma_2^2}{E_2} \right) \frac{4}{\pi} WR \right\}^{\frac{1}{2}} \tag{2.27}$$

$$p_0 = \frac{2W}{\pi a} \tag{2.28}$$

$$p = p_0 \left(1 - \frac{x^2}{a^2}\right)^{\frac{1}{2}} \qquad \left(\left|\frac{x}{a}\right| < 1\right) \tag{2.29a}$$

$$= 0 \qquad \left(\left|\frac{x}{a}\right| > 1\right) \tag{2.29b}$$

equation (2.26) yields [15]

$$h - h_0 = \bar{\bar{h}} = \frac{a^2}{2R} \left[\left|\frac{x}{a}\right| \left| \left(\frac{x^2}{a^2} - 1\right)^{\frac{1}{2}} \right| - \ln \left| \left|\frac{x}{a}\right| + \left(\frac{x^2}{a^2} - 1\right)^{\frac{1}{2}} \right| \right]$$

$$\left(\left|\frac{x}{a}\right| > 1\right) \tag{2.30a}$$

$$= 0 \qquad \left(\left|\frac{x}{a}\right| < 1\right) \tag{2.30b}$$

2.5. Property Relations

Viscosity and density of the fluid are functions of pressure and temperature. Following Cheng [23] the following property relations

are assumed

$$\mu = \mu_s \exp\left(\alpha p + \frac{\beta}{T} - \frac{\beta}{T_s} + \frac{\gamma p}{T}\right) \tag{2.31}$$

$$\rho = \rho_s \left\{1 + \frac{C_A p}{1+C_B p} + D_t(T-T_s)\right\} \tag{2.32}$$

For the 'isothermal' case these relations reduce to

$$\mu = \mu_s \exp(\bar{\bar{\alpha}} p) \tag{2.33}$$

$$\rho = \rho_s \left\{1 + \frac{C_A p}{1+C_B p}\right\} \tag{2.34}$$

where $$\bar{\bar{\alpha}} = \left(\alpha + \frac{\gamma}{T_s}\right) \tag{2.35}$$

2.6. Non-dimensional Procedures

The equations can be non-dimensionalised by introducing the following non-dimensional variables. Within the fluid:

$$\bar{x} = \frac{x}{L}, \quad \bar{y} = \frac{y}{h}, \quad \bar{u} = \frac{u}{U}, \quad \bar{h} = \frac{h}{h_o}, \quad \bar{\mu} = \frac{\mu}{\mu_s}, \quad \bar{\rho} = \frac{\bar{\rho}}{\rho_s},$$

$$\bar{T} = \frac{T}{T_s}, \quad \bar{p} = \frac{pa}{W}, \quad Pr = \frac{C_p \mu_s}{k}, \quad E = \frac{U^2}{C_p T_s}, \quad Re = \frac{\rho_s UL}{\mu_s}$$

$$\bar{\alpha} = \frac{\alpha W}{a}, \quad \bar{\beta} = \frac{\beta}{T_s}, \quad \bar{\gamma} = \frac{\gamma W}{aT_s}, \quad \bar{D}_t = D_t T_s \tag{2.36}$$

Within the solid:

$$\bar{\bar{y}}_1 = \frac{y}{h_{r_1}}, \quad \bar{\bar{y}}_2 = \frac{y}{h_{r_2}} \tag{2.37}$$

Then equations (2.8a) to (2.8e) are non-dimensionalised. to

$$\frac{1}{\bar{\bar{\mu}}_e} = \int_0^1 \frac{1}{\bar{\bar{\mu}}} \, d\bar{\bar{y}} \tag{2.38a}$$

$$\frac{1}{\bar{\bar{\mu}}'_e} = 2\int_0^1 \frac{\bar{\bar{y}}}{\bar{\bar{\mu}}} \, d\bar{\bar{y}} \tag{2.38b}$$

$$\frac{1}{\bar{\bar{\mu}}''_e} = 3\int_0^1 \frac{\bar{\bar{y}}}{\bar{\bar{\mu}}} \, d\bar{\bar{y}} \tag{2.38c}$$

$$t_1 = 12 \left[\frac{\bar{\bar{\mu}}_e}{3\bar{\bar{\mu}}''_e} - \left(\frac{\bar{\bar{\mu}}_e}{2\bar{\bar{\mu}}'_e}\right)^2 \right] \tag{2.38d}$$

$$t_2 = 1 + \frac{U_2 - U_1}{U_2 + U_1} \left[1 - \frac{\bar{\bar{\mu}}_e}{\bar{\bar{\mu}}'_e}\right] \tag{2.38e}$$

respectively.

The equations (2.14), (2.16) and (2.3) are non-dimensionalised to

$$\frac{d\bar{\bar{p}}}{d\bar{\bar{x}}} = \frac{\lambda \bar{\bar{\mu}}_e}{t_1 \bar{\bar{h}}^2} \left[t_2 - \frac{\bar{\bar{h}}^*}{\bar{\bar{h}}} \frac{\bar{\bar{\rho}}^*}{\bar{\bar{\rho}}} t_2^*\right] \tag{2.39}$$

$$\frac{d\bar{p}}{d\bar{x}} = \frac{\lambda\bar{\mu}}{\bar{h}^3}\left[\bar{h} - \frac{\bar{h}^*\bar{\rho}^*}{\bar{\rho}}\right] \tag{2.40}$$

$$\bar{p}(-\infty) = \bar{p}(0.5) = 0 = \left.\frac{d\bar{p}}{d\bar{x}}\right|_{\bar{x}\,=\,0.5} \tag{2.41}$$

respectively, where

$$\lambda = \frac{6aL\mu_s}{W}\,\frac{(U_1+U_2)}{h_o^2} \tag{2.42}$$

The elastic equation (2.26) is non-dimensionalised to

$$\bar{h} = 1 + G\bar{x}^2 - F\int_{-\infty}^{0.5} \bar{p}(\bar{\xi})\ln\left|\frac{\bar{x}-\bar{\xi}}{\bar{x}_o-\bar{\xi}}\right| d\bar{\xi} \tag{2.43}$$

where.

$$G = \frac{L^2}{2R\,h_o} \tag{2.44}$$

and

$$F = \frac{2WL}{ah_oE'} \tag{2.45}$$

The energy equation for the fluid (2.17) is non-dimensionalised to

$$PrRe\left(\frac{h_o^2}{L^2}\right)\bar{\rho}\bar{u}\,\frac{\partial\bar{T}}{d\bar{x}} = Pr\,\frac{h_o^2}{L^2}\,M\varepsilon\bar{U}\bar{T}\,\frac{d\bar{p}}{d\bar{x}} + PrE\,\frac{\bar{\mu}}{\bar{h}^2}\left(\frac{\partial\bar{u}}{\partial\bar{y}}\right)^2 + \frac{1}{\bar{h}^2}\,\frac{\partial^2\bar{T}}{\partial\bar{y}^2} \tag{2.46}$$

where

$$M = \frac{W}{C_p\rho_sT_saJ} \tag{2.47}$$

$$\bar{\varepsilon} = -\frac{1}{\bar{\rho}} \frac{\partial \bar{\rho}}{\partial \bar{T}}\Big|_{\bar{p}} \tag{2.48}$$

J = Joule's constant

One may also define a modified Reynolds number

$$Re^* = \frac{\rho_s U h_o^2}{\mu_s L} \tag{2.49}$$

Equation (2.46) could then be rewritten as

$$PrRe^* \bar{\rho}\bar{u} \frac{\partial \bar{T}}{\partial \bar{x}} = PrM \frac{h_o^2}{L^2} \bar{\varepsilon}\bar{u}\bar{T} \frac{d\bar{p}}{d\bar{x}} + PrE \frac{\bar{\mu}}{\bar{h}^2} \left(\frac{\partial \bar{z}}{\partial \bar{y}}\right) + \frac{1}{\bar{h}^2} \frac{\partial^2 \bar{T}}{\partial \bar{y}^2} \tag{2.50}$$

Boundary conditions given by equations (2.18a), (2.18b) and (2.18c) are non-dimensionalised to

$$\bar{T}\ (-\infty,\ 0) = 1 \tag{2.51a}$$

$$\frac{\partial \bar{T}}{\partial \bar{y}}\Big|_{\bar{y}=0} = \left(\frac{K_1}{K}\right) \frac{\partial \bar{T}_1}{\partial \bar{y}_1}\Big|_{\bar{y}=0} \tag{2.51b}$$

$$\frac{\partial \bar{T}}{\partial \bar{y}}\Big|_{\bar{y}=1} = \left(\frac{K_2}{K}\right) \frac{\partial \bar{T}_2}{\partial \bar{y}_2}\Big|_{\bar{y}=1} \tag{2.51c}$$

respectively.

The energy equations for the solids (2.19) and (2.20) are non-dimensionalised to

$$\frac{\partial^2 \bar{T}_1}{\partial \bar{y}_1^{\,2}} = RS_1 \frac{\partial \bar{T}_1}{\partial \bar{x}} \tag{2.52}$$

$$\frac{\partial^2 \bar{T}_2}{\partial \bar{y}_2^{\,2}} = RS_2 \frac{\partial \bar{T}_2}{\partial \bar{x}} \tag{2.53}$$

respectively, where

$$RS_1 = \left(\frac{L\rho_1 C_{p_1} U_1}{K_1}\right)\left(\frac{h_{r_1}}{L}\right)^2 \tag{2.54a}$$

$$RS_2 = \left(\frac{L\rho_2 C_{p_2} U_2}{K_2}\right)\left(\frac{h_{r_2}}{L}\right)^2 \tag{2.54b}$$

and they denote a reference solid non-dimensional number pertaining to bottom and top solids respectively. The boundary conditions on temperature are given by equations (2.51a), (2.51b), (2.51c) and by

$$\bar{T}_1\,(\bar{x}, \bar{h}_{r_1}) = \bar{T}_2\,(\bar{x}, \bar{h}_{r_2}) = 1 \tag{2.55}$$

The property expressions (2.31) and (2.32) are non-dimensionalised to

$$\bar{\mu} = \exp\left(\bar{\alpha}\bar{p} + \frac{\bar{\beta}}{\bar{T}} - \bar{\beta} + \frac{\bar{\gamma}\bar{p}}{\bar{T}}\right) \tag{2.56}$$

$$\bar{\rho} = 1 + \frac{\bar{C}_A \bar{p}}{1 + C_B \bar{p}} + \bar{D}_t\,(\bar{T} - 1) \tag{2.57}$$

respectively.

For the 'isothermal case' equations (2.33) and (2.34) are similarly non-dimensionalised to

$$\bar{\mu} = \exp\{\bar{p}\bar{\phi}\} \tag{2.58}$$

$$\bar{\rho} = 1 + \frac{\bar{C}_A \bar{p}}{1+\bar{C}_B \bar{p}} \tag{2.59}$$

respectively, where

$$\bar{\phi} = \bar{\alpha} + \bar{\gamma} \tag{2.60}$$

The non-dimensionalisation adopted transfers the original solid-fluid-solid field into a rectangular field shown in Fig. 2.

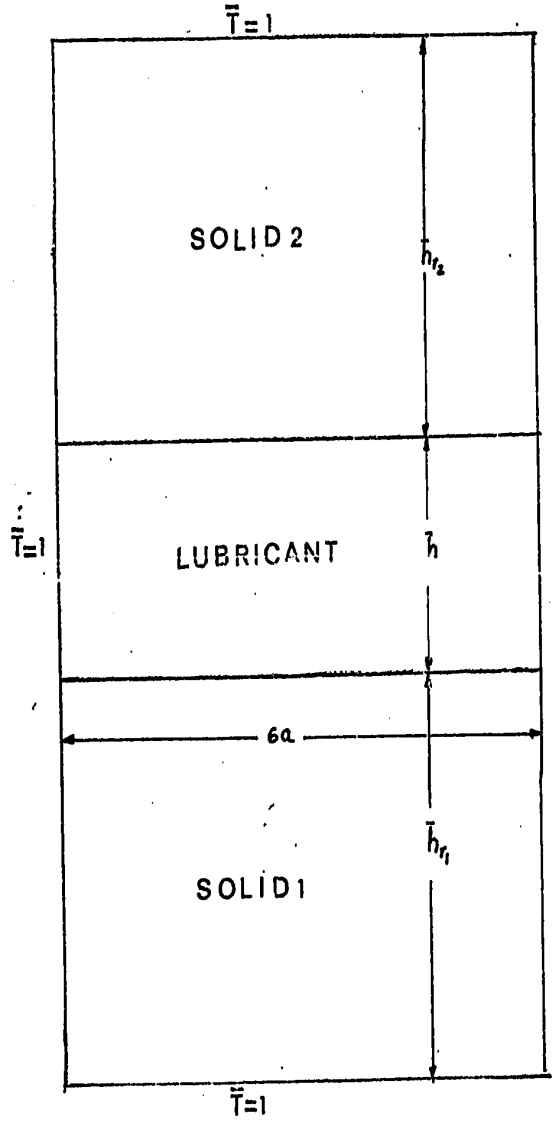

FIGURE 2 Solid-Fluid-Solid Field

CHAPTER III

SOLUTION TO THE ISOTHERMAL PROBLEM

3.1. General Approach

The 'isothermal' problem requires the simultaneous solution of the Reynolds equation (2.40) along with the elasticity equation (2.43) taking into account the variation of viscosity and density with pressure as given by equations (2.58) and (2.59) respectively. As a closed form solution of the coupled integro-differential system of equations could not be found, a suitable numerical method had to be adopted.

In relatively low load cases, a straightforward converging iterative procedure of assuming a pressure distribution, calculating the film shape through the elastic equations and re-evaluating the pressure distribution by integrating the Reynolds equation can be devised [12, 18]. However, for high loads, this procedure fails to converge.

The next important consideration is whether to keep a fixed centre-line film thickness and calculate the pressure distribution suitable for this assumed thickness or else to assume a given load and calculate the centre film thickness. Osterle and Stephenson [18] assumed a fixed centre-line film thickness and their results show poor convergence even for light loads. Further, even from the design point of view, only the load to be transmitted and surface speeds are usually

known apriori. In the present work, load is considered known and the numerical procedure developed yields the film profile and pressure distribution. Earlier work [15, 19] has also revealed that the convergence is much better when load is taken as an input.

It is convenient to divide the contact region into subregions A, B, C and D, as is shown in Fig. 3. The methods adopted in each of these regions to solve the elastic and Reynolds equations together have been detailed in the subsequent articles.

3.2. Initial Considerations for Integration in Region A

From the consideration that

$$\frac{d\bar{p}}{d\bar{x}}\Big|_{\bar{x} = \bar{x}_0} = \frac{d\bar{p}}{d\bar{x}}\Big|_{\bar{x} = \bar{x}^*} = 0, \tag{3.1}$$

and using the viscosity equation (2.58) we can rewrite equation (2.40) in the form

$$\frac{d}{dx}\left(e^{-\bar{\phi}\bar{p}}\right) = -\frac{\lambda\bar{\phi}}{\bar{h}^3}\left[\bar{h} - \frac{\bar{h}_0\bar{\rho}_0}{\bar{\rho}}\right] \tag{3.2}$$

with the boundary condition (2.41)

$$\bar{p}\ (-\infty) = 0$$

Thus, if in the entrance region A (Fig. 3) one could calculate $\bar{h}$, then for any assumed value of h_0, equation (3.2) can be numerically integrated. For the initial cycle of calculations the film profile in region A was assumed to correspond to the Hertzian profile of dry contact. This assumption has been adopted by many investigators

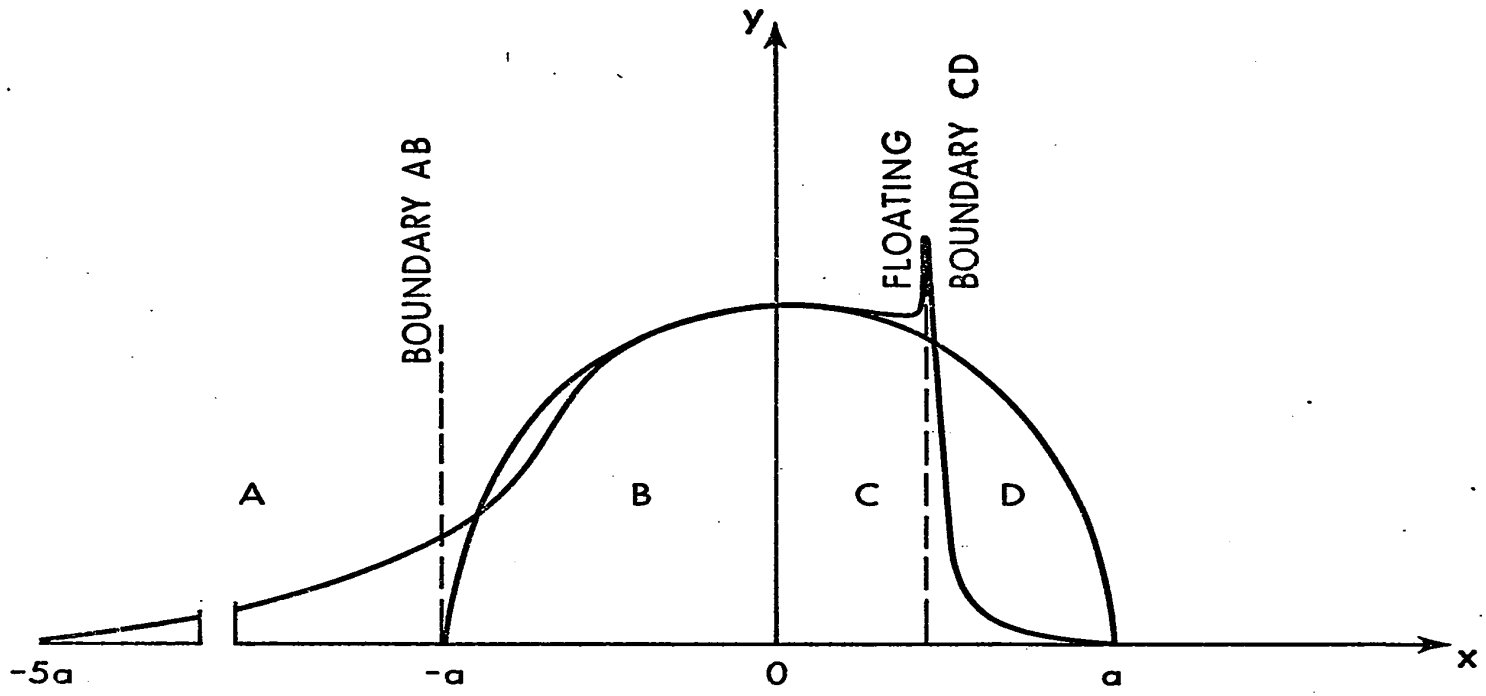

FIGURE 3 Typical Elastohydrodynamic Contact Regions for Numerical Integration

[15, 17, 38] and has been used by Grubin and Vinogradova [11] to considerable advantage when they derived their well known film thickness formula. The applicable Hertzian relations have been listed under article 2.3, equations (2.27) to (2.30b).

A Runge-Kutta fourth order integration technique in double precision arithmetic (detailed in appendix A) was adopted to carry out the numerical integration. The choice of this method depended on the considerations that the method is self-starting and has a low truncation error [62] and at any stage the step size can be varied. For numerical purposes $-\infty$ was located at $x = -5a$ ($\bar{x} = -2.5$). This assumption has been made on the basis of experimental evidence [52, 53]. Various authors have chosen basically similar criteria to fix the value of the pressure at the boundary AB. Dowson and Whitaker [19] calculated a number of pressure curves, each one corresponding to an assumed h_0 and selected that pressure curve which can be extrapolated to run smoothly into the elliptical pressure profile of dry contact. This called for human intervention and judgement. In the present work, following Archard, Gair and Hirst [15] it was postulated that had h_0 been guessed correctly in the first instance, the extrapolated value of the pressure at $\bar{x} = -0.4$ will be the same as the value of the Hertzian pressure at that point. At any rate, this is just a first step to get the procedure started and the iterative procedure takes care of the shape of the final curve. As will be seen later, the values of the final film thickness calculated agree quite well with film thicknesses calculated with these criteria. Several guesses of h_0 may be necessary to meet the aforementioned initial criterion but this is easily programmed in a

computer since increasing h_0 decreases the pressures in region A and vice-versa. If h_0 is chosen too small one obtains an error message from the computer that logarithm of a negative quantity is attempted to be computed.

3.3. Numerical Integration of the Elastic Equation

The next step is to calculate the displacements in region B due to pressures in region A through equation (2.43). However, equation (2.43) has a singularity at $\bar{x} = \bar{\xi}$. Various authors [13, 15, 18] have used different devices to remove this singularity. In effect, these consist of dividing the pressure curve into small segments and consider $p(\bar{\xi})$ as a second order polynomial [13] or a first order polynomial [18, 15] and formally integrate the assumed pressure function. Wernick [63] found that such methods introduced a ripple in the film profile which he attributed to the neglect of the effect of curvature in the pressure that was not fully taken care of in the foregoing methods. His method has been indicated briefly in appendix B. Since there was a rapid change of curvature in the pressure profile in the entrance region and as will be seen later in the region near the spikes, this method was considered the most appropriate and was used. In order to have a check on the accuracy of the calculations to be expected of this method, the values of the film thickness as calculated through equation (2.30a) and through Wernick's method for a Hertzian dry contact are compared at discrete points in Table I.

The displacements in region B due to the pressures in region A are added to the Hertzian displacements in B.

Table I

Position	-5a	-4a	-3a	-2a	-a
Through equation (2.30a)	7.045×10^{-4}	4.635×10^{-4}	2.793×10^{-4}	1.537×10^{-4}	9.476×10^{-5}
Through Wernick's method Appendix B	7.047×10^{-4}	4.637×10^{-4}	2.795×10^{-4}	1.537×10^{-4}	9.458×10^{-5}

Position	o	a	2a	3a	4a
Through equation (2.30a)	9.476×10^{-5}	9.476×10^{-5}	1.537×10^{-4}	2.793×10^{-4}	4.635×10^{-4}
Through Wernick's method Appendix B	9.476×10^{-5}	9.462×10^{-5}	1.537×10^{-4}	2.795×10^{-4}	4.637×10^{-4}

COMPARISON OF ELASTIC DISPLACEMENTS FOR $\bar{U} = 400$ and $W = 0.32$ TON/IN.

3.4. Centre-Line Shift Technique

It will be seen that while the Hertzian pressure profile for a dry contact is symmetrical about the centre line, the hydrodynamic pressure profiles are not. For this reason, when the surface displacements are calculated taking into account the hydrodynamic pressures in region A, the elastic displacements will be tilted with respect to the line of centres of cylinders. This leads to an oil-film thickness of decreasing height in the direction of surface motion. But a feature of the elastohydrodynamic contact is that $\bar{h}$ must be sensibly constant over a major portion of the Hertzian zone and particularly in the central region. This problem is conveniently overcome by employing what is known as the centre-line shift technique [64, 59]. This technique has been indicated in appendix D.

3.5. Inverse Hydrodynamic Relation

In region B (Fig. 3), the pressures and viscosities are high. A straightforward integration of Reynolds equation in this region leads to inaccuracies [19]. It has been found [13, 15, 17] better to compare the film shapes calculated by the elastic and hydrodynamic relations and modify the pressure curve to ensure close agreement. For this purpose it is convenient to rewrite equation (2.40) in the form of a cubic equation

$$\bar{h}^3 \frac{d\bar{p}}{d\bar{x}} - \lambda\bar{\mu}\bar{h} + \frac{\bar{h}^*\bar{\rho}^*}{\bar{\rho}} = 0 \qquad (3.3)$$

A rapid and accurate solution to the equation could be had by adopting a Newton-Raphson iterative technique. This procedure has been

described in appendix C. For the initial cycle of calculation pressure is assumed Hertzian (except at boundary AB, where the value already calculated is used) and the pressure gradients are calculated at discrete points in region B. The values so calculated are used in the solution of equation (3.3) which yields $\bar{h}$ at the points chosen. The values of $\bar{h}$ are compared to the elastic displacements at the very same points as calculated through methods developed under article 3.3.

The differences in the film thicknesses as calculated through the elastic and inverse hydrodynamic relations are a measure for the amendment of pressures needed at these points. An inverted Wernick method was developed to calculate the change of pressures needed and this procedure has been indicated in appendix B. With these new pressures, pressure gradients can be calculated and the cycle starts once again with the solution of equation (3.3). It is illustrative at this stage to present the block diagram (Fig. 4) to indicate the procedure adopted for the iterative solution of the elastic and Reynolds equations in regions A and B of Fig. 3. It will be noticed that one is solving for the centre film thickness by considering pressures and displacements in regions A and B and Hertzian pressures in C and D. The mathematical argument for the procedure adopted is given below. Expression (2.16) can be rewritten as

$$\frac{h^3}{\mu}\frac{dp}{dx} = 6U\left(h - \frac{h_o\rho_o}{\rho}\right) \qquad (3.4)$$

Differentiating both sides with respect to x and rearranging

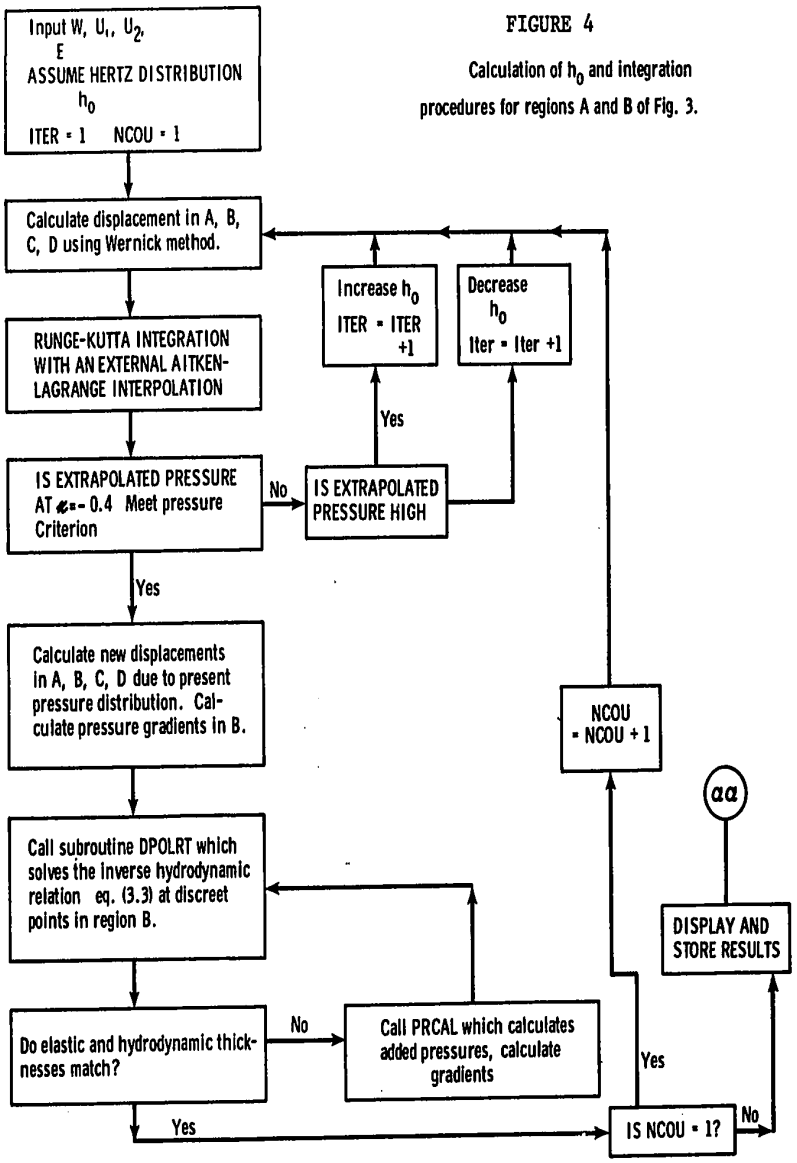

FIGURE 4

Calculation of h_0 and integration procedures for regions A and B of Fig. 3.

BLOCK DIAGRAM

$$\frac{h^3}{\mu}\left[\frac{d^2p}{dx^2} - \frac{1}{\mu}\frac{d\mu}{dx}\frac{dp}{dx}\right] + \frac{dh}{dx}\left[-6U + \frac{3h^2}{\mu}\frac{dp}{dx}\right]$$

$$= 6U\frac{\rho_o h_o}{\rho^2}\frac{d\rho}{dx} \qquad (3.5)$$

For Hertzian pressure distribution $\frac{dp}{dx} = 0$ at $x = 0$ and expression (3.5) reduces to

$$\left.\frac{dh}{dx}\right|_{x=0} = \frac{h_o^3}{6U\mu_o}\left.\frac{d^2p}{dx^2}\right|_{x=0} \qquad (3.6)$$

For Hertzian pressure distribution from expression (2.29b)

$$\left.\frac{d^2p}{dx^2}\right|_{x=0} = -\frac{p_o}{a^2}$$

Thus,

$$\left.\frac{dh}{dx}\right|_{x=0} = \frac{-p_o h_o^3}{6U\mu_o a^2} \qquad (3.7)$$

Hence, if h_o is small and μ_o is large (as is the case)

$$\left.\frac{dh}{dx}\right|_{x=0} \simeq 0$$

This shows that under the conditions of our present problem, one may solve for the regions A and B entirely before going on to the regions C and D.

3.6. Integration Procedure for Regions C and D

Different procedures have been suggested by various authors [15, 19, 24] for the integration in regions C and D. The choice of the technique depends on the assumption of the existence of the pressure 'spike'. Investigating the problem for low loads, Stephenson and Osterle [18] did not find any spikes. Herrebrugh [20] investigating the problem for an isoviscous lubricant also did not find any 'spikes'. The existence of the spike has however been authenticated by other authors working under less restrictive assumptions [15, 19, 21, 24, 38] and also verified by experiment [52, 53, 54]. Cheng and Sternlicht [21] avoided the problem of hunting for the location of the 'spike'. They fixed the location and found the corresponding rolling velocity which will yield the spike at the chosen location. However, in any design problem it is the surface speeds that are known apriori.

In this work, a simpler and quicker method to locate fairly closely the approximate location of the spike (within 4% of the semi-Hertzian width) was found and this was subsequently refined by an iterative procedure. Initially the floating boundary CD was located say at $\bar{x} = 0.4$. In the regions C and D the pressures are assumed Hertzian and zero respectively. For the already found pressure distributions in regions A and B and the presently assumed pressure distribution in regions C and D the elastic equation (2.43) is used to obtain the displacements at discreet points in D. For the displacements found for discreet points in D, equation (2.40) is integrated. The integration starts from $\bar{x} = 0.5$ with the boundary

condition $\bar{p}(0.5) = 0$. Simpson's rule is found sufficient for integration in this region. Integration is carried out till CD is reached. The value of the pressure at CD serves as a sensitive indicator for the location of the spike. If, for example, CD is to the right of the actual location of the spike, pressure found by the integration at CD is small. If CD is to the left of the actual location, the pressure will attempt to pass through an infinite value with an error message from the computer that the logarithm of a negative number is attempted to be computed. Thus, the direction in which CD has to be moved becomes known and CD can be loacted. Pressures in region D are calculated for this tentative location of CD. With the present pressure distribution in D, the already calculated pressure distribution in A and B and assumed Hertzian pressure distribution in C, the elastic displacements at discrete points in C are calculated through equation (2.43). For the Hertzian pressure distribution in C (Fig. 3) solution of the cubic relation (3.3) will yield the hydrodynamic thicknesses at the chosen discrete points in C. As before, the differences in the film thicknesses calculated through the elastic and inverse hydrodynamic relations are a measure for the amendment of pressures needed at these points. The inverted Wernick method (described already) is used to calculate the pressure amendments needed. It is illustrative at this stage to present the block diagram (Fig. 5) to indicate the procedure adopted for the iterative solution of the elastic and Reynolds relations in regions C and D.

FIGURE 5

Location of the pressure 'spike' and the integration procedures for regions C and D of Fig. 3.

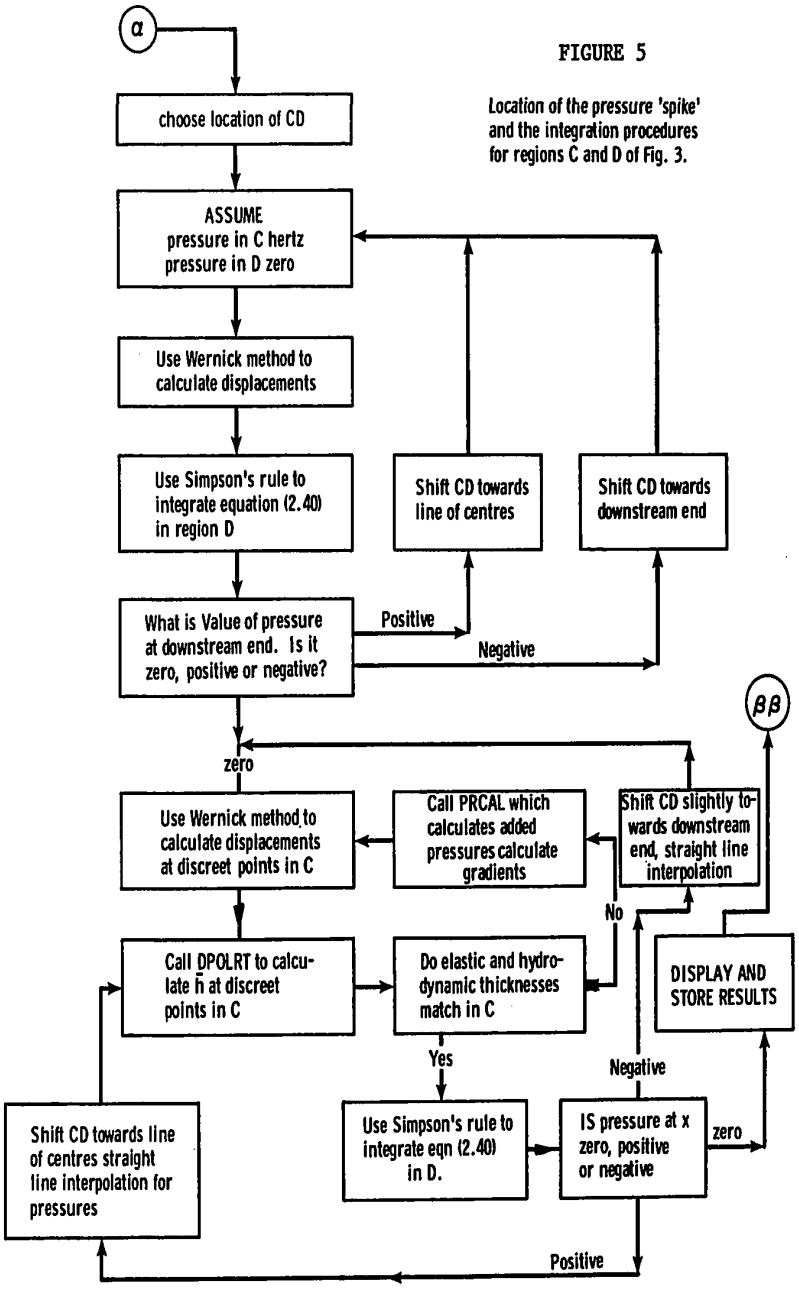

BLOCK DIAGRAM

As is shown in the block diagram, the new pressures in C are used to calculate the elastic displacements in D. And when these displacements are used to integrate for pressures in region D, it may become necessary to shift the floating boundary CD to achieve closer agreement of pressures. In actual calculations it was found that only a very slight shift to the left was necessary to obtain satisfactory agreement and between two to four iterations were enough to locate the position of the spike within $^1/1000$ of the Hertzian semi-width.

3.7. Discussion on the Numerical Scheme

One of the contributions of the present study is that a completely automatic scheme has been developed which can be extended to the study of the thermal system as will be seen in Chapter IV. We had to make a few assumptions in developing the scheme and the purpose of this article is to discuss the validity of the assumptions made in the light of experimental findings and theoretical work. The first assumption that was made was that the integration can be started in region A from $\bar{x} = -2.5$ $(x/a = -5.0)$. The results that are presented in the next article show that this is adequate, as the pressure becomes significant only from $\bar{x} = -1.0$. This is also in agreement with the experimental findings of Kannel [52] and Longfeld [53]. In starting the iterative process for finding the centre-line film thickness, it was assumed that the extrapolated pressure should match the Hertzian pressure at $\bar{x} = -0.4$. This consideration is based upon the following reasoning. The hydrodynamic equation (3.2) shows that $\bar{h} - \bar{h}_0$ has to be small when the pressures are high. From the elastic standpoint,

the Hertzian pressure distribution yields the flatness that is observed and verified. Hence the system should be closer to the Hertzian pressure distribution. Since the hydrodynamic equations reveal a pressure build-up in the entrance region, a certain amount of pressure must be subtracted from the Hertzian distribution to compensate for the external excess pressure. The true pressure curve may be expected to cut the Hertzian curve at a value of $\bar{p}$ well below the maximum since the depression caused by a force diminishes slowly with the distance and the flatness at the high pressure region has to be maintained to correspond with the experimental findings [46, 47, 52, 53]. Thus, for the starting of the schemes it was assumed that the extrapolated pressure should match the Hertzian pressure at $\bar{x} = -0.4$ where the pressures are well below the maximum. The iterative procedure improves the approximation.

Different schemes are adopted in regions A, B, C and D to find iterative solutions to the elastic and hydrodynamic equations. Previous studies by others have shown the necessity for such a step. The numerical method to solve for the inverse hydrodynamic equation, adopted in the present work, is new to the elastohydrodynamic studies and has been found to be quick and accurate. The inversion of the Wernick method to find the amendment to the pressure curve is also a new feature. As this method takes into account both the pressure gradients and pressures, the results are likely to be more accurate as is seen by comparison with an analytical solution (Table I). A simpler method to locate the spike, reducing the tedious hunting process, has been deve-

loped and has been explained in some detail under article 3.6. The use of the Runge-Kutta procedure in the entrance is numerically more accurate and is also new in elastohydrodynamic studies.

3.8. Non-Dimensional Parameters

Dowson and Higginson [59] have formulated three non-dimensional parameters, viz. load parameter, speed parameter and materials parameter for isothermal elastohydrodynamic contacts. In terms of the notation used in this study they are

$$\text{Load parameter} \qquad LP = \frac{W}{ER} \tag{3.8}$$

$$\text{Speed parameter} \qquad SP = \frac{\mu_s \bar{U}}{ER} \tag{3.9}$$

$$\text{Materials parameter} \qquad MP = \phi E \tag{3.10}$$

It has also been shown [59] that the effect of load on film thickness is very little. For ordinary elastohydrodynamic contacts the variation in the materials parameter is also small. Thus, the speed parameter emerges as the dominant variable in controlling film thickness. In the present study both the load parameter and the materials parameter have been kept constant. The effect of speed parameter on the film thickness has been studied over the range SP varying between 10^{-12} to 10^{-10}. It may however be pointed out that the same numerical scheme can be adopted for studying the effect of the other parameters. By varying the slip for the same effective rolling velocity temperature effects have been studied which form the subject matter of Chapters IV.

3.9. Results and Discussion

The input data and the isothermal results are given in appendices E and F respectively. Dowson and Whitaker [19] have presented a minimum film thickness diagram showing the three regions encountered in cylinder lubrication. This diagram has been reproduced in Fig. F.1 and the range of the present study has been marked therein. It is seen that the present investigation is inside the elastic range and that the ranges of speed covered are between moderately low and moderately high. The pressure distribution and the film profiles have been obtained for different rolling velocities and are presented in Figures F.2 and F.3 respectively. Referring to Fig. F.2, it is observed that with the increase in rolling velocity the pressure 'spike' moves towards the line of centres. The magnitude of the pressure at the 'spike' increases with rolling velocity though not proportionately. At low rolling velocities the pressure distribution is closer to the Hertzian pressure distribution.

Referring to Fig. F.3, it is noted that the film profiles are parallel in the high pressure region with a depression developing in the down-stream end. The area of the depression increases with increase in rolling velocity. The film thickness increases appreciably with speed but the rate of variation tends to diminish at higher speeds. All the above results are in good qualitative agreement with other results [14, 15, 17, 19, 21, 24].

Cheng [65] has indicated the three thicknesses in common use in elastohydrodynamic work. These are the nominal, centre-line

and minimum film thickness and are indicated in Fig. 1. Cheng [65] has also given a table of the isothermal elastohydrodynamic film thickness formulae based upon a correlation of the results of various authors. A good quantitative check on the results of the present study will be to compare the results on the film thicknesses with those of other authors, as per Cheng's [65] table. This has been done in Fig. F.4 to F.6. Experimental results due to Sibley and Orcutt [45] and Crook [47] have been superimposed. It is clear that the present studies correlate favourably with experimental results. Fig. F.6 also yields a correlation of the form $h_0 \alpha \bar{U}^{0.66}$.

3.10 Conclusions

The Dowson-Higginson [59] formula or the Grubin [11] formula have a narrow range of validity. They yield good results for velocities not exceeding 400 inches per second and for Hertzian maximum pressure not exceeding 100,000 psi. Also the materials parameter αE has to be high in these formulae. This is a severe restriction. At low values of the materials parameter the thicknesses predicted are much lower than is actually the case. For example both these formulae predict zero film thickness for an isoviscous lubricant. This is absurd as Herrebrugh's [20] analysis and the measurements of Kannel et al [67] have shown. Thus a rapid and accurate numerical scheme becomes necessary to calculate the film thickness for all ranges of the materials parameter. The numerical scheme devised for the present study is good for this purpose.

The favourable correlation with experimental work and theoretical results also shows that accuracy at every stage is important and balancing of the elastic and hydrodynamic film thickness has to be done carefully. The closer agreement also shows that the errors in the numerical scheme keep within agreeable limits and justify the assumptions made in developing the scheme.

CHAPTER IV

THERMAL ELASTOHYDRODYNAMIC PROBLEM

4.1. General Approach

The thermal elastohydrodynamic problem requires the simultaneous solution of the Reynolds equation (2.39), the energy equations (2.50), (2.52) and (2.53) along with the elasticity equation (2.43), taking into account the variation of fluid properties given by equations (2.56) and (2.57). As a closed form solution of these coupled non-linear integro-differential systems of equations could not be found suitable numerical methods had to be used. The method adopted here is to use the results obtained in Chapter III as the initial input and devise a cycle of operations that will take into account the thermal effect on the system.

4.2. Simplifying Assumptions

In order to obtain a solution to this highly complicated problem, it is necessary to make some simplifying assumptions. Cheng and Sternlicht [21] made an assumption of a mean viscosity across the film. Cheng [23] removed this restrictive assumption but his form of the Reynolds equation has been found to be in error (Chapter II). Dowson and Whitaker [24] have used thermal factors, considered functions of $\bar{x}$ to obtain property values at any given $\bar{x}$ location. This again is an assumption of mean property values. Further, all the above authors [21, 23, 24] have used a surface energy equation as the

boundary condition for the energy equation of the lubricant. The assumption that is inherent in deriving the surface temperature equation is that the problem can be treated as a case of linear heat flow [24, 23, 29, 60] and that the dimensionless parameter

$$\frac{UL}{2}\,\frac{\rho_1 C_{p_1}}{K_1} > 10.$$

This is generally true in high speed contacts, but in the case of low speed, light-weight highly conductive contacts this condition may not be satisfied. A less restrictive boundary condition would be to equate the heat fluxes at the fluid-solid interface and this has been done in the present work. Also, this method yields the temperature distribution in the solids.

4.3. Numerical Method for solving Energy Equations

A finite difference formulation has been adopted for solving the energy equations of the solid-fluid-solid together as a unified field. The grid diagram and the finite difference formulae to be used are shown in Fig. 6. With the finite difference computational molecules adopted, the energy equations could be written as a system of algebraic equations as shown below. The energy equation (2.52) is written as

$$\chi_m = a_1 \bar{T}_{1_{i,m}} + b_1 \bar{T}_{1_{i,m+1}} + C_1 \bar{T}_{1_{i,m-1}} + d_m = 0 \qquad (4.3)$$

FIGURE 6 Grid Diagram

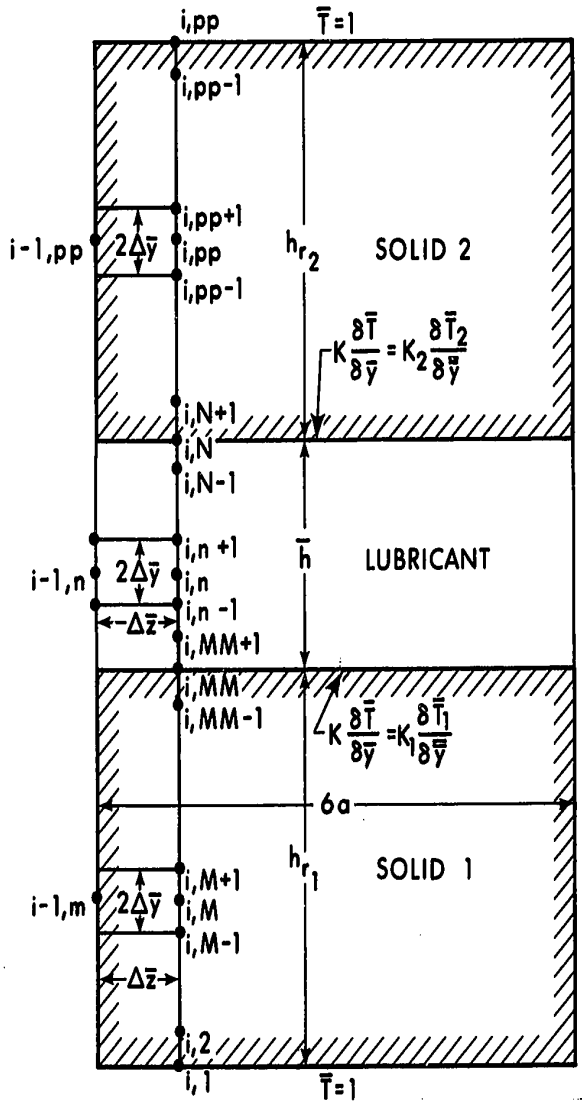

First step $$\left(\frac{\partial\bar{T}}{\partial\bar{x}}\right)_{i,j} = \frac{\bar{T}_{i,j} - \bar{T}_{i-1,j}}{\Delta\bar{x}} \qquad (4.1a)$$

Subsequent step $$\left(\frac{\partial\bar{T}}{\partial\bar{x}}\right)_{i,j} = \frac{3\bar{T}_{i,j} - 4\bar{T}_{i-1,j} + \bar{T}_{i-2,j}}{2\Delta\bar{x}} \qquad (4.1b)$$

$$\frac{\partial^2\bar{T}}{\partial\bar{y}^2} = \frac{\bar{T}_{i,j+1} - 2\bar{T}_{i,j} + \bar{T}_{i,j-1}}{\Delta\bar{y}^2} \qquad (4.2)$$

where

$$a_1 = 3RS_1 + 4\Delta\bar{x}/\Delta\bar{\bar{y}}_1^2 \tag{4.4}$$

$$b_1 = -2\Delta\bar{x}/\Delta\bar{\bar{y}}_1^2 \tag{4.5}$$

$$c_1 = -2\Delta\bar{x}/\Delta\bar{\bar{y}}_1^2 \tag{4.6}$$

$$d_m = -4RS_1\,\bar{T}_{i-1,m} + RS_1\,\bar{T}_{i-2,m} \tag{4.7}$$

$$m = 2, \text{ ---------- } MM-1$$

The boundary condition equation (2.51b) is expressed as

$$\chi_m = -\bar{T}_{i,m+1} + \bar{T}_{i,M}\left(1 + \frac{K_1}{K}\frac{\Delta\bar{y}}{\Delta\bar{\bar{y}}_1}\right) - \frac{K_1}{K}\frac{\Delta\bar{y}}{\Delta\bar{\bar{y}}_1}\bar{T}_{1_{i,M-1}} = 0 \tag{4.8}$$

The energy equation (2.50) for the lubricant is expressed as

$$\chi_n = a_{n_1}\bar{T}_{i,n-1} + b_n\bar{T}_{i,n} + a_{n_3}\bar{T}_{i,n+1} + \omega_n\bar{u}_{i,n} + d_n = 0 \tag{4.9}$$

where

$$a_{n_1} = \frac{-2\Delta\bar{x}}{\Delta\bar{y}^2\bar{h}_i^2} \tag{4.10}$$

$$b_n = \frac{4\Delta\bar{x}}{\Delta\bar{y}^2\bar{h}_i^2} + 3\,PrRe^*\bar{\rho}_{i,n}\bar{u}_{i,n} - 2\,PrMh_o^2\,\bar{\bar{\varepsilon}}\bar{u}_{i,n}\frac{d\bar{p}_i}{d\bar{x}_1}\frac{\Delta\bar{x}}{L^2} \tag{4.11}$$

$$a_{n_3} = -\frac{-2\Delta\bar{x}}{\Delta\bar{y}^2\bar{h}_i^2} \tag{4.12}$$

$$\omega_n = -2\Delta\bar{x}\ PrE\ \left(\frac{\partial\bar{u}}{\partial\bar{y}}\right)^2_{i,n} / \bar{h}_i \qquad (4.13)$$

$$d_n = -PrRe^*\bar{\rho}_{i,n}\bar{u}_{i,n}\ (\bar{T}_{i-2,n} - 4\bar{T}_{i-1,n}) \qquad (4.14)$$

and

$$n = MM+1, \text{ ---------- } N-1$$

The boundary condition equation (2.51c) is expressed as

$$\chi_N = \bar{T}_{i,N}\left(1 + \frac{\Delta\bar{y}}{\Delta\bar{\bar{y}}_2}\frac{K_2}{K}\right) - \bar{T}_{i,N-1} - \frac{\Delta\bar{y}}{\Delta\bar{\bar{y}}_2}\frac{K_2}{K}\bar{T}_{2_{i,N+1}} = 0 \qquad (4.15)$$

The energy equation (2.53) is expressed as

$$\chi_{pp} = -\bar{T}_{2_{i,pp+1}}\left(\frac{2\Delta\bar{x}}{\Delta\bar{\bar{y}}_2^2}\right) + \bar{T}_{2_{i,pp}}\left(3RS_2 + \frac{4\Delta\bar{x}}{\Delta\bar{\bar{y}}_2^2}\right) -$$

$$\bar{T}_{2_{i,pp-1}}\left(\frac{2\Delta\bar{x}}{\Delta\bar{\bar{y}}_2^2}\right) - 4RS_2\,\bar{T}_{i-1,pp} + RS_2\,\bar{T}_{i-2,pp} = 0 \qquad (4.16)$$

$$pp = N+1, \text{ ---------- } PP-1$$

From equation (2.4) and (2.5) one obtains the normalised velocity gradient and velocity. They are

$$\frac{\partial\bar{u}}{\partial\bar{y}} = \frac{Wh^2}{\mu_s UaL}\frac{d\bar{p}}{d\bar{x}}\frac{1}{\bar{\mu}}\left\{\bar{y} - \frac{\mu_e}{2\mu_e'}\right\} + \frac{U_2-U_1}{U}\frac{\bar{\mu}_e}{\bar{\mu}} \qquad (4.17)$$

$$\bar{u} = \frac{Wh^2}{\mu_s UaL}\frac{d\bar{p}}{d\bar{x}}\int_0^{\bar{y}}\frac{\bar{\eta}d\bar{\eta}}{\bar{\mu}} + \frac{U_2-U_1}{U}\bar{\mu}_e\int_0^{\bar{y}}\frac{d\bar{\eta}}{\bar{\mu}} -$$

$$\frac{Wh^2}{2\mu_s UaL}\frac{d\bar{p}}{d\bar{x}}\frac{\bar{\mu}_e}{\bar{\mu}_e}\int_0^{\bar{y}}\frac{d\bar{\eta}}{\bar{\mu}} + \frac{U_1}{U} \qquad (4.18)$$

where $\bar{\eta}$ is an auxiliary non-dimensional y-coordinate. Equations (4.3), (4.8), (4.9), (4.15) and (4.16) constitute a system of non-linear algebraic equations and the following procedure is adopted to solve them numerically.

For the solution of the energy equation the pressure gradients and the film thicknesses are considered known [21]. For the first cycle of calculations the values calculated from the isothermal solutions (Chapter III) are adopted. (In the subsequent cycles, the pressure gradients are amended by the iterative solution of the modified Reynolds equation (2.39) along with the elasticity equation (2.43) and the temperature as calculated in the previous cycle are used.) Further, for the starting of the iterative solution, the density and viscosity of the lubricant are considered as functions of pressure only. This reduces the system of energy equations to a tri-diagonal linear system and rapid and efficient algorithms are available to solve this system. Thomas algorithm [66] was adopted. The adoption of this method reduces the storage difficulties and the grid can be made as small as is desired. The solution can now proceed column-wise. As soon as the temperatures have been calculated in a particular column, the property values are recalculated, adopting the

presently calculated temperatures and once again the system is solved for that column. The iteration is stopped as soon as the criterion

$$\frac{|\bar{T}_j^{\,r} - \bar{T}_j^{\,r+1}|}{|\bar{T}_j^{\,r}|} \leq 0.001 \tag{4.19}$$

was met. It was found that in high speed cases acceleration parameters [68] of the form

$$\bar{T}^{r+1} = \bar{T}^{r+1}\,(1-\upsilon) + \sigma\,(\bar{T}^{r}) \tag{4.20}$$

$$\upsilon = 0.47 \text{ to } 0.61$$

were useful. The convergence was slower in the spike region. The Newton-Raphson method was also used in some cases and this also improved convergence [68]. The block diagram illustrating the numerical procedure described is presented in Fig. 7. Simpson's rule was used to calculate the integrals in the equations (2.38a to 2.38c) and in equation (4.18).

4.4. Modified inverse hydrodynamic Relation

It is now necessary to find the changes induced in the pressure gradient and in the film profile due to the modifications in the temperature field. The methods detailed in chapter III can now be used with a modified inverse hydrodynamic relation. Equation (2.39) can be rewritten as

$$t_1\bar{h}^3\frac{d\bar{p}}{d\bar{x}} - \lambda\bar{\mu}_e t_2\bar{h} + \frac{\bar{h}^*\bar{\rho}^* t_2^*}{\bar{\rho}} = 0 \tag{4.21}$$

FIGURE 7

Column - Wise Matrix Solution Of Energy Equations

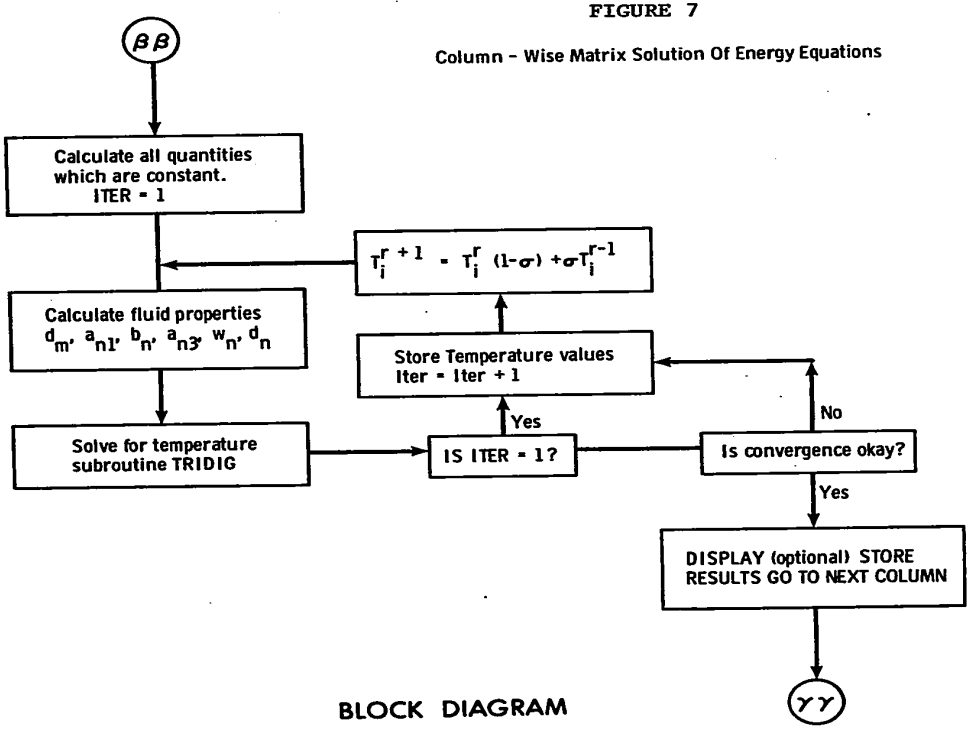

BLOCK DIAGRAM

For discreet points in region B (Fig. 3) the values of t_1, μ_e, t_2 can be calculated from our knowledge of temperature distribution. Further, we can also calculate from the determined temperatures at the down-stream end the values of t_2^* and $\bar{\rho}^*$. Since the pressure gradients at both the line of centres and the down-stream end are zero, expression (4.21) applied at these points yields

$$(-\lambda\bar{\mu}_e t_2\bar{h})_o + \frac{\bar{h}^*\bar{\rho}^* t_2^*}{\bar{\rho}} = (-\lambda\bar{\mu}_e t_2\bar{h})_* + \frac{\bar{h}^*\bar{\rho}^* t_2^*}{\bar{\rho}^*} \qquad (4.22)$$

where subscript o and $*$ indicate evaluation of the quantities in the brackets at the line of centres and the down-stream end respectively. Equation (4.22) is a first order relation in $\bar{h}^*$ (remembering our basic assumption that the centre-line film thickness is insensitive to change of temperature) and $\bar{h}^*$ can be evaluated. The procedure to be followed hereafter is identical to that described in articles 3.5 and 3.6 with the modifications indicated below.

1. The inverse hydrodynamic relation to be solved is given by equation (4.21).
2. For finding the position of the spike, computer time is saved if one starts from the location of the spike obtained from the previous cycle. Usually only a slight shift towards the line of centres is necessary.

4.5. Further Temperature Calculations

The temperature field needs to be checked on the basis of the modifications in film profile and pressure gradient. One repeats

the procedure detailed under article 4.3 with the presently found values of the pressure gradient and $\bar{h}$. If the presently calculated temperatures do not differ by more than 1% of the values obtained in earlier cycles, the calculated values are accepted as the solution of the problem. Convergence in the temperature field was faster than in the case of pressure and film profile calculations. However, 3 to 5 full cycles were found enough for the range of the present work.

4.6. Calculations for the Frictional Force

Following Cheng [23], the friction factor is defined as the ratio of the frictional force to the load per unit width of the roller. This may be written as

$$f_r = \frac{1}{W} \int_{-\infty}^{0.5} \left(\mu \frac{\partial u}{\partial y}\right)_{\bar{y}=1} L \, d\bar{x} \tag{4.23}$$

$$= \frac{h_0}{a} \int_{-\infty}^{0.5} \bar{h} \frac{d\bar{p}}{d\bar{x}} \left(1 - \frac{\bar{\mu}_e}{2\bar{\mu}'_e}\right) d\bar{x}$$

$$+ \frac{\mu_s (U_2 - U_1)}{W h_0} L \int_{-\infty}^{0.5} \frac{\bar{\mu}_e}{\bar{h}} d\bar{x} \tag{4.24}$$

One may define

$$f_s = \frac{\mu_s (U_2 - U_1)}{W h_0} L \int_{-\infty}^{0.5} \frac{\bar{\mu}_e}{\bar{h}} d\bar{x} \tag{4.25}$$

Simpson's rule was used for integration purposes.

CHAPTER V

DISCUSSIONS AND CONCLUSIONS

5.1. Discussion of the Results

Using a modified Reynolds equation for a lubricant whose density and viscosity are functions of pressure and temperature, the thermal elastohydrodynamic problem between two rolling and sliding cylinders has been investigated. The numerical scheme developed analyses the 'isothermal system' and the results serve as an input to the thermal problem. One of the contributions of the present work is the derivation of the correct thermal form of the Reynolds equation. Also, instead of using a surface temperature equation [24, 23, 21], the energy equations for the solid-liquid-solid combination has been solved as a unified field. This approach extends the validity of the solution and has been discussed in Chapter IV.

A detailed discussion of the numerical scheme for the isothermal problem has already been presented in Chapter III. The reasons for adopting a tri-diagonal matrix solution for the temperature equations and the iterative methods used have been detailed in Chapter IV.

In the present chapter, the results of the 'thermal' problem, which are presented in Appendix G, are discussed. The slip ratio which is defined as

$$\text{Slip Ratio} = \frac{U_2 - U_1}{U_2} \tag{5.1}$$

has been varied from zero to a moderately high value of 0.25.

Figure G.1 relates the position of the pressure spike with the slip ratio and rolling velocity. Also indicated in the same figure is the magnitude of the pressure at the spike. It is observed that at constant rolling velocity the position of the spike is moved towards the line of centres as the slip ratio is increased. This result is in agreement with the result of other workers [21, 24]. It is also seen that the magnitude of the pressure at the spike is reduced with the increase of slip. This finding is in agreement with the conclusions of Dowson and Whitaker [24] and is in conflict with the results of Cheng and Sternlicht [21]. It may be observed that with the increase in slip the temperature of the lubricant increases with corresponding decrease in viscosity. Herrebrugh [20] did not find any spikes for an iso-viscous lubricant and came to the conclusion that spikes are due to increase in the absolute viscosity of the lubricant. Thus, any reduction in viscosity should reduce the magnitude of the spike and the present results conform to this reasoning. Figures G.2 (a and b) and G.3 (a and b) represent the temperature distribution across the film at different $\bar{x}$ locations for rolling velocities 400 in/sec. and 30 in/sec. respectively and for a constant slip ratio of 0.25. The presentation of each figure has been subdivided into two parts a and b in order to achieve clarity. Thus, the figure G.2.a represents the temperature distributions up to the position of the spike and G.2.b shows the temperature distribution from the position of the spike to the down-stream

end ($\bar{x} = 0.5$). Similarly for the figures G.3.a and G.3.b. Referring to figure G.2.a, the temperature rise is seen to be moderate till about $\bar{x} = -0.3$. Thereafter the temperature increase is more rapid and this is attributed to the increase in viscosity in the high pressure region. The temperature rise near the fluid-solid interface is however moderate. The significant increase in temperature at the region of the spike is evident where the non-dimensional temperature rise is about 0.185 between $\bar{x} = 0$ to $\bar{x} = 0.06$. This is due to the rapid increase of viscosity due to high pressures at the spike region. The mid-stream temperatures are seen to fall beyond the spike (Fig. G.2.b). Here, the lubricant temperatures near the walls are seen to increase slightly. Both figures, G.2.a and G.2.b, show that the viscous heat generated at the centre across the film is much higher than that generated near the boundaries. Figures G.3.a and G.3.b follow a slightly different pattern. The temperature rise is moderate till $\bar{x} = -0.2$. This is attributed in part to the low rolling velocity ($\bar{u} = 30$). The temperature rise is less rapid in this case and at $\bar{x} = 0$ the non-dimensional mid-film temperature is 1.14. The mid-film temperature then falls slowly to 1.09 at location $\bar{x} = 0.32$ (not shown in figure G.3.a) due to the fall in pressure. The spike occurs further away from the line of centres in the case of low rolling velocity. Thus, the effects of decompression cooling and conduction are more evident. At the region of the pressure spike the temperature rises rapidly. Maximum mid-film temperature occurs at the spike. Beyond the spike (Fig. G.3.b) the mid-film temperature

falls till at $\bar{x} = 0.5$ the temperature across the film is almost uniform. A comparison of the figures G.2 and G.3 reveals that the solids with a lower rolling velocity reach higher temperatures for the same slip ratio. This finding is in agreement with Cheng and Sternlicht [21]. It is also observed that in both cases represented by figures G.2 and G.3, the lower solid which moves more slowly than the top solid attains the highest temperature. This result is in agreement with other results [24, 21, 23]. Checking the temperature distribution at the down-stream end $\bar{x} = 0.5$ it is observed that the variation of temperature across the film is significant at $\bar{U} = 400$ in/sec. Thus, the assumption of Cheng [23] that $t_2 = 1$ at $\bar{x} = 0.5$ is inaccurate for high velocities.

Figures G.4 and G.5 represent the mid-film temperatures along the contact for several slip ratios at $\bar{U} = 130$ in/sec. and $\bar{U} = 200$ in/sec. respectively. The temperature profiles follow the pressure distribution and maximum mid-film temperature is at the position of the pressure spike. In both cases, for zero slip the temperature rise is negligible, showing the insignificant effects of compressive heating. For other slip ratios the temperature rise is moderate till $\bar{x} = -0.3$ and thereafter the temperature rise is rapid till the line of centres is reached. For rolling velocities $\bar{U} = 130$ in/sec. (Fig. G.4) we notice that for low to moderate slip ratios of 1%, 5% and 10%, there is a slight cooling till the spike region is reached. This is attributed to the fall in pressure and hence fall in viscosity and the decompression cooling effects. At higher slip

ratios of 15% and 25%, the temperature remains constant till the region of spike is reached. This is attributed to the fact that at higher slips the spike moves towards the line of centres and thus the pressure falls slower than in low slip cases. The temperature falls after the spike and at low slip ratios the temperature at the down-stream end is moderate. As was to be expected, the temperatures are higher at the down-stream end for higher slip velocities. A similar pattern is followed for the case $\bar{U}$ = 200 in/sec. (Fig. G.5). Figure G.6 shows the maximum rise in mid-film temperatures reached at various slip ratios for different rolling velocities. It is observed that for a constant slip ratio the temperature rises steadily with rolling velocity till about $\bar{U}$ = 200 in/sec. Further increase in rolling velocity causes the temperature to rise much slower than before. Fig. G.7 shows the maximum film temperatures plotted against slip velocity for different rolling velocities. It is observed that for low values of $(U_2 - U_1)$ there is a rapid rise in temperature. Further substantial increases in $(U_2 - U_1)$ causes only slow rise in temperature. This is attributed to the rapid fall in viscosity at high temperatures. Also it is seen that the increase in rolling velocity causes slight increase in temperature, showing the major role played by slip velocity in the generation of heat. Fig. G.8 shows the temperature rise above ambient reached by the lower solid at the position of the spike for various slip velocities. At zero (and near about zero) slip velocity for $\bar{U}$ = 400 in/sec. the temperature rise is 4°F and for $\bar{U}$ = 30 in/sec. the temperature rise is negligible. As $(U_2 - U_1)$ is increased, it is

observed that the temperature rise is more rapid in the case of lower rolling velocities than in higher rolling velocities. This leads to the conclusion that thermal stresses are likely to be less severe at higher rolling speeds. When it is remembered that the dip in the down-stream end is more pronounced at lower rolling speeds, one may conclude that if fatigue and thermal stresses are considered important, they should be provided for at the lowest rolling velocity the system is likely to encounter.

Fig. G.9 shows the surface temperature rise above the ambient for the lower solid along the length of the contact for $\bar{U}$ = 30 in/sec. for different slip ratios. It is seen that the temperature rise at the entrance to the high pressure region is of the order of 1°F. The film thickness has been found to depend on the viscosity of the lubricant at the temperature of the surrounding solids at inlet. The insignificant rise in temperature at inlet shows that film thicknesses calculated on the isothermal assumption are valid for the thermal case as well. Fig. G.10 shows the plot of friction factor f_s against $(U_2 - U_1)$. Super-imposed are the experimental plots of Crook [49] and Bell and Kannel reported in the discussion in Reference [23]. It is seen that friction factor increases initially with increase in slip velocity and then decreases. This is due to the fact that the friction factor depends on $\bar{\mu}_e (U_2 - U_1)$ and initial increase of $(U_2 - U_1)$ increases the friction factor. As $(U_2 - U_1)$ is further increased, $\bar{\mu}_e$ decreases due to rise in temperature and the product $\bar{\mu}_e (U_2 - U_1)$ decreases. The trends predicted in the present work and

in the experiment are the same. Quantitatively the agreement is moderate. The discrepancy may be due to an overestimation of the viscosity near the peak pressure. The assumption of a Newtonian fluid near the vicinity of the peak tends to overestimate the peak as the isothermal analysis of Chow and Saibel [38] has shown. Cheng [23] has reported that a slight change of the temperature viscosity exponent β causes a significant change in the predicted friction factors.

The problem being non-linear, analytically there is no general proof of the uniqueness of the solution [66]. If comparable results are obtained by using two different numerical procedures, the solution is considered correct. This was done in the present study for $\bar{u}$ = 30 in/sec. The film thickness results of the present study which compare well with experimental results also show the consistency of the numerical solution.

Assessment of error is very difficult for the problem under study. However, conservative error estimates can be made. Pressures in the inlet region have been calculated by fourth order Runge-Kutta method with a step size $\Delta\bar{x}$ = 0.1. Computation of the non-dimensional pressures have been carried out with computer errors less than one percent. In regions B, C, D the numerical procedures are different but the non-dimensional pressures have been calculated with computer errors less than one percent. The temperatures are calculated to an accuracy of better than ninety-nine percent in all regions. The numerical procedures used are stable [66] and it is well known that if consistency is satisfied, then stability of the system also ensures

convergence.

5.2 *Conclusion and Scope for further Work*

The pressure, temperature and film thickness between two rolling and sliding cylinders have been determined by solving numerically the coupled Reynolds, elasticity and energy equations. The isothermal problem was solved first and an iterative procedure was developed to solve the thermal problem. The results show that a pressure peak exists in the down-stream end of the film for all heavily loaded cases. The effect of temperature was to reduce the pressure peak slightly in all cases. Increase in rolling velocity shifts the location of the pressure peak towards the line of centres. Increase in the slip velocity also moves the peak towards the line of centres. At low speeds the surface temperature was higher. The slip velocity has been shown to be the major factor in the temperature rise. Friction factor increases initially with sliding velocity and later decreases. The present results compare more closely as regards the film thicknesses with experimental findings. The comparison of the friction factor with experimental findings shows moderate quantitative agreement.

The present numerical procedure can be effectively used to investigate the effects of the material parameter and the load parameter. The effects of non-Newtonian behaviour of the lubricant is worthy of study. Study of the dissipation of heat for low reference solid numbers Rs_1 and Rs_2 will be of interest in thermal elastohydrodynamic studies.

BIBLIOGRAPHY

1. Hertz, H., "Ueber die Beruehrung fester elastischer Koerper", 1881, "Ueber die Beruehrung fester elastischer Koerper und ueber die Haerte", 1882, reprinted in Gesammelte Werke von Heinrich Hertz, Vol. I., pp. 155 - 173, 174 - 196, Leipzig, 1895, English translation in: Hertz, H., Miscellaneous Papers, translation by Jones, D.E., and Schott, G.A., pp. 146 - 162, 163 - 183, Macmillan, New York, N.Y., 1896.
2. Crook, A.W., "Developments in Elastohydrodynamic Lubrication", Journal of the Institute of Petroleum, Vol. 49, No. 478, Oct. 1963, pp. 295 - 307.
3. Martin, H.M., "Lubrication of Gear Teeth", ENGINEERING, Vol. 102, 1916, p. 199.
4. Peppler, W., "Druckuebertragung an geschmierten zylindrischen Gleit- und Waelzflaechen", V.D.I. Forschungsheft, 1938, p. 391.
5. Meldahl, A., "Contribution to the Theory of the Lubrication of Gears and of the Stressing of the Lubricated Flanks of Gear Teeth", Brown Boveri Review, Vol. 28, No. 11, 1941, p. 374.
6. Gatcombe, E.K., "Lubrication Characteristics of Involute Spur Gears - A Theoretical Investigation", Transactions of the A.S.M.E., Vol. 67, 1943, p. 177.
7. Hersey, M.D., and Lowdenslager, D.B., "Film Thickness Between Gear Teeth", Transactions of the A.S.M.E., Vol. 72, 1950, p. 1035.
8. Cameron, A., "Hydrodynamic Theory in Gear Lubrication", Journal of the Institute of Petrol, Vol. 38, 1952, p. 614.

9. Mcewen, E., "The Effect of Variation of Viscosity with Pressure on the Load Carrying Capacity of Oil Film between Gear Teeth", Journal of the Institute of Petrol, Vol. 38, 1952, p. 646.

10. Blok, H., "Discussion. Gear Lubrication Symposium. Part I, The Lubrication of Gears", J. Inst. Petrol, Vol. 38, P. 673.

11. Grubin, A.N., and Vinogradova, I.E., "Central Scientific Research Institute for Technology and Mechanical Engineering, Book No. 30", Moscow, 1949, D.S.I.R. Translation No. 337.

12. Weber, C., and Saalfeld, K., "Schmierfilm bei Walzen mit Verformung", Zeits. ang. Math. Mech., Vol. 34, 1954, p. 54.

13. Dowson, D., and Higginson, G.R., "A numerical Solution to the Elastohydrodynamic Problem", Journal of Mechanical Engineering Science, Vol. I, No. 1, 1959, pp. 6 - 15.

14. Dowson, D., and Higginson, G.R., "The Effect of Material Properties on the Lubrication of Elastic Rollers", Journal of Mechanical Engineering Science, Vol. 2, No. 3, 1960, pp. 188 - 194.

15. Archard, G.D., Gair, F.C., and Hirst, W., "The Elastohydrodynamic Lubrication of Rollers", Proc. Roy. Soc. Series A., Vol. 262, 1961, pp. 51 - 72.

16. Archard, J.F., and Kirk, M.T., "Lubrication at Point Contacts", Proc. Roy. Soc. Series A., Vol. 262, 1961, pp. 532 - 550.

17. Dowson, D., Higginson, G.R., and Whitaker, A.V.,"Elastohydrodynamic Lubrication: A Survey of Isothermal Solutions", Journal of Mechanical Engineering Science, Vol. 4, No. 2, 1962, pp. 121 - 126.

18. Rhoads Stephenson, R., and Fletcher Osterle, J., "A Direct Solution of the Elastohydrodynamic Lubrication Problem", A.S.L.E. Trans-

actions, Vol. 5, 1962, pp. 365 - 374.

19. Dowson, D., and Whitaker, A.V., "The Isothermal Lubrication of Cylinders", A.S.L.E. Transactions, Vol. 8, 1965, pp. 224 - 234.

20. Herrebrugh, K., "Solving the Incompressible and Isothermal Problem in Elastohydrodynamic Lubrication through an Integral Equation", Journal of Lubrication Technology, Transactions of the A.S.M.E., Jan. 68, pp. 262 - 270.

21. Cheng, H.S., and Sternlicht, B., "A Numerical Solution for the Pressure, Temperature and Film Thickness Between Two Infinitely Long, Lubricated Rolling and Sliding Cylinders, Under Heavy Loads", Journal of Basic Engineering, Transactions of the A.S.M.E., Sept. 1965, pp. 695 - 707.

22. Dowson, D., Discussion to Reference 21, Journal of Basic Engineering, Transaction of the A.S.M.E., Sept. 1965, pp. 705 - 706.

23. Cheng, H.S., "A Refined Solution to the Thermal-Elastohydrodynamic Lubrication of Rolling and Sliding Cylinders", A.S.L.E. Transactions, Vol. 8, 1965, pp. 397 - 410.

24. Dowson, D., and Whitaker, A.V., "A Numerical Procedure for the Solution of the Elastohydrodynamic Problem of Rolling and Sliding Contacts Lubricated by a Newtonian Fluid", Proceedings of the Institution of Mechanical Engineers, London, Vol. 180, Part 3B, Paper 4, 1965, pp. 57 - 71.

25. O'Donoghue, J.P., and Cameron, A., "Friction and Temperature in Rolling Sliding Contacts", A.S.L.E. Transactions, Vol. 9, 1966, pp. 186 - 194.

26. O'Donoghue, J.P., and Cameron, A., "Temperature at Scuffing",

Proc. Instn. Mech. Engrs., London, Vol. 180, Part 3B, 1965-66, pp. 85 - 94.

27. Blok, H., "Theoretical Study of Temperature Rise at Surfaces of Actual Contact Under Oiliness Lubricating Conditions", General Discussion, Lubrication, Institution of Mech. Engineers, Vol. 2, 1937, pp. 222 - 235.

28. Carslaw, H.S., and Jaeger, J.C., "Conduction of Heat in Solids", Oxford University Press, Second Edition, 1959.

29. Jaeger, J.C., "Moving Sources of Heat and the Temperature at Sliding Contacts", Journal and Proc. Roy. Soc. New South Wales, Vol. 76, 1943, pp. 203 - 224.

30. Allen, D.N. de G., "A Suggested Approach to Finite Difference Representation of Differential Equations with an Application to Determine Temperature Distribution Near a Sliding Contact", Quarterly Journal of Mechanics and Applied Mathematics, Vol. 15, 1962, pp. 11 - 33.

31. Symm, G.T., Cameron, A., and Gordon, A.N., "Contact Temperatures on Sliding/Rolling Surfaces, Proc. Roy. Soc. Series A.,Vol. 286, pp. 45 - 61.

32. Francis, H.A., "Interfacial Temperature Distribution Within a Sliding Hertzian Contact", A.S.L.E. Transactions, Vol. 14, 1971, pp. 41 - 54.

33. Cheng, H.S., and Orcutt, F.K., "A Correlation between the Theoretical and Experimental Results on the Elastohydrodynamic Lubrication of Rolling and Sliding Contacts", Paper No. 13, Proc. Inst. Mech. Engrs., London, Vol. 180, 1965-66, p.158.

34. Milne, A.A., "A Theory of Hydrodynamic Lubrication for a Maxwell Liquid", Proceedings of the Conference of Lubrication and Wear, Instn. of Mech. Engrs., London, 1957, Paper 41.

35. Tanner, R.I., "Full Film Lubrication Theory for Maxwell Fluid", International Journal of Mechanical Sciences, Vol. I, 1960, pp. 206 - 215.

36. Bell, I.F., "Elastohydrodynamic Effects in Lubrication", M.Sc., Thesis, 1961, University of Manchester.

37. Bell, J.C., "Lubrication of Rolling Surfaces by a Ree-Eyring Fluid", Transactions of the American Society of Lubrication Engrs., Vol. 5, 1962, p. 160.

38. Chow, T.S., and Saibel, T.S., "The Elastohydrodynamic Problem with a Viscoelastic Fluid", Transactions of the A.S.M.E., Paper No. 70 - LubJ.

39. Merritt, H.E., "Worm Gear Performance", Proc. Instn. Mech. Engrs., London, Vol. 129, 1935, p. 127.

40. Lane, T.B., and Hughes, J.R., "A Study of the Oil Film Formation in Gears by Electrical Resistance Measurements", British Journal of Applied Physics, Vol. 3, 1952, pp. 315 - 318.

41. Crook, A.W., "Simulated Gear Tooth Contacts", Proc. Instn. Mech. Engrs. London, Vol. 171, 1957, pp. 187 - 214.

42. El-Sisi, S.I., and Shawki, G.S.A., "Measurement of Oil Film Thickness between Discs by Electrical Conductivity", Trans. A.S.M.E. Journal of Basic Engineering, Vol. 82 D, 1960, pp. 12 - 18.

43. Leach, E.F., and Kelley, B.W., "Temperature - The Key to Lubricant Capacity", A.S.L.E. Transactions, Vol. 8, 1965, pp. 271 - 285.

44. Tallian, T.E., Chiu, Y.P., Huttenlocher, D.F., Kamenshine, J.A., Sibley, L.B., and Sindlinger, N.E., "Lubricant Films in Rolling Contact of Rough Surfaces", A.S.L.E. Transactions, Vol. 7, 1964, pp. 109 - 126.

45. Sibley, L.B., and Orcutt, F.K., "Elastohydrodynamic Lubrication of Rolling Contact Surfaces", A.S.L.E. Transactions, Vol. 4, 1961, pp. 234 - 249.

46. Crook, A.W., "The Lubrication of Rollers", Philosophical Transactions, Series A., Vol. 250, 1958, pp. 387 - 409.

47. Crook, A.W., "The Lubrication of Rollers. II. Film Thickness with Relation to Viscosity and Speed", Phil. Trans. Series A., Vol. 254, 1961, pp. 223 - 236.

48. Crook, A.W., "The Lubrication of Rollers. III. A Theoretical Discussion of Friction and Temperatures in the Oil Film", Phil. Trans., Series A., Vol. 254, pp. 237 - 258.

49. Crook, A.W., "The Lubrication of Rollers. IV. Measurements of Friction and Effective Viscosity", Phil. Trans. Series A., Vol. 255, 1963, pp. 281 - 312.

50. Dyson, A., and Wilson, A.R., "Film Thicknesses in Elastohydrodynamic Lubrication at High Slide/Roll Ratios", Proc. Instn. Mech. Engrs., Vol. 183, Part 3P, Paper II, 1968 - 69, pp. 81 - 97.

51. Kannel, J.W., Bell, J.C., and Allen, C.M., "Methods for Determining Pressure Distributions in Lubricated Rolling Contact", A.S.L.E. Transactions, Vol. 8, 1965, pp. 250 - 270.

52. Kannel, J.W., "Measurements of Pressures in Rolling Contact", Proc. Instn. Mech. Engrs., Vol. 180, Part 3B, Paper 11, 1965-66, pp. 135 - 142.

53. Longfeld, M.D., "Pressure Distributions in a Highly Loaded Lubricated Contact", Proc. Instn. Mech. Engrs., Vol. 180, Part 3B, pp. 113 - 118.

54. Orcutt, F.K., "Experimental Study of Elastohydrodynamic Lubrication", A.S.L.E. Transactions, Vol. 8, 1965, pp. 381 - 396.

55. Cameron, A., and Gohar R., "Theoretical and Experimental Studies of the Oil Film in Lubricated Point Contact", Proc. Roy. Soc. A., Vol. 291, 1966, pp. 520 - 536.

56. Westlake, F.J., and Cameron, A., "Optical Elastohydrodynamic Fluid Testing", A.S.L.E./A.S.M.E. Lubrication Conference, Pittsburgh, Pennsylvania, October 1971, pp. 101 - 111.

57. Sanborn, D.M., and Winer, W.O., "Fluid Rheological Effects in Sliding Elastohydrodynamic Point Contacts with Transient Loading: 1 - Film Thickness", Transactions of the A.S.M.E., Journal of Lubrication Technology, April 71, pp. 262 - 271.

58. Sanborn, D.M., and Winer, W.O., "Fluid Rheological Effects in Sliding Elastohydrodynamic Point Contacts with Transient Loading: 2 - Traction", Transactions of the A.S.M.E., Journal of Lubrication Technology, July 71, pp. 342 - 348.

59. Dowson, D., and Higginson, G.R., "Elastohydrodynamic Lubriaction", Pergamon Press, First Ed., 1966.

60. Cameron, A., "Principles of Lubrication", Longmans Green and Co. Ltd., First Ed., 1966.

61. Timoshenko and Goodier, "Theory of Elasticity", Mcgraw-Hill Book Co., Inc., Second Ed., 1951.

62. Conte, S.D., "Elementary Numerical Analysis", Mcgraw-Hill Book Co., 1965, First Ed.

63. Wernick, R.J., "Some Computer Results in the Direct Iteration Solution of the Elastohydrodynamic Equations", 62-TR38, Mechanical Technology Incorporated, Rport, Feb. 1963.

64. Poritsky, H., "Lubrication of Gear Teeth including the Effect of Elastic Desplacement", First National Symposium (Fundamentals of Friction and Lubrication in Engineering), American Society of Lubrication Engineers, 1952.

65. Cheng, H.S., "Isothermal Elastohydrodynamic Theory for the full range of Pressure-Viscosity Coefficient", Journal of Lubrication Technology, Transactions of the A.S.M.E., Jan. 1972, P. 35 - 43.

66. Lee, Stanley E., "Quasilinearisation and Invariant Imbedding", Academic Press, New York, First Ed., 1968.

67. Kannel, J.W., et al, "A Study of the Influence of Lubricants on High-Speed Rolling Contact Bearing Performance", ASD Tech. Rep. No. ASD-TDR-61-643, 1969, Part VIII, June 1968.

68. Hahn, E.J. and Kettleborough, C.F., "Solution for the Pressure and Temperature in an Infinite Slider Bearing of an Arbitrary Profile", Transactions of A.S.M.E., Journal of Lubrication Technology, Oct. 1967, pp. 445 - 452.

APPENDIX A

RUNGE-KUTTA 4TH ORDER INTEGRATION TECHNIQUE

Consider an equation of the form $y' = f(x,y)$ where the prime denotes the derivative dy/dx. The value of y at station x_{n+1} in terms of its values at x_n is obtained by Taylor's series expansion as

$$y_{n+1} = y_n + hy'_n + \frac{h^2}{2!} y''_n + \frac{h^3}{3!} y'''_n + \text{--------} \qquad (A.1)$$

$$x_{n+1} = x_n + h \quad \text{where } h \text{ is the step size}$$

The Runge-Kutta method proceeds from station x_n to station x_{n+1} using values of the first derivative only calculated at a number of intermediate points. They are chosen to give agreement with the first few terms of the Taylor's series shown in (A.1) above. A commonly used set is

$$K_1 = f(x_n, y_n)$$

$$K_2 = f\left(x_n + h/2, y_n + \frac{K_1 h}{2}\right)$$

$$K_3 = f\left(x_n + h/2, y_n + \frac{K_2 h}{2}\right)$$

$$K_4 = f(x_n + h, y_n + K_3 h)$$

$$y_{n+1} = y_n + \frac{h}{6} [K_1 + 2K_2 + 2K_3 + K_4] \qquad (A.2)$$

The local truncation error of algorithm (A.2) is $0 (h^5)$. The method requires the evaluation of the first derivative four times per each step but this is not much of a problem in a computer. It has the important advantage that it is self-starting, i.e. it requires only the value of y at a point $x = x_n$ in order to find y and y' at $x = x_{n+1}$.

In the present study, equation (2.40) along with equation (2.41) can be solved directly through this method if $\bar{h}$ can be calculated. In the first cycle of calculation, $\bar{h}$ can be calculated from the Hertzian relations (2.27 to 2.30a). In the second sycle of calculations $\bar{h}$ is calculated at discreet points through equation (2.26) and the intermediate values of $\bar{h}$ needed for the Runge-Kutta technique is obtained through an Aitken-Lagrange interpolation.

APPENDIX B

CALCULATION OF ELASTIC DISPLACEMENT

In the calculation of the elastic displacement of the cylinders we encounter an integral of the form

$$I(x) = \int_{-A}^{B} p(\xi) \ln|\xi - x| d\xi \qquad (B.1)$$

If care is not exercised in the evaluation of (B.1), the singularity in the integrand can cause large errors. The singularity is removable by adopting the technique of approximating the function p by a polynomial in each sub-interval, performing the integration in closed form in the sub-interval and summing over the whole region of integration.

The choice of the degree of the polynomial approximation to p is arbitrary depending on the nature of p. In the literature both linear approximation [18] and zero degree approximation [15] have been used. However, since the pressure function can have considerable curvature, the method developed by Wernick [63] is adopted.

Wernick [63] subdivided the interval $-A$ to B into N sub-intervals requiring only that the value of $p(\xi)$ be available at the end points and mid-point of each sub-interval. He represented

$$I(x) = \sum_{j=1}^{N} I_j(x), \qquad (B.2)$$

where

$$I_j(x) = \int_{\xi_j}^{\xi_{j+1}} p(\xi) \ln|\xi - x| \, d\xi \tag{B.3}$$

and obtained

$$I_j(x) = [(\xi-x)\{\ln|\xi-x|-1\}\{p(\xi)-\tfrac{1}{2}(\xi-x)p'(\xi) + (\xi-x)^2 p''(\xi)/6\} + (\xi-x)^2\{p'(\xi)-5(\xi-x)p''(\xi)/9\}/4]_{\xi_j}^{\xi_{j+1}} \tag{B.4}$$

where

$$\left.\begin{aligned} p'_j &= p'(\xi_j) = (-3p_j + 4p_{j+\frac{1}{2}} - p_{j+1})/2\Delta_j \\ p'_{j+1} &= p'(\xi_{j+1}) = (p_j - 4p_{j+\frac{1}{2}} + 3p_{j+1})/2\Delta_j \\ p''_j &= p''_{j+1} = (p_j + 2p_{j+\frac{1}{2}} + p_{j+1})/\Delta^2_j \end{aligned}\right\} \text{Error} = O(\Delta_j^2) \tag{B.5}$$

and

$$\Delta_j = \tfrac{1}{2}(\xi_{j+1} - \xi_j) \tag{B.6}$$

This method can be further extended to yield the pressure distribution if the deformation is available and the pressures at the two end points of the interval where the deformation is available is known. A series of linear simultaneous equations can be set up and solved for the pressure distribution. This has been called in the present study

as the 'inverted Wernick' method. It will be noticed that the sub-intervals need not be uniform. A comparison of the results obtained through Wernick's method and an analytical solution has been presented in Table I.

APPENDIX C

ITERATIVE METHOD FOR CALCULATING POLYNOMIAL ROOTS

Given a polynomial

$$f(z) = \sum_{n=0}^{N} a_n z^n \tag{C.1}$$

Let $z = x + iy$ be a starting value for a root of $f(z)$. Then

$$z^n = (x + iy)^n \tag{C.2}$$

Define x_n as real terms of expanded equation (C.2). Define y_n as imaginary terms of expanded equation (C.2). Then for

$$n = 0$$

$$x_0 = 1.0$$

$$y_0 = 0.0$$

$$n > 0$$

$$x_n = xx_{n-1} - yy_{n-1} \tag{C.3}$$

$$y_n = xy_{n-1} + yx_{n-1} \tag{C.4}$$

Let U be the real terms of (C.1), V be imaginary terms of (C.1)

$$U = \sum_{n=0}^{N} a_n x_n \qquad (C.5)$$

$$V = \sum_{n=0}^{N} a_n y_n \qquad (C.6)$$

or

$$U = a_0 + \sum_{n=1}^{N} a_n x_n \qquad (C.7)$$

$$V = \sum_{n=1}^{N} a_n y_n \qquad (C.8)$$

$$\frac{\partial U}{\partial x} = \sum_{n=1}^{N} n x_{n-1} a_n \qquad (C.9)$$

$$\frac{\partial U}{\partial y} = - \sum_{n=1}^{N} n y_{n-1} a_n \qquad (C.10)$$

Equations (C.3), (C.4), (C.7), (C.8), (C.9) and (C.10) can be performed iteratively for $n = 1$ to $n = N$ by saving x_{n-1} and y_{n-1}. Using Newton-Raphson method for computing Δx and Δy the result is

$$\Delta x = \frac{(v \frac{\partial u}{\partial y} - u \frac{\partial u}{\partial x})}{[(\frac{\partial u}{\partial x})^2 + (\frac{\partial u}{\partial y})^2]}$$

$$\Delta y = - \frac{(u \frac{\partial u}{\partial y} + v \frac{\partial u}{\partial x})}{[(\frac{\partial u}{\partial x})^2 + (\frac{\partial u}{\partial y})^2]}$$

after applying Cauchy-Rieman equations. Thus, for the next iteration

$$x' = x + \Delta x$$

$$y' = y + \Delta y$$

This procedure was found accurate for solving the cubic inverse hydrodynamic relation (3.3).

APPENDIX D

CENTRE-LINE SHIFT TECHNIQUE

The elastic displacement (equation 2.26) can be written in the form

$$h = h_0 + \frac{x^2}{2R} + v \qquad (D.1)$$

Dowson and Higginson [59] have shown that any linear correction to the displacement can be done arbitrarily. If the centre-line of the cylinders be moved a distance Δc relative to the pressure distri-- bution, the film thickness becomes

$$h' = h + \frac{(x-\Delta c)^2}{2R} + v \qquad (D.2)$$

The change in film thickness is $\frac{-\Delta c\, x}{R}$ + constant. Therefore a centre-line shift of Δc produces a linear change in the film thick- ness, or in other words, a change in the slope of the datum of $-\Delta c/R$.

APPENDIX E

INPUT DATA

Diameter of rollers (R_1, R_2)	3 inches
Material of rollers	steel
Load (W)	0.32 tons/in.
Pressure viscosity exponent (α)	- 0.214 $in.^2$/ton
Temperature viscosity exponent (β)	8300° R
Pressure temperature viscosity exponent (γ)	350 $in.^2{}^{\circ}F$/ton
Inlet viscosity (μ_s)	0.4 poise
Modulus of elasticity (E_1, E_2)	13500 tons/sq.in.
Poisson's ratio (σ_1, σ_2)	0.3
Inlet temperature (T_s)	110°F
Thermal conductivity of oil (K)	0.1 B/ft.°F hr.
Specific heat of oil (C_p)	0.4 B/lb.deg.F
Density of oil (ρ)	0.0325 $lb./in.^3$
Thermal conductivity of solids (K_1, K_2)	26.6 B/ft.°F hr.
Density of solids (ρ_1, ρ_2)	0.283 $lb./in.^3$
Specific heat of solids (C_{p_1}, C_{p_2})	0.1 B/lb.°F
Pressure density coefficient (C_A)	0.009 sq.in./ton
Pressure density coefficient (C_B)	0.026 sq.in./ton
Coefficient of thermal expansivity (ε)	0.000348 per °F

APPENDIX F

RESULTS OF ISOTHERMAL SOLUTION

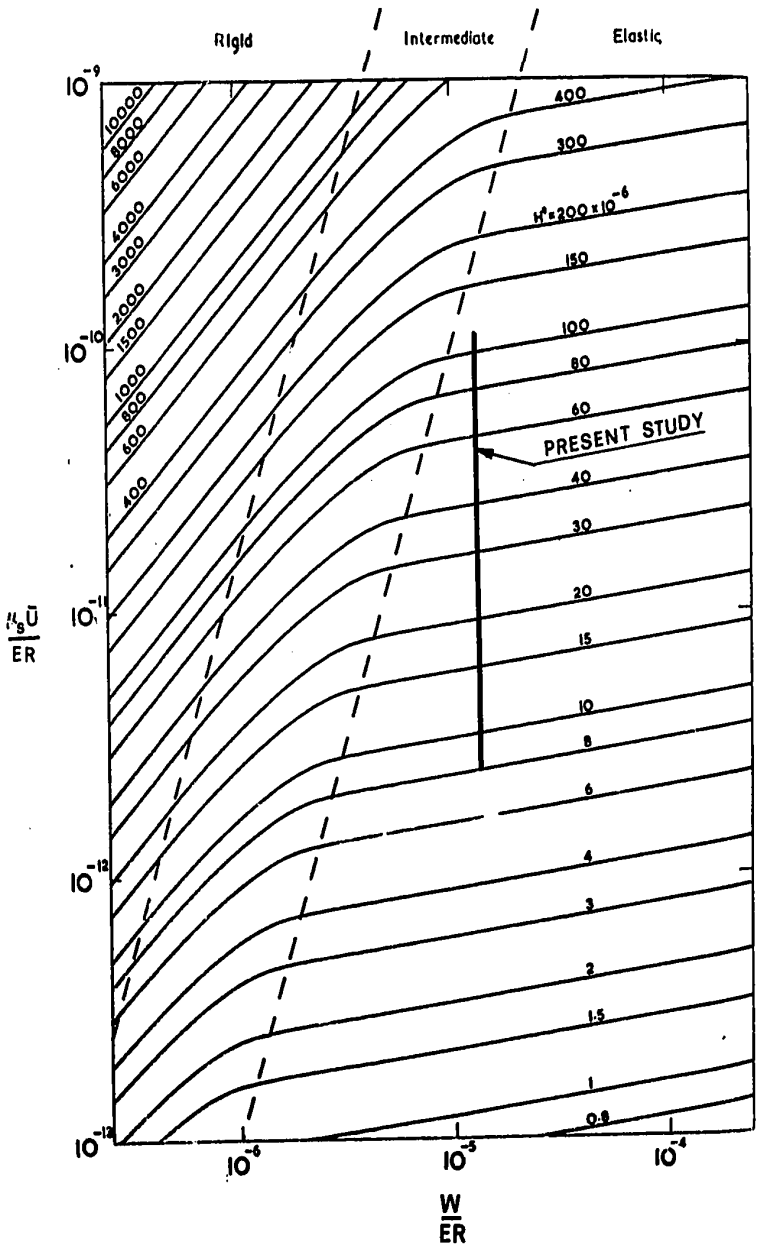

FIGURE F.1 Minimum Film Thickness Contours and Range of Present Study

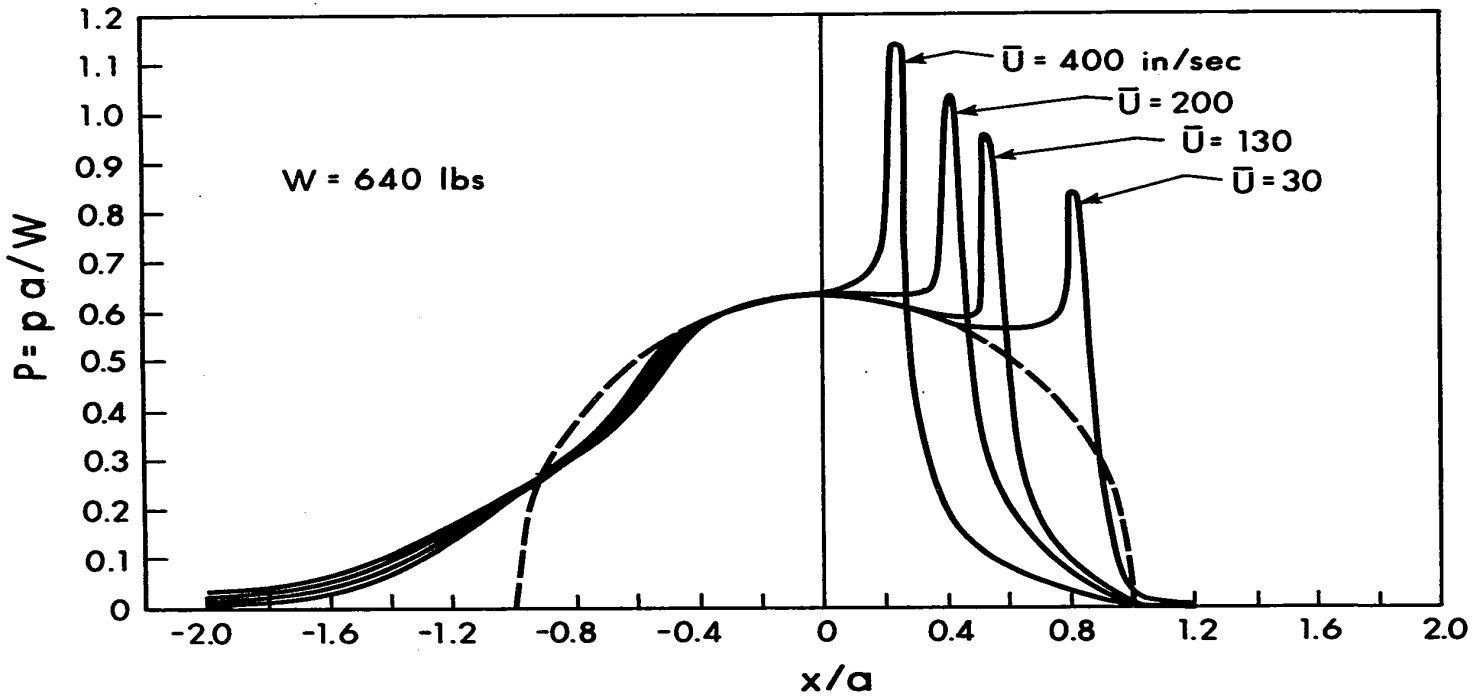

FIGURE F.2 Pressure Distributions

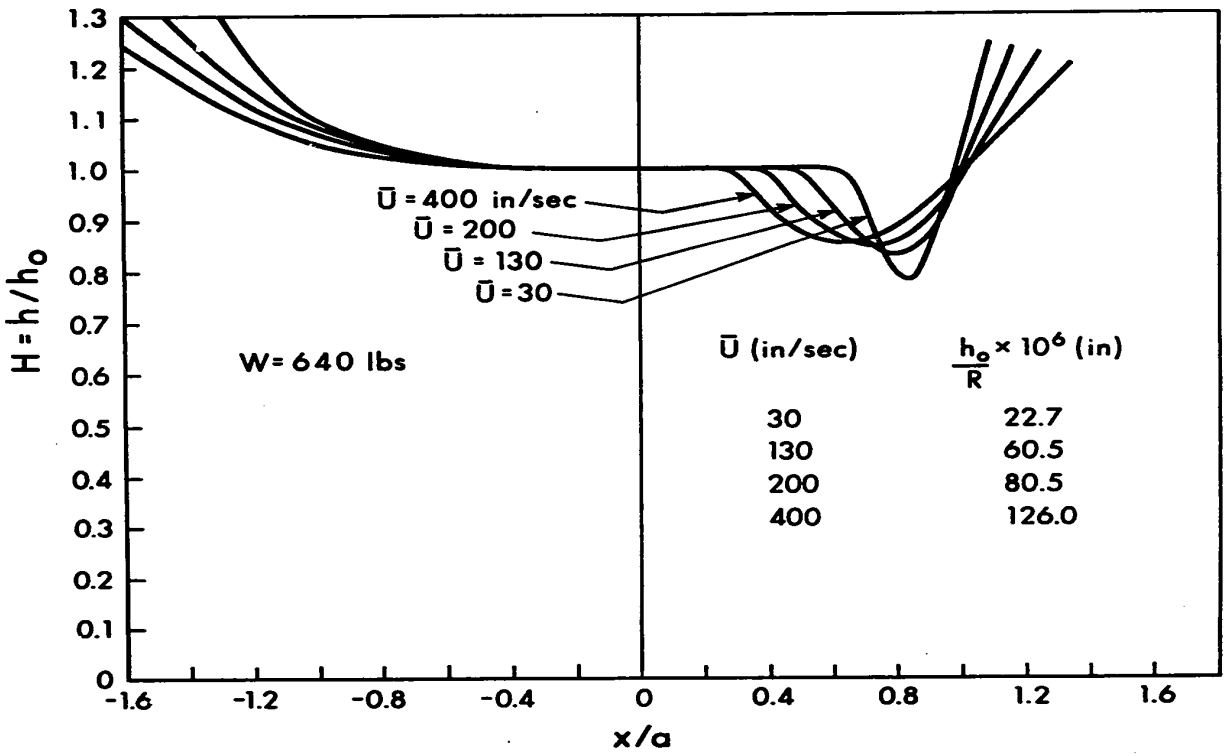

FIGURE F.3 Film Profiles

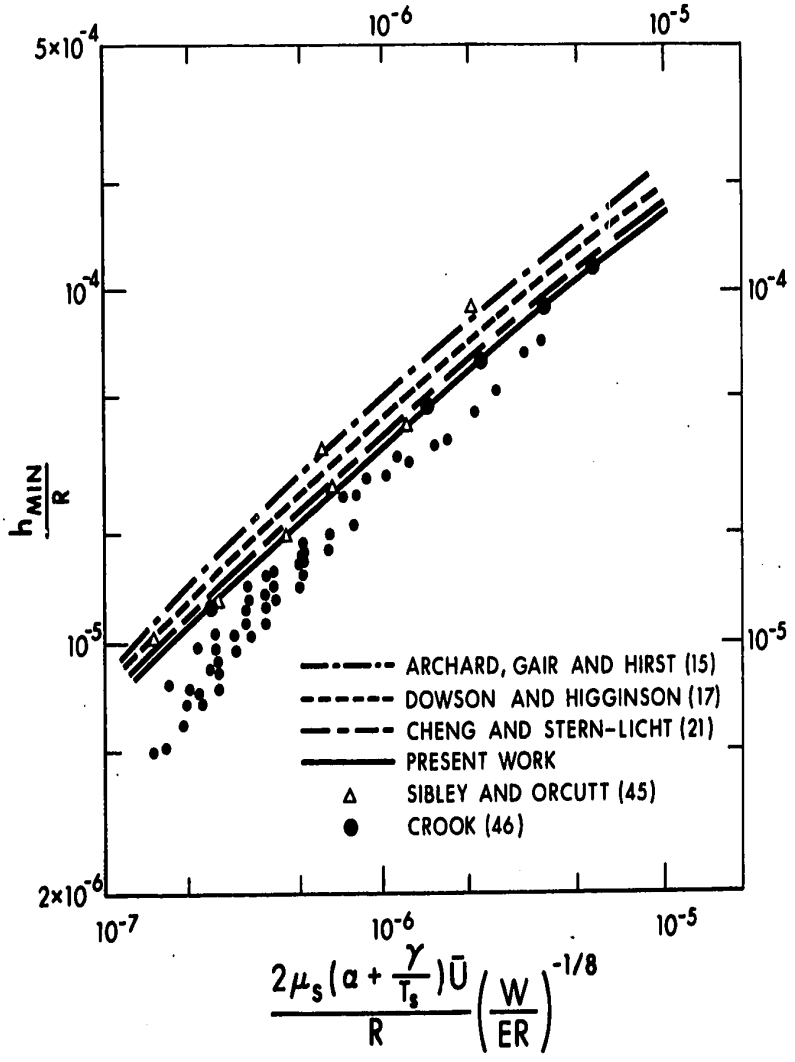

FIGURE F.4 Comparison of Theoretical and Experimental Minimum Film Thicknesses

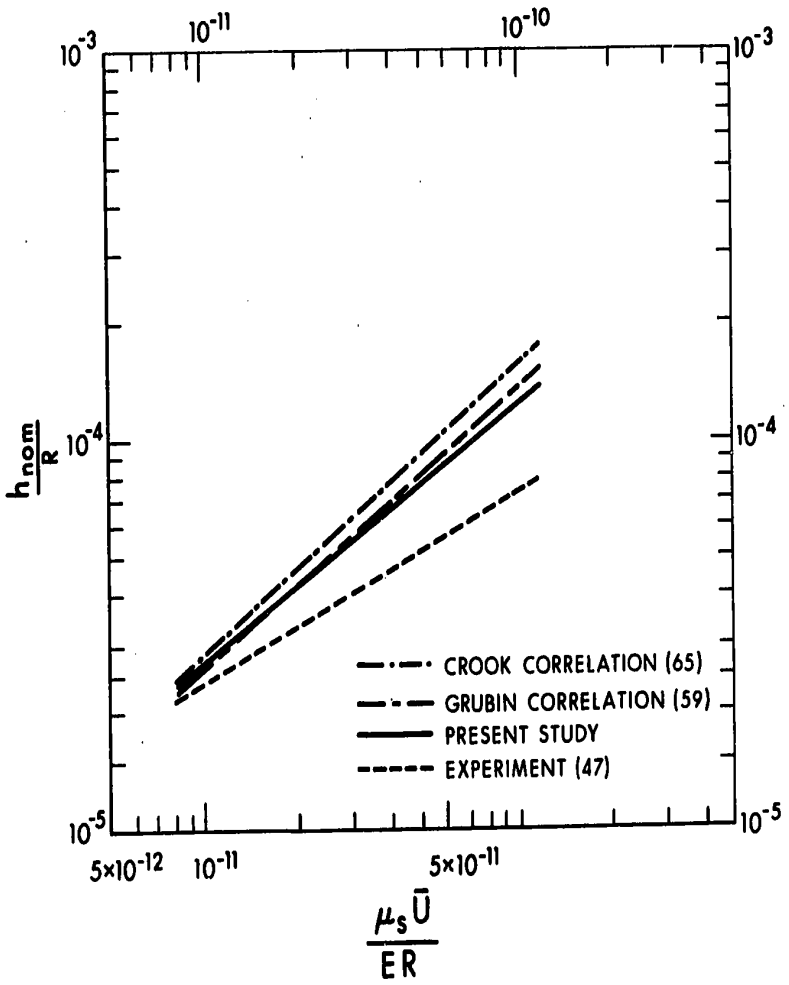

FIGURE F.5 Comparison of Theoretical and Experimental Nominal Film Thicknesses

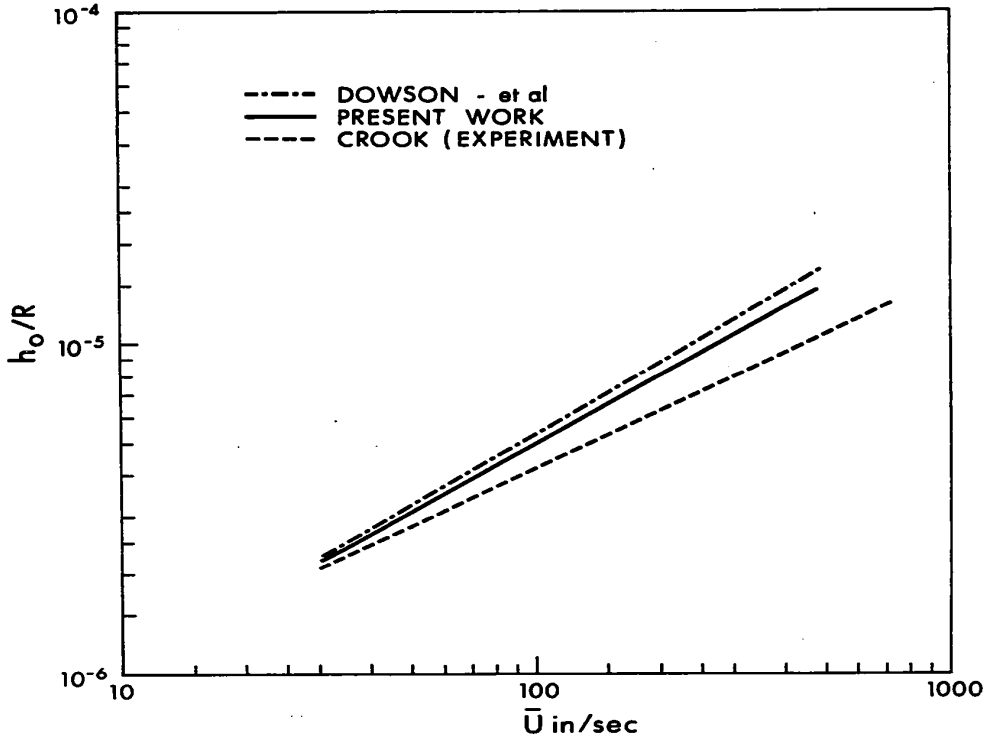

FIGURE F.6 Comparison of Theoretical and Experimental Centre-line Film Thicknesses

APPENDIX G

CURVES AND RESULTS FOR THERMAL SOLUTION

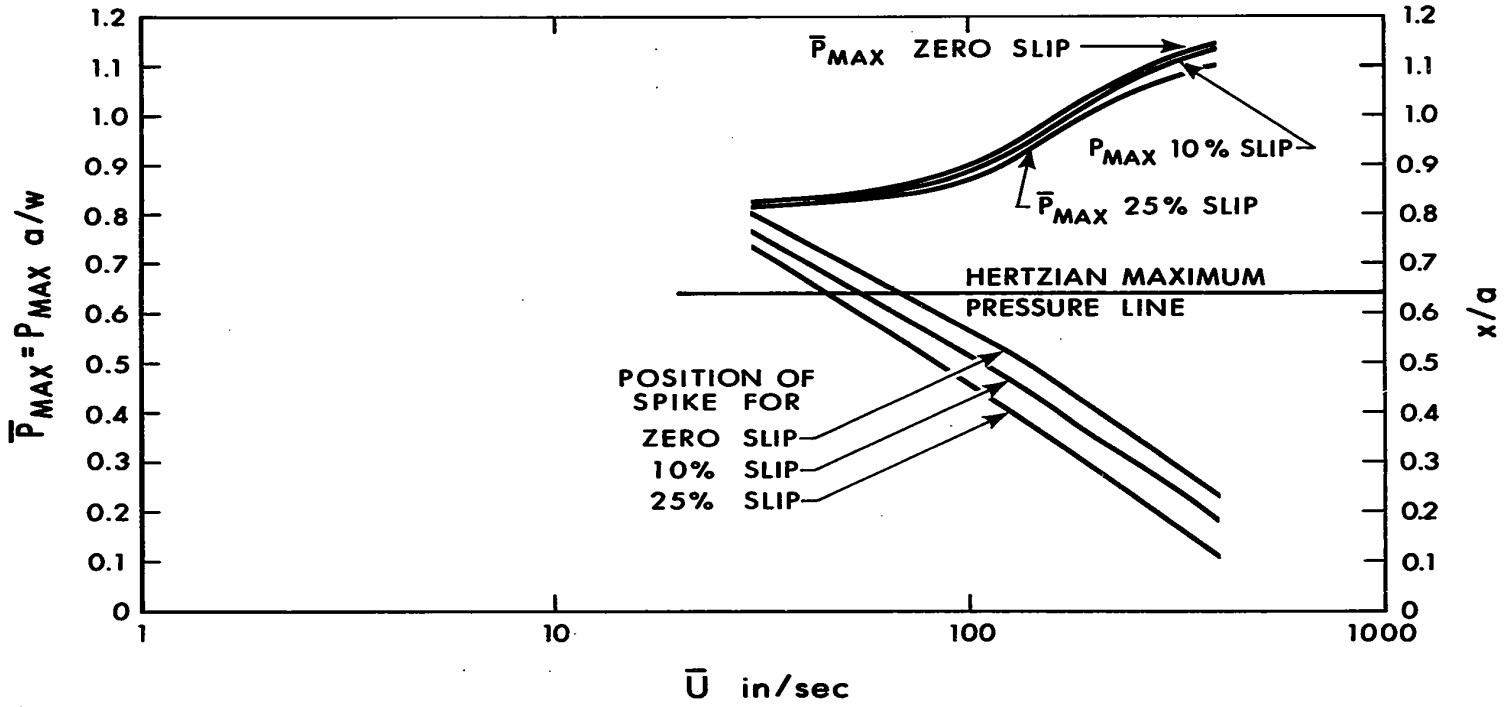

FIGURE G.1 Position and Magnitude of Pressure Spike for Various Rolling Velocities and Slip Ratios

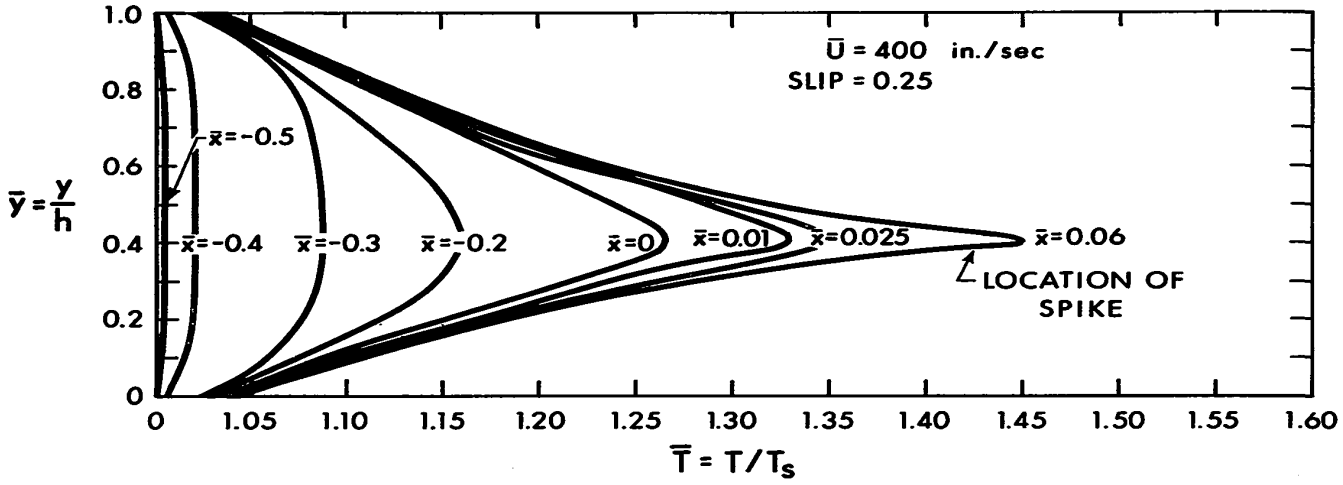

FIGURE G.2.a Temperature Distribution up to Location of Spike for $\bar{U}$ = 400 in./sec. and Slip = 0.25

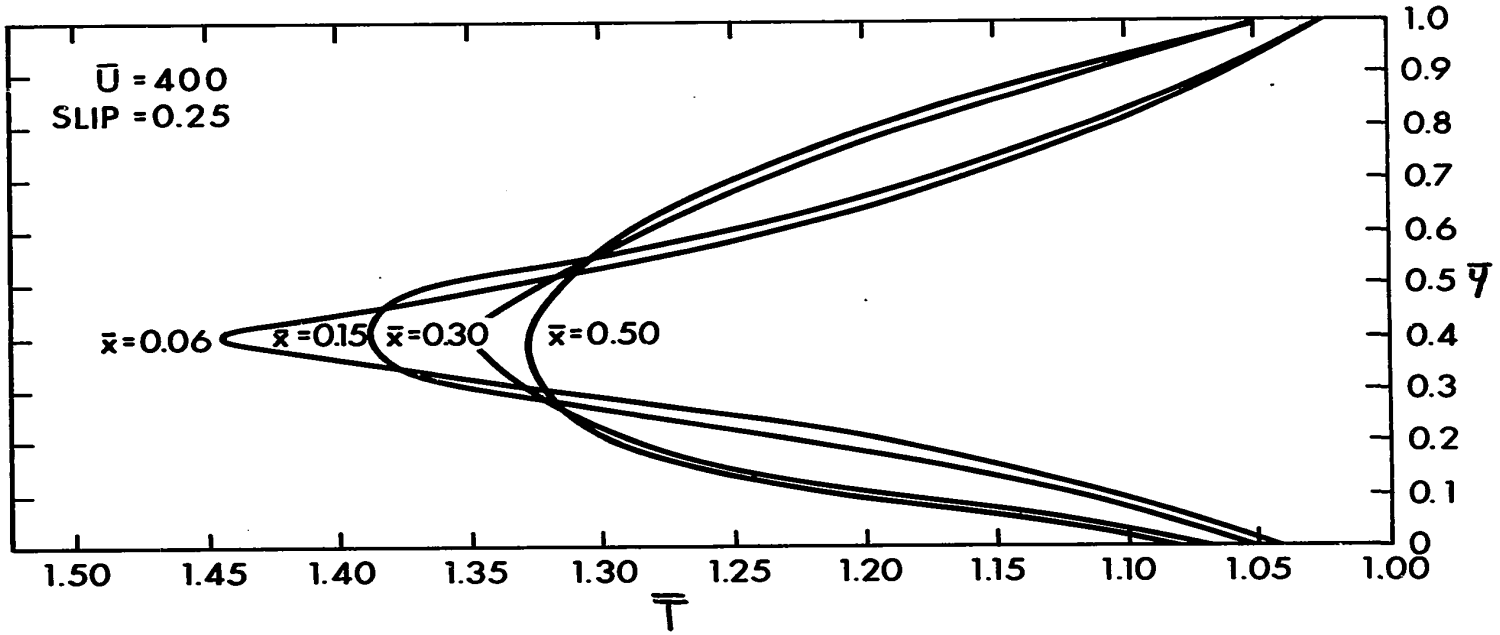

FIGURE G.2.b Temperature Distribution between the Spike Position and the Down-stream End for $\bar{U}$ = 400 in./sec. and Slip = 0.25

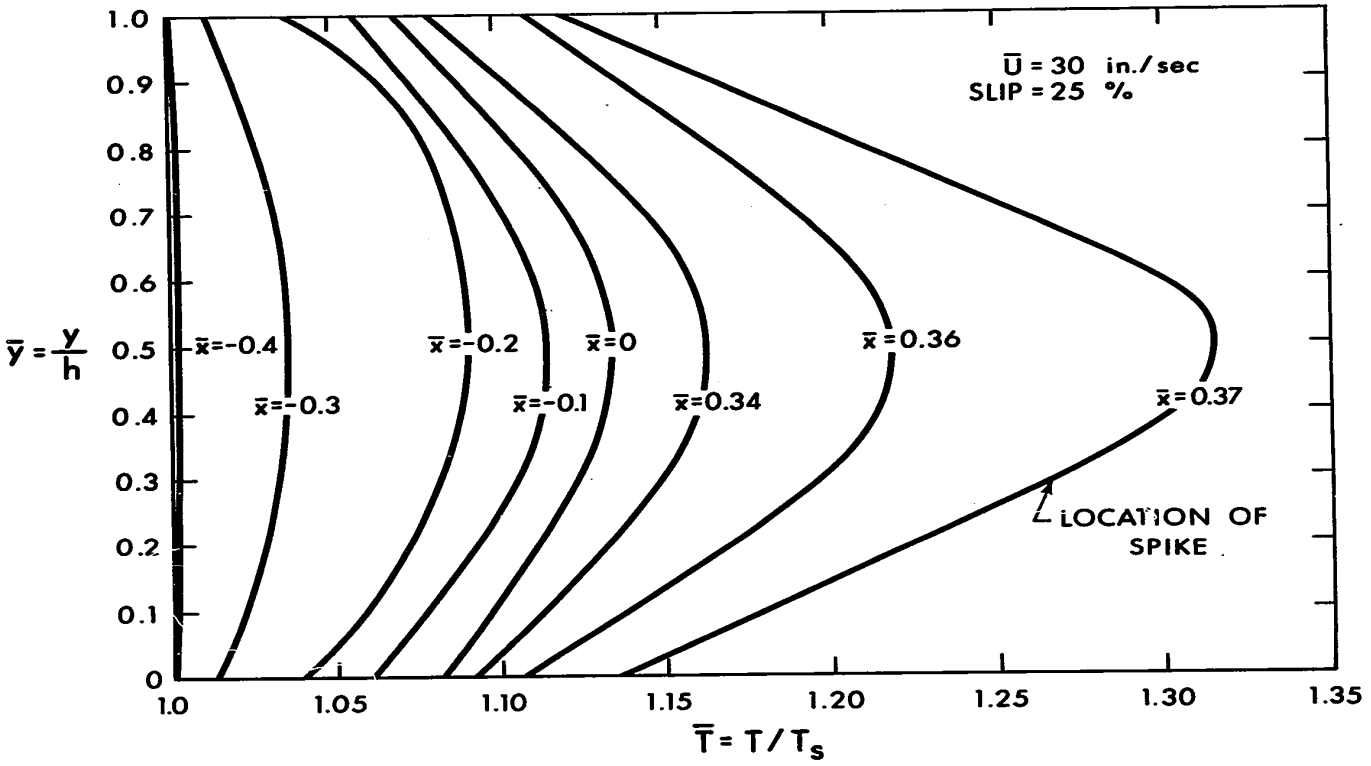

FIGURE G.3.a Temperature Distribution up to Location of Spike for $\bar{U}$ = 30 in./sec. and Slip = 0.25

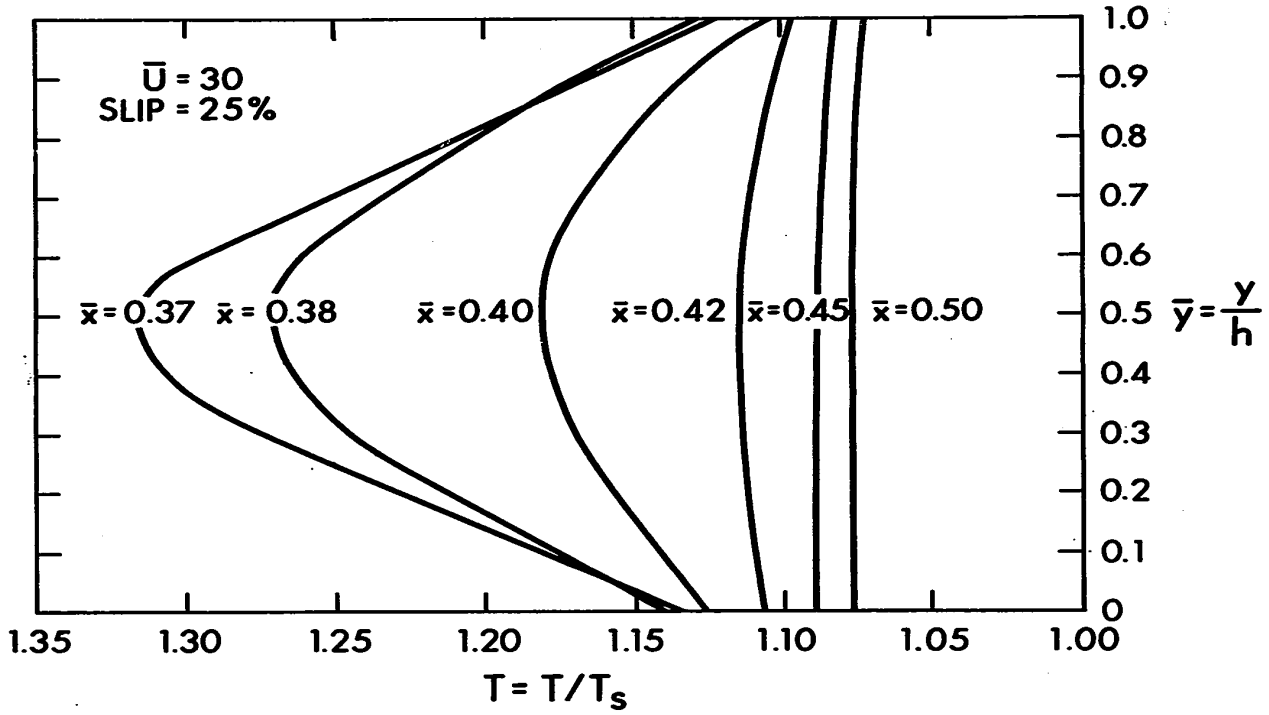

FIGURE G.3.b Temperature Distribution between the Spike Position and the Down-stream End for $\bar{U}$ = 30 in./sec. and slip = 0.25

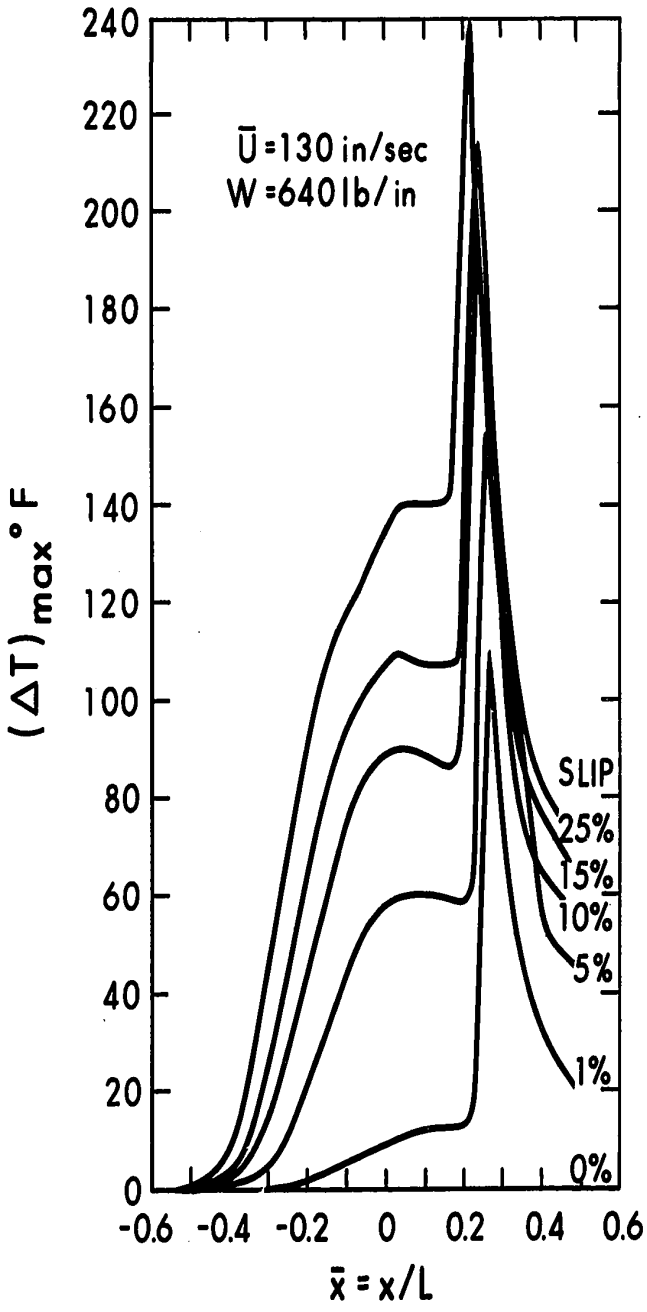

FIGURE G.4 Mid-film Temperature Rise for $\bar{U}$ = 130 in./sec. and different Slip Ratios

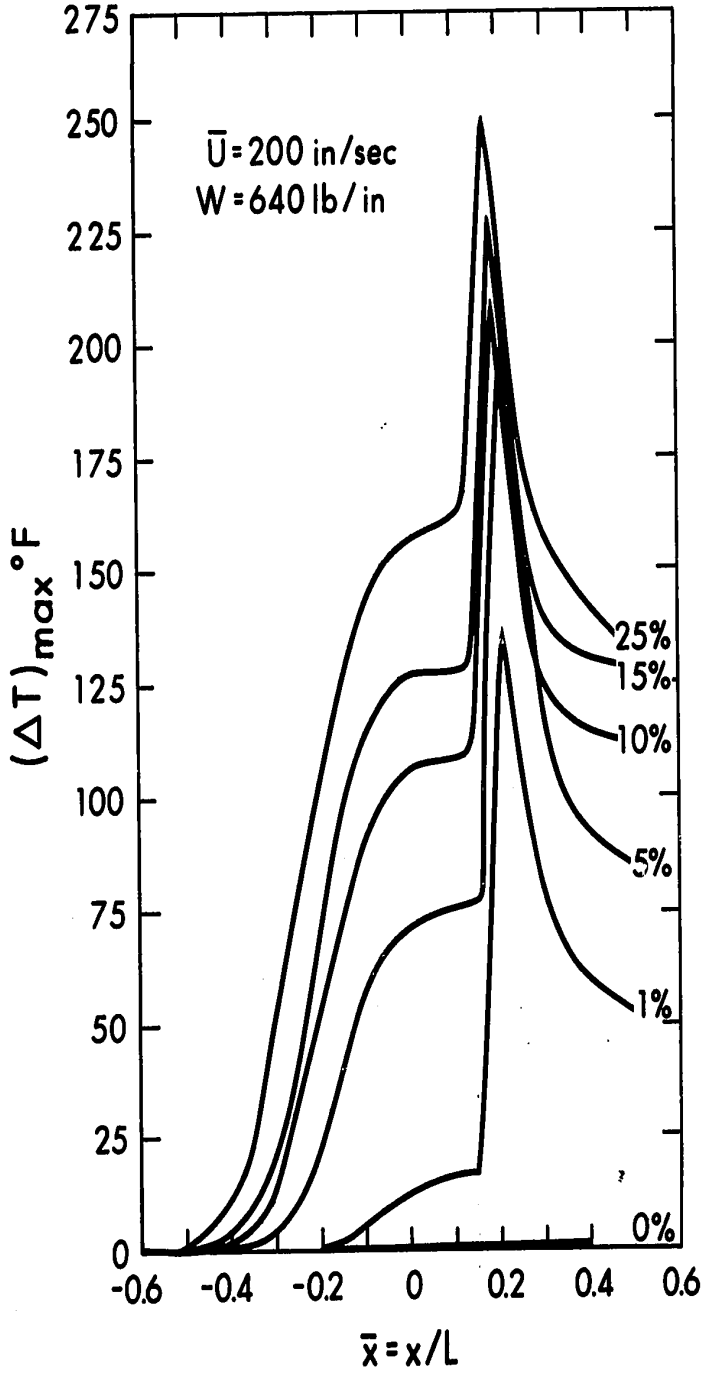

FIGURE G.5 Mid-film Temperature Rise for $\bar{U}$ = 200 in./sec. and different Slip Ratios

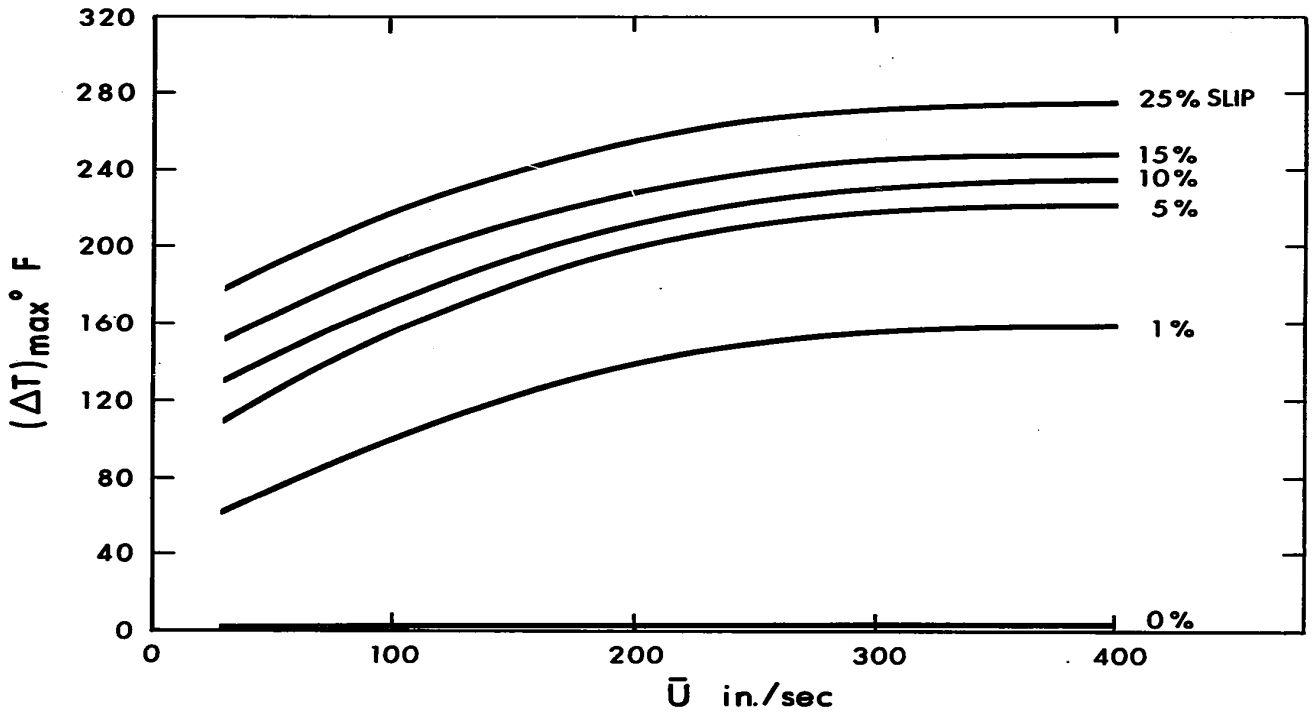

FIGURE G.6 Maximum Temperature Rise in the Lubricant

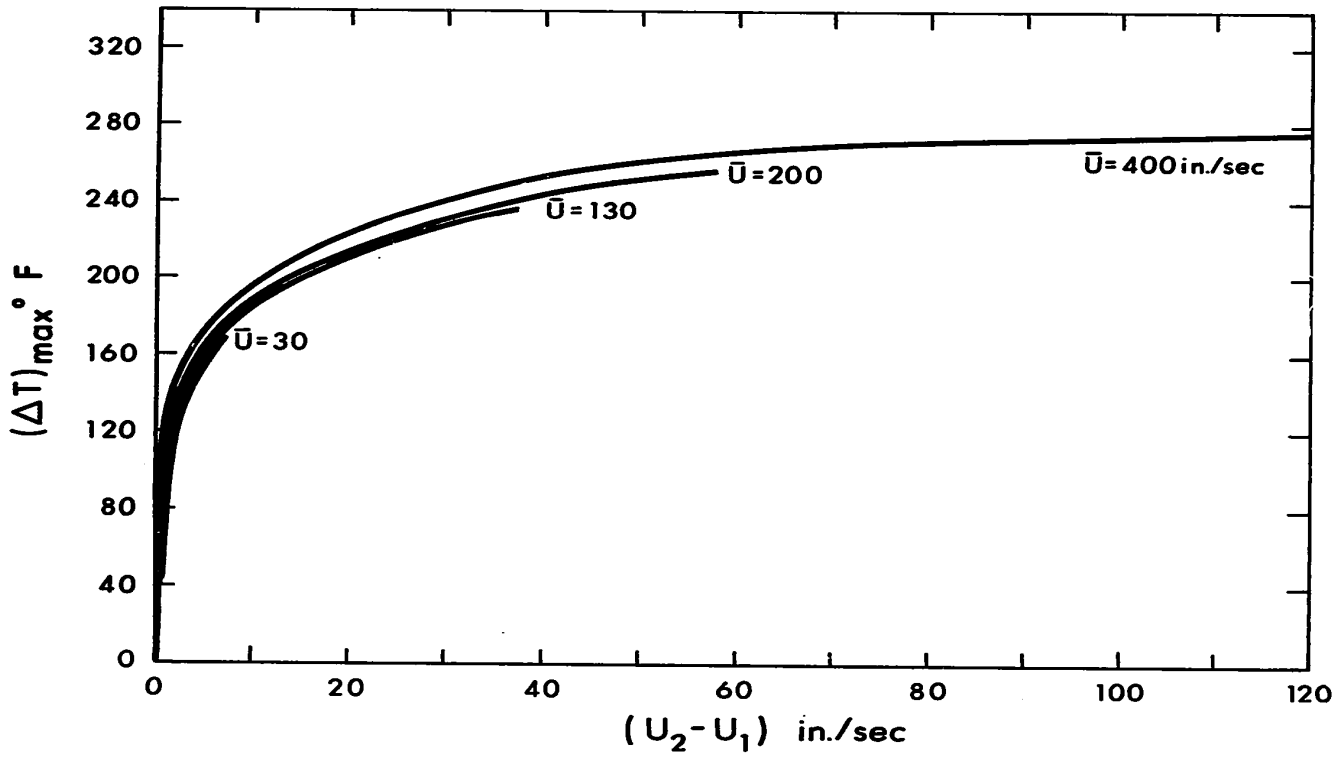

FIGURE G.7 Correlation of Maximum Temperature Rise in Lubricant with Slip Velocity at different Rolling Velocities

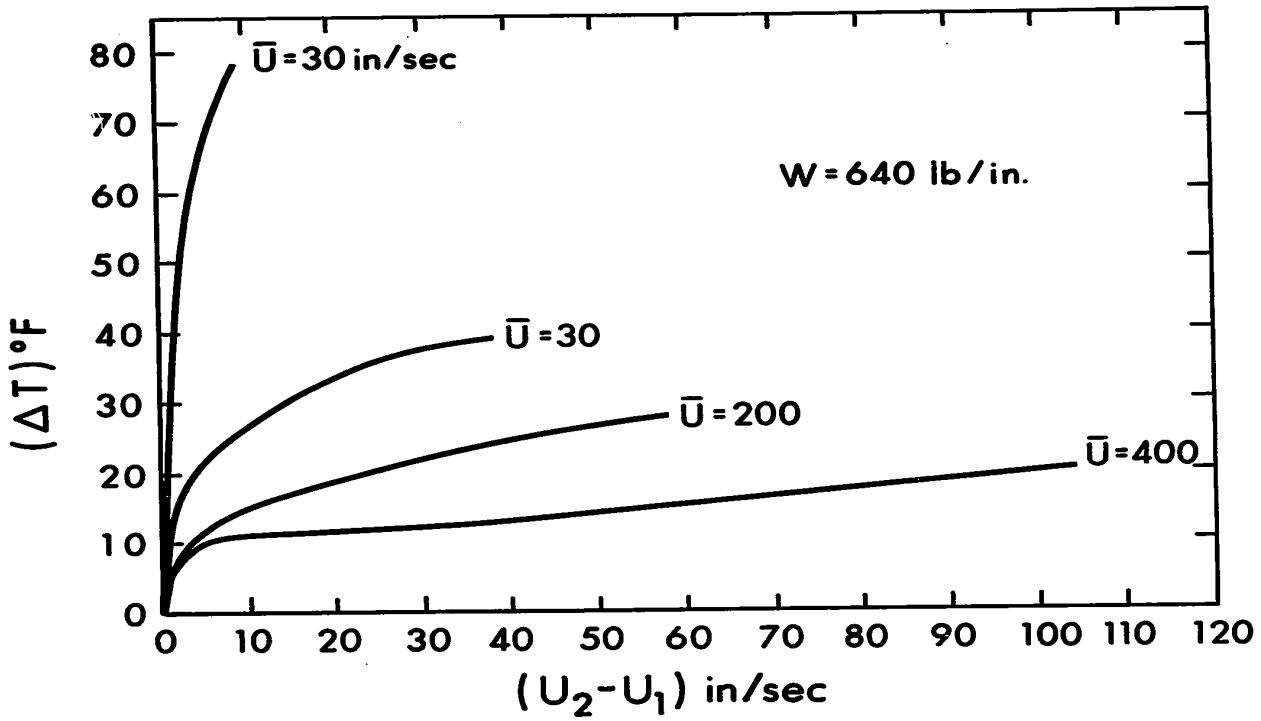

FIGURE G.8 Correlation of Temperature Rise at the Spike in the Lower Solid with Slip Velocity at different Rolling Velocity

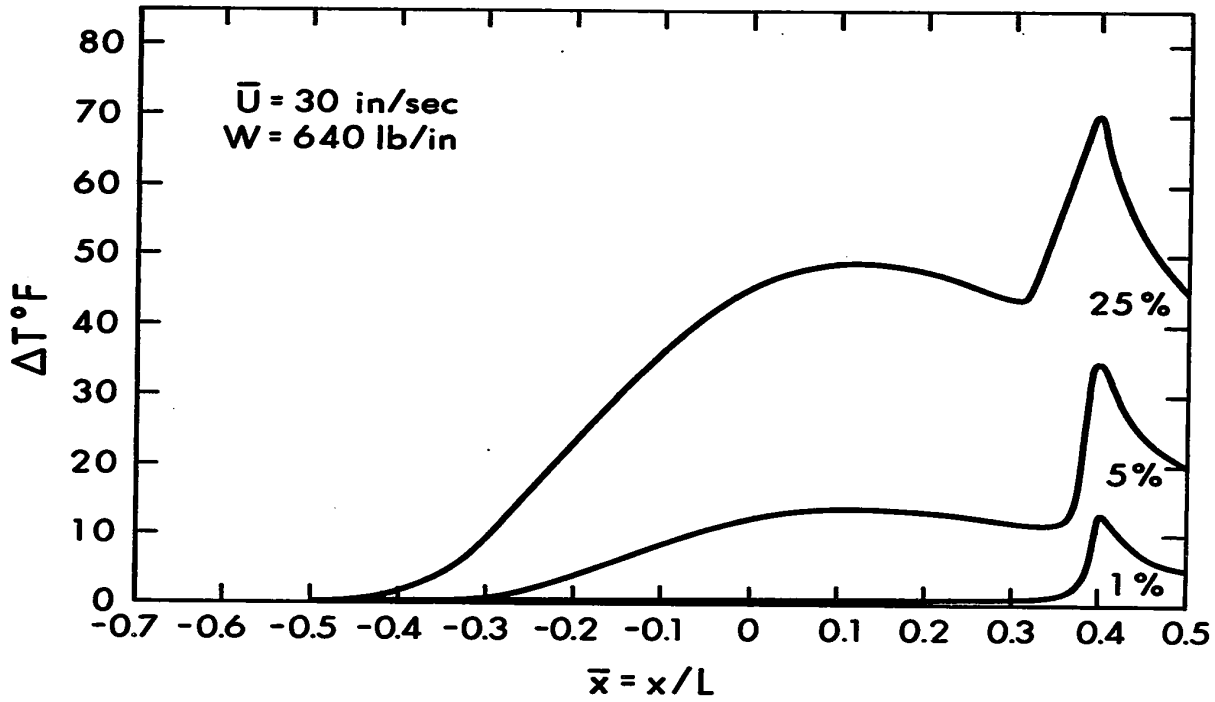

FIGURE G.9 Temperature of the Lower Solid for different Slip Ratios for $\bar{U}$ = 30 in./sec.

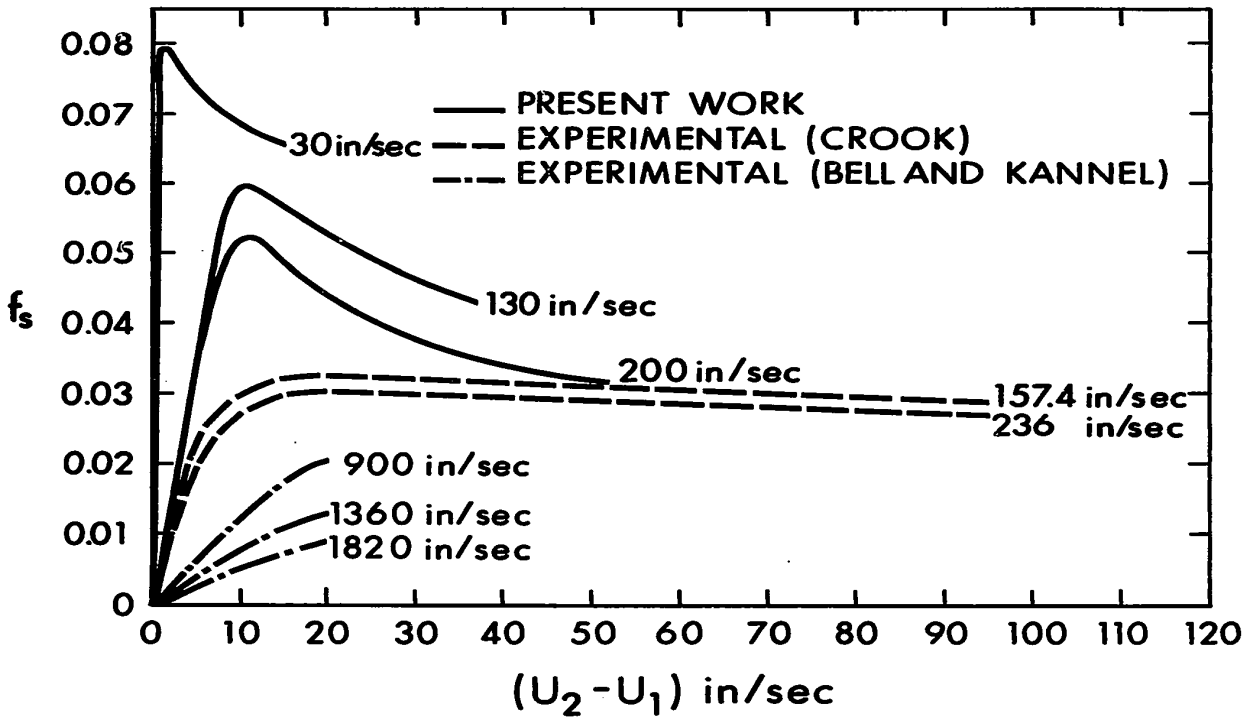

FIGURE G.10 Correlation of Friction Factor with Experimental Results

TEMPERATURE DISTRIBUTION IN LUBRICANT

$\bar{U}$ = 30 IN/SEC SLIP = 5%

$\bar{x}$ \ $\bar{y}$	0.0	0.1	0.2	0.3	0.4	0.5	0.6	0.7	0.8	0.9	1.0
- 0.5	1.000	1.000	1.000	1.000	1.000	1.000	1.000	1.000	1.000	1.000	1.000
- 0.4	1.000	1.000	1.000	1.000	1.000	1.000	1.000	1.000	1.000	1.000	1.000
- 0.3	1.001	1.001	1.002	1.002	1.002	1.002	1.002	1.002	1.002	1.001	1.001
- 0.2	1.006	1.009	1.012	1.014	1.015	1.015	1.015	1.014	1.012	1.009	1.006
- 0.1	1.011	1.016	1.020	1.023	1.025	1.025	1.025	1.023	1.020	1.016	1.011
- 0	1.022	1.028	1.033	1.036	1.039	1.039	1.039	1.036	1.033	1.028	1.022
0.1	1.025	1.029	1.033	1.035	1.037	1.037	1.037	1.035	1.032	1.029	1.024
0.2	1.023	1.025	1.027	1.029	1.030	1.030	1.029	1.029	1.027	1.025	1.023
0.3	1.020	1.021	1.022	1.023	1.024	1.024	1.024	1.023	1.022	1.021	1.019
0.35	1.019	1.020	1.022	1.023	1.023	1.023	1.023	1.023	1.022	1.021	1.019
0.4	1.063	1.096	1.129	1.160	1.185	1.195	1.184	1.159	1.128	1.095	1.062
0.5	1.034	1.036	1.037	1.037	1.037	1.037	1.037	1.037	1.037	1.036	1.034

TEMPERATURE DISTRIBUTION IN LUBRICANT

$\bar{U}$ = 130 IN/SEC — SLIP = 10%

$\bar{x}$ \ $\bar{y}$	0	0.1	0.2	0.3	0.4	0.5	0.6	0.7	0.8	0.9	1.0
- 0.5	1.000	1.000	1.000	1.000	1.000	1.000	1.000	1.000	1.000	1.000	1.000
- 0.4	1.000	1.001	1.001	1.002	1.002	1.002	1.002	1.002	1.002	1.002	1.001
- 0.3	1.005	1.012	1.017	1.021	1.023	1.024	1.023	1.021	1.018	1.013	1.005
- 0.2	1.014	1.035	1.054	1.070	1.080	1.084	1.080	1.069	1.053	1.034	1.014
- 0.1	1.023	1.052	1.080	1.106	1.125	1.131	1.124	1.104	1.078	1.050	1.022
0	1.030	1.063	1.095	1.126	1.148	1.156	1.147	1.124	1.094	1.061	1.028
0.1	1.035	1.067	1.099	1.127	1.147	1.154	1.146	1.125	1.097	1.066	1.033
0.2	1.040	1.075	1.114	1.157	1.201	1.224	1.198	1.154	1.112	1.074	1.038
0.23	1.046	1.090	1.141	1.202	1.276	1.342	1.269	1.196	1.136	1.087	1.043
0.3	1.048	1.089	1.126	1.154	1.172	1.177	1.171	1.152	1.123	1.087	1.046
0.4	1.041	1.064	1.084	1.099	1.109	1.112	1.109	1.099	1.083	1.063	1.039
0.5	1.043	1.071	1.084	1.092	1.097	1.098	1.096	1.091	1.083	1.069	1.041

TEMPERATURE DISTRIBUTION IN LUBRICANT

$\bar{U}$ = 130 IN/SEC SLIP = 15%

$\bar{x}$ \ $\bar{y}$	0.0	0.1	0.2	0.3	0.4	0.5	0.6	0.7	0.8	0.9	1.0
- 0.5	1.000	1.000	1.000	1.000	1.000	1.000	1.000	1.000	1.000	1.000	1.000
- 0.4	1.001	1.002	1.003	1.004	1.004	1.005	1.005	1.005	1.004	1.003	1.001
- 0.3	1.008	1.021	1.031	1.038	1.042	1.044	1.043	1.039	1.032	1.022	1.008
- 0.2	1.020	1.047	1.074	1.098	1.116	1.122	1.114	1.096	1.071	1.045	1.019
- 0.1	1.029	1.064	1.098	1.131	1.156	1.165	1.154	1.127	1.094	1.061	1.027
0	1.036	1.075	1.114	1.150	1.178	1.189	1.176	1.146	1.110	1.072	1.034
0.1	1.042	1.081	1.118	1.152	1.177	1.186	1.176	1.149	1.115	1.078	1.040
0.2	1.048	1.088	1.133	1.182	1.233	1.260	1.228	1.177	1.128	1.085	1.044
0.23	1.054	1.104	1.160	1.228	1.307	1.375	1.296	1.217	1.152	1.098	1.050
0.3	1.056	1.102	1.142	1.174	1.194	1.199	1.192	1.171	1.139	1.098	1.052
0.4	1.049	1.076	1.099	1.117	1.129	1.132	1.128	1.116	1.097	1.073	1.045
0.5	1.051	1.083	1.099	1.109	1.116	1.117	1.115	1.108	1.097	1.080	1.048

TEMPERATURE DISTRIBUTION IN LUBRICANT

$\bar{U}$ = 130 IN/SEC SLIP = 25%

$\bar{x}$ \ $\bar{y}$	0.0	0.1	0.2	0.3	0.4	0.5	0.6	0.7	0.8	0.9	1.0
- 0.5	1.000	1.000	1.001	1.001	1.001	1.001	1.001	1.001	1.001	1.001	1.000
- 0.4	1.003	1.007	1.010	1.012	1.013	1.014	1.014	1.013	1.011	1.008	1.003
- 0.3	1.014	1.036	1.055	1.069	1.078	1.081	1.077	1.068	1.053	1.035	1.014
- 0.2	1.027	1.063	1.099	1.135	1.162	1.170	1.155	1.126	1.091	1.057	1.024
- 0.1	1.038	1.081	1.124	1.165	1.198	1.209	1.191	1.155	1.115	1.073	1.033
0	1.046	1.092	1.138	1.183	1.219	1.233	1.214	1.176	1.132	1.086	1.041
0.1	1.055	1.104	1.152	1.198	1.234	1.247	1.229	1.191	1.145	1.097	1.049
0.15	1.058	1.106	1.154	1.200	1.237	1.252	1.234	1.195	1.147	1.099	1.051
0.18	1.062	1.115	1.174	1.240	1.312	1.356	1.297	1.225	1.162	1.106	1.054
0.30	1.067	1.114	1.154	1.182	1.199	1.203	1.196	1.177	1.147	1.107	1.059
0.40	1.058	1.087	1.111	1.129	1.140	1.144	1.139	1.127	1.107	1.081	1.051
0.50	1.065	1.106	1.120	1.128	1.134	1.136	1.133	1.126	1.116	1.100	1.058

TEMPERATURE DISTRIBUTION IN LUBRICANT

$\bar{U}$ = 200 IN/SEC SLIP = 10%

$\bar{x}$ \ $\bar{y}$	0.0	0.1	0.2	0.3	0.4	0.5	0.6	0.7	0.8	0.9	1.0
- 0.5	1.000	1.000	1.000	1.000	1.000	1.000	1.000	1.000	1.000	1.000	1.000
- 0.4	1.001	1.001	1.002	1.002	1.003	1.003	1.003	1.004	1.004	1.003	1.001
- 0.3	1.006	1.017	1.023	1.026	1.028	1.029	1.029	1.028	1.025	1.018	1.007
- 0.2	1.014	1.039	1.060	1.078	1.089	1.094	1.090	1.079	1.062	1.040	1.014
- 0.1	1.021	1.054	1.088	1.123	1.152	1.164	1.152	1.123	1.088	1.054	1.021
0	1.026	1.064	1.104	1.143	1.176	1.189	1.175	1.142	1.102	1.063	1.026
0.1	1.031	1.071	1.111	1.149	1.178	1.190	1.177	1.147	1.110	1.070	1.030
0.15	1.033	1.074	1.118	1.168	1.226	1.265	1.224	1.167	1.117	1.073	1.032
0.19	1.035	1.081	1.133	1.198	1.279	1.354	1.275	1.194	1.130	1.079	1.034
0.30	1.049	1.113	1.158	1.189	1.206	1.211	1.204	1.185	1.154	1.109	1.046
0.40	1.054	1.122	1.163	1.187	1.199	1.202	1.197	1.183	1.158	1.118	1.052
0.50	1.083	1.195	1.191	1.196	1.200	1.201	1.199	1.194	1.188	1.192	1.080

TEMPERATURE DISTRIBUTION IN LUBRICANT

$\bar{U}$ = 200 IN/SEC SLIP = 15%

$\bar{x}$ \ $\bar{y}$	0.0	0.1	0.2	0.3	0.4	0.5	0.6	0.7	0.8	0.9	1.0
- 0.5	1.000	1.000	1.000	1.000	1.000	1.000	1.000	1.000	1.000	1.000	1.000
- 0.4	1.001	1.004	1.005	1.006	1.007	1.007	1.008	1.008	1.007	1.006	1.002
- 0.3	1.010	1.027	1.038	1.046	1.051	1.052	1.052	1.048	1.041	1.029	1.010
- 0.2	1.018	1.048	1.078	1.105	1.125	1.133	1.125	1.105	1.078	1.048	1.018
- 0.1	1.025	1.063	1.104	1.147	1.186	1.203	1.183	1.144	1.101	1.061	1.024
0	1.031	1.075	1.121	1.168	1.208	1.225	1.205	1.163	1.117	1.072	1.029
0.1	1.036	1.083	1.129	1.174	1.210	1.224	1.207	1.170	1.126	1.080	1.034
0.15	1.038	1.086	1.137	1.193	1.258	1.303	1.252	1.188	1.132	1.083	1.036
0.19	1.041	1.093	1.152	1.223	1.310	1.387	1.302	1.214	1.145	1.089	1.039
0.30	1.057	1.131	1.182	1.215	1.233	1.237	1.229	1.209	1.174	1.123	1.052
0.40	1.064	1.143	1.189	1.215	1.227	1.230	1.225	1.210	1.182	1.136	1.060
0.50	1.094	1.211	1.219	1.225	1.229	1.230	1.227	1.221	1.215	1.214	1.090

TEMPERATURE DISTRIBUTION IN LUBRICANT

$\bar{U}$ = 200 IN/SEC SLIP = 25%

$\bar{x}$ \ $\bar{y}$	0.0	0.1	0.2	0.3	0.4	0.5	0.6	0.7	0.8	0.9	1.0
- 0.5	1.000	1.001	1.001	1.001	1.001	1.001	1.001	1.001	1.001	1.001	1.000
- 0.4	1.004	1.011	1.015	1.017	1.019	1.019	1.020	1.020	1.018	1.014	1.005
- 0.3	1.015	1.042	1.065	1.082	1.092	1.095	1.091	1.081	1.064	1.042	1.015
- 0.2	1.024	1.062	1.102	1.142	1.175	1.186	1.167	1.132	1.094	1.057	1.022
- 0.1	1.032	1.078	1.128	1.183	1.233	1.251	1.217	1.165	1.114	1.069	1.027
0	1.039	1.093	1.149	1.207	1.258	1.274	1.241	1.187	1.132	1.081	1.033
0.1	1.046	1.102	1.159	1.216	1.255	1.283	1.253	1.201	1.146	1.091	1.039
0.2	1.056	1.125	1.197	1.268	1.328	1.350	1.316	1.250	1.178	1.110	1.047
0.25	1.057	1.123	1.185	1.238	1.273	1.282	1.265	1.227	1.174	1.113	1.049
0.30	1.061	1.131	1.190	1.231	1.254	1.259	1.248	1.220	1.177	1.119	1.053
0.40	1.056	1.110	1.158	1.196	1.220	1.227	1.217	1.191	1.152	1.103	1.049
0.50	1.057	1.109	1.152	1.185	1.206	1.212	1.204	1.181	1.147	1.102	1.050

TEMPERATURE DISTRIBUTION IN LUBRICANT

$\bar{U}$ = 400 IN/SEC SLIP = 5%

$\bar{x}$ \ $\bar{y}$	0.0	0.1	0.2	0.3	0.4	0.5	0.6	0.7	0.8	0.9	1.0
- 0.5	1.000	1.000	1.000	1.000	1.000	1.000	1.000	1.000	1.000	1.000	1.000
- 0.4	1.000	1.000	1.000	1.001	1.001	1.001	1.001	1.001	1.001	1.001	1.000
- 0.3	1.002	1.007	1.008	1.008	1.008	1.009	1.009	1.009	1.009	1.008	1.003
- 0.2	1.007	1.022	1.026	1.027	1.028	1.029	1.029	1.029	1.029	1.024	1.008
- 0.1	1.015	1.045	1.062	1.069	1.073	1.075	1.076	1.075	1.068	1.050	1.017
0.0	1.019	1.055	1.083	1.102	1.114	1.120	1.120	1.113	1.093	1.061	1.021
0.08	1.021	1.059	1.097	1.138	1.188	1.268	1.254	1.171	1.114	1.067	1.024
0.10	1.021	1.059	1.097	1.140	1.202	1.358	1.296	1.179	1.116	1.068	1.024
0.20	1.045	1.128	1.151	1.196	1.262	1.316	1.295	1.239	1.173	1.151	1.052
0.30	1.041	1.115	1.164	1.208	1.260	1.299	1.286	1.242	1.190	1.133	1.047
0.40	1.043	1.115	1.169	1.213	1.259	1.292	1.282	1.244	1.194	1.131	1.048
0.50	1.046	1.124	1.177	1.218	1.260	1.289	1.281	1.246	1.200	1.140	1.051

TEMPERATURE DISTRIBUTION IN LUBRICANT

$\bar{U}$ = 400 IN/SEC SLIP = 10%

$\bar{x}$ \ $\bar{y}$	0.0	0.1	0.2	0.3	0.4	0.5	0.6	0.7	0.8	0.9	1.0
- 0.5	1.000	1.003	1.004	1.004	1.004	1.004	1.004	1.004	1.004	1.003	1.000
- 0.4	1.001	1.002	1.003	1.003	1.003	1.003	1.004	1.004	1.004	1.004	1.001
- 0.3	1.007	1.021	1.025	1.027	1.027	1.028	1.028	1.029	1.028	1.024	1.007
- 0.2	1.014	1.041	1.055	1.060	1.062	1.064	1.064	1.063	1.061	1.041	1.014
- 0.1	1.020	1.059	1.091	1.113	1.127	1.135	1.136	1.127	1.104	1.067	1.023
0.0	1.022	1.063	1.103	1.139	1.171	1.193	1.193	1.164	1.121	1.073	1.025
0.5	1.023	1.065	1.108	1.155	1.211	1.285	1.273	1.194	1.131	1.077	1.027
0.06	1.023	1.065	1.109	1.157	1.219	1.336	1.303	1.198	1.131	1.077	1.027
0.07	1.023	1.065	1.109	1.158	1.226	1.387	1.321	1.202	1.132	1.077	1.027
0.08	1.023	1.065	1.109	1.159	1.230	1.410	1.325	1.204	1.133	1.077	1.027
0.15	1.025	1.068	1.117	1.181	1.276	1.370	1.321	1.225	1.144	1.082	1.029
0.30	1.040	1.109	1.172	1.232	1.288	1.320	1.307	1.260	1.197	1.127	1.045
0.50	1.045	1.119	1.183	1.237	1.282	1.307	1.297	1.260	1.204	1.134	1.050

TEMPERATURE DISTRIBUTION IN LUBRICANT

$\bar{U}$ = 400 IN/SEC SLIP = 15%

$\bar{x}$ \ $\bar{y}$	0.0	0.1	0.2	0.3	0.4	0.5	0.6	0.7	0.8	0.9	1.0
- 0.5	1.000	1.001	1.001	1.001	1.001	1.001	1.001	1.001	1.001	1.001	1.000
- 0.4	1.002	1.006	1.007	1.007	1.007	1.008	1.008	1.008	1.008	1.008	1.003
- 0.3	1.012	1.035	1.044	1.047	1.048	1.049	1.049	1.049	1.047	1.038	1.013
- 0.2	1.018	1.053	1.076	1.087	1.092	1.095	1.095	1.093	1.082	1.058	1.020
- 0.1	1.023	1.066	1.107	1.143	1.169	1.181	1.176	1.153	1.117	1.072	1.025
0.0	1.025	1.070	1.117	1.167	1.216	1.247	1.230	1.181	1.128	1.076	1.027
0.05	1.026	1.072	1.122	1.179	1.252	1.340	1.279	1.198	1.133	1.079	1.028
0.06	1.026	1.072	1.123	1.182	1.259	1.388	1.289	1.201	1.135	1.079	1.028
0.07	1.026	1.073	1.124	1.183	1.266	1.430	1.294	1.203	1.135	1.079	1.028
0.15	1.028	1.077	1.133	1.207	1.308	1.393	1.318	1.221	1.144	1.083	1.030
0.30	1.046	1.124	1.195	1.259	1.315	1.342	1.318	1.265	1.199	1.127	1.046
0.50	1.051	1.135	1.205	1.264	1.309	1.329	1.311	1.267	1.208	1.136	1.050

APPENDIX H

FORTRAN PROGRAM

RESULTS OF THE ISOTHERMAL SOLUTION WERE STORED

IN LINE FILES AND USED FOR THERMAL SOLUTION

```
C
C       THERMAL SOLUTION OF ELASTO-HYDRODYNAMIC PROBLEM B
     * Y MATRIX METHODS
C
      IMPLICIT REAL*8(A-H,O-Z)
      DIMENSION DUY(11,101),DSX(11,101),DSY(11,101),S(11
     *,101),T(11,101),V(11,101),Z1(11,11),GXB(101),FXB(1
     *01),H(101),HD(101),PD(101),PT(101),Z2(1,11),A(101)
     *,P(101),D(101),U(11,101),TLC1(200),TLC2(200),DMUE(
     * 200)
      COMMON R,AL,HO,VS,PS,PMAX,UD
C
C     INITIAL VALUES ARE ASSIGNED
C
      READ(5,101)U2,U1,DS,VS
 101  FORMAT(4F10.6)
C
C     ASSIGN INITIAL VALUES OF PRESSURE
C
C
C
C     NONDIMENSIONALISE
C
      UD=U1+U2
      CALL HERTZ(HD,PD)
      CALL THERMA(HD,PD,TLC1,TLC2     )
       STOP
      END
```

```
      SUBROUTINE HERTZ(HD,PD)
      IMPLICIT REAL*8(A-H,O-Z)
      DIMENSION HD(101),HND(101),PD(101),PND(101),DPXND(
     *(101),D(101),V(101),XCOF(4),ROOTR(3),ROOTI(3),HTT(
     *101),COF(4),DELPD(11,1),PDR(101),PSPI(191),HSPI(19
     *1),PDIP(191),HTT1(101),HSPI1(191),HT(101)
      COMMON R,A,HO,VS,PS,PMAX,U
      EXTERNAL FUN
      HO=0.1620E-04
      READ(5,10)PL,S1,S2,E1,E2,R1,R2
      T=(1.-(S1*S1))/E1+(1.-(S2*S2))/E2
      PI=3.1416D00
      EC=T/PI
      R=R1*R2/(R1+R2)
      A=2.*DSQRT(R*PL*EC)
      PMAX=2.*PL/(PI*A)
C
C       CALCULATE HERTZIAN PRESSURE AND DISPLACEMENT
      PS=2.5D00
      WRITE(6,20)PL,S1,S2,E1,E2,R1,R2,R,A,HO
 20   FORMAT(10F13.6)
      WRITE(6,25)
 25   FORMAT(T10,'HERTZIAN PRESSURE AND DISPLACEMENT'//T
     * 15,'NODE',T40,'P
     ARESSURE IN TONS/SQ.IN.',T75,'DISPLACEMENT IN INCHE
     * S')
      X=-5.
      DO 30 I=1,41
      Z1=(A*A)/(2.*R)
      Z2=DSQRT(DABS(X*X-1.))
      HD(I)=Z1*(DABS(X*Z2)-DLOG(DABS(DABS(X)+Z2)))+HO
      PD(I)=0.
 30   X=X+0.1
      X=-1.
      DO 35 I=41,61
      PD(I)=PMAX*DSQRT(DABS(1.-X*X))
      HD(I)=HO
 35   X=X+0.1
      J=41
      DO 40 I=61,101
      HD(I)=HD(J)
      PD(I)=0.
 40    J=J-1
      DO 50 I=1,101
      WRITE(6,45)I,PD(I),HD(I)
 45   FORMAT(T15,I2,T45,F15.8,T75,F15.8)
 50   CONTINUE
C
      CALL ECAL(R,EC,HO,A,PD,HT,101,101,99,HD,1)
C     CALCULATE OPTIMUM FILM THICKNESS
C     A RUNGE-KUTTA ALGORITHM IS USED
      ITER=1
```

```
 55   CALL RRK2(FUN,0.1,-5.0,0.0,1,40,PND)
      DO 60 I=1,41
      PD(I)=PND(I)*PS
 60   CONTINUE
C
C     CHECK WHETHER ASSUMED VALUES OF MIN. THICKNESS IS
     * O.K.
C
      A1=2.*PD(40)-PD(38)
      EPS=0.1
      A2=PD(42)-A1
      IF(A2.GT.EPS)GO TO 70
      IF(DABS(A2).GT.EPS)GO TO 80
      GO TO 90
 70    HO=HO-1.0E-07
      ITER=ITER+1
      IF(ITER-100)55,55,64
 64    WRITE(6,100)HO,ITER
      STOP
 80    HO=HO+1.0E-08
      ITER=ITER+1
      IF(ITER-100)55,55,61
 61   WRITE(6,100)HO,ITER
      STOP
 90    WRITE(6,100)HO,ITER
      DO 110 I=1,101
      PD(41)=(PD(42)+PD(40))/2.
      WRITE(6,120)PD(I)
 120  FORMAT(T10,E15.6)
 110  CONTINUE
      ITER=1
      DO 190 J=1,101
 190  HT(I)=HD(I)
      CALL ECAL(R,EC,HO,A,PD,HTT1,101,101,99,HD,1)
      CALL CLSHIF(HTT1,A,R,HO)
      CALL ECAL(R,EC,HO,A,PD,HTT,101,101,99,HD,1)
      CALL CLSHIF(HTT,A,R,HO)
      DO 196 I=1,101
      WRITE(6,197)HTT1(I),HTT(I),I
 197  FORMAT(T10,2E15.8 ,T60,I3)
 196  CONTINUE
C
C     COMPARE DEFLECTIONS DUE TO MOMENTUM EQNS.AND ELAST
     * IC EQNS
C
C     SOLVE 'INVERSE 'EQUATIONS
 111  ACONS=PS*HO*HO*2000./(12.*A*0.4*1.4503*1.0E-05 )
      BCONS=U/2.
      CCONS=U/2.
      DCONS=1.+(0.009*PD(51)/(1.+.0260*PD(51) ) )
      DO 130 I=41,61
 130    PND(I)=PD(I)/PS
```

```
      DO 140 I=41,60
  140   DPXND(I)=(PND(I+1)-PND(I-1))/0.2
      DPXND(61)=0.
      J=1
      M=3
      MM=41
      NN=61
      DO 150 I=MM,NN
      D(I)=1.+(0.009*PD(I)/(1.+0.0260*PD(I)) )
      V(I)=DEXP(PND(I))
      XCOF(J)=DCONS*CCONS
      XCOF(J+1)=-D(I)*CCONS
      XCOF(J+2)=0.
      XCOF(J+3)=ACONS*DPXND(I)*D(I)/V(I)
      CALL DPOLRT(XCOF,COF,3,ROOTR,ROOTI,IER)
      WRITE(6,160)ROOTR(1),ROOTI(1),ROOTR(2),ROOTI(2),RO
     * OTR(3),ROOTI(3),
     AIER
  160   FORMAT(6E15.8,T100,I3)
      HT(I)=ROOTR(1)*HO
      WRITE(6,250)HT(I)
  250 FORMAT(T10,E15.8)
  150 CONTINUE
      HT(61)=HO
      CALL HELMAT(HT,EC,P,A)
      CALL ECAL1(HTT,HT,PD,EC,A)
C
C
      IFLAG=1
      IFLAG=5
      IF(IFLAG.EQ.1)GO TO 900
C     WE WRITE VALUES SO FAR CALCULATED AS DATA IN FILE
     * BRIGU -3
      WRITE(3,10)PL,S1,S2,E1,E2,R1,R2
      WRITE(3,11)EC,R,A,PMAX,PS
  11  FORMAT(T5,5E15.8)
      WRITE(3,100)HO ,ITER
      DO 191 I=1,101
      WRITE(3,192)PD(I),HD(I),HTT(I)
  192 FORMAT(T10,3E15.8)
  191 CONTINUE
      DO 194 I=41,61
      WRITE(3,193)HT(I)
  193 FORMAT(T10,E15.8)
  194 CONTINUE
      GO TO 901
C     WE READ BACK  DATA FROM FILE 3
  900 READ(3,10)PL,S1,S2,E1,E2,R1,R2
  10  FORMAT(F10.5,2F5.3,2F10.2,2F5.3)
      READ(3,11)EC,R,A,PMAX,PS
       READ(3,100)HO,ITER
  100 FORMAT(E15.6,T40,I3)
```

```
      DO 296 I=1,101
      READ(3,192)PD(I),HD(I),HTT(I)
  296 CONTINUE
      DO 297 I=41,61
      READ(3,193)HT(I)
  297 CONTINUE
  901 DO 151 I=1,191
  151 PDIP(I)=0.
      D(51)=1.0D00+(0.009*PD(51))/(1.+0.026*PD(51))
      DO 101 I=1,51
  101  PSPI(I)=PD(I)
      J=151
      DO 102 I=61,101
      PSPI(J)=PD(I)
  102 J=J+1
      IJ=1
      IKN=72
      JJJ=1
      SPIX=0.760001D00
      SPIX=0.800001D00
      LL=25
      LL=35
      LL=21
  262 DO 400 IQ=1,JJJ
      SPIX=SPIX-0.01
      LL=LL+1
      IKN=IKN+1
      L=SPIX/0.01
      LP51=L+51
      LP52=L+52
C     THE SPICAL ROUTINE FIXES SPIKE POSITION
  251 DO 253 I=LP52,151
  253  PSPI(I)=0.
      JUK=3
      DO 399 NI=1,JUK
  255 CALL SPICAL(R,EC,A,HT,HTT,PD,D ,PMAX,HO,HSPI,PSPI,
     *IJ,PDIP,SPIX,NI,HSPI1,IKN)
      CALL DIPCAL(HO,VS,PS,HSPI1,PSPI,U,A,D,LL,PDIP)
      CALL CHEDIP(PDIP,IJ)
C     THE DIPCAL ROUTINE FIXES PRESSURE IN DIP
  399 CONTINUE
  400 CONTINUE
  170 RETURN
      END
```

```
      SUBROUTINE SPICAL(R,EC,A,HT,HTT,PD,D,PMAX ,HO,HSPI
     *,PSPI,IJ,PDIP,SPIX,NI,HSPI1,IKN)
      IMPLICIT REAL*8(A-H,O-Z)
       DIMENSION HTT(101),HT(101),PD(101),D(101),PSPI(19
     *1),DD(191),HSPI(191),HSPI1(191),PDIP(191),A1(191),
     *PDP(191)
C     DIVIDE REGION C AND D INTO 100 EQUAL PARTS
      L=SPIX    /0.01
      LP53=L+53
      LP51=L+51
      LP52=L+52
      X=0.
      IF(NI.GT.1)GO TO 80
      DO 20 I=51,LP51
      Q1=DABS(1.-X**2)
      PSPI(I)=PMAX*DSQRT(Q1)
 20   X=X+0.01D00
      READ(5,27)(PSPI(I),I=113,LP53)
 27   FORMAT(20F5.2)
 80   DO 21 I=1,191
 21   PDP(I)=PSPI(I)
C     WE NOW HAVE ASSUMED PRESSURE IN REGION D AS ZERO
C
C     CALCULATE THE ELASTIC DISPLACEMENT
      CALL ESPCAL(R,EC,A,PSPI,HSPI1,HO)
C
C     DO CENTRE LINE SHIFT
C
      DO 75 K=52,151
      DD(K)=1.0D00+(0.009*PSPI(K))/(1.+0.026*PSPI(K))
      A1(K)=D(51)*HO/DD(K)
 75   CONTINUE
      C=(HSPI1(52)-HSPI1(102))*R/(A*0.50)
      CONST=HO-HSPI1(52)+C*0.01*A/R
      DO 22 I=52,151
      SHINC=C*(I-51)*A*0.01/R
 22   HSPI1(I)=HSPI1(I)+CONST+SHINC
C     IN ORDER TO MAKE THE FILM SENSIBLY PARALLEL FILM P
C     RESSURES IN REGION C ARE INCREASED
C
      DO 300 K=52,151
      WRITE(6,301)K,PSPI(K),HSPI1(K),A1(K)
 301  FORMAT(T10,I3,T45,3E15.8)
 300  CONTINUE
      RETURN
      END
```

```
      SUBROUTINE ESPCAL(R,EC,A,PSPI,HSPI,HO)
      IMPLICIT REAL*8(A-H,O-Z)
      DIMENSION E(191),U(191),AK(191),PD1(191) ,PDD (191
     *),PSPI(191),HSPI(191),SUM2(191),SUM3(191)
      DO 10 J=1,51
10    E(J)=(J-1)*0.1-5.
      DO 15 J=52,151
15    E(J)=(J-51)*0.01
      DO 20 J=152,191
20    E(J)=(J-151)*0.1+1.
      X=-5.
      DO 40 K=1,191
      SUM=0.
      DO 30J=1,189,2
      U(J)=E(J)-X
      U(J+2)=E(J+2)-X
      A1=DABS(U(J))
      A2=1.0E-03
      IF(A1-A2)25,25,26
25    AK(J)=0.
      GO TO 17
26    AK(J)=0.5*U(J)*U(J)*(DLOG(DABS(U(J)))-1.5)
17    M=J+2
      A1=DABS(U(M))
      IF(A1-A2)18,18,19
 18   AK(M)=0.
      GO TO 21
19    AK(M)=0.5*U(M)*U(M)*(DLOG(DABS(U(M)))-1.5)
21    IF(J-49)22,22,23
22    PD1(J)=(-3.*PSPI(J)+4.*PSPI(J+1)-PSPI(J+2))/(0.2)
      PD1(J+2)=( PSPI(J)-4.*PSPI(J+1)+3.*PSPI(J+2))/(0.2
     * )
      PDD(J)=(PSPI(J)-2.*PSPI(J+1)+PSPI(J+2))/0.01
      SUM1=(PD1(J)*AK(J)-PD1(J+2)*AK(J+2))-PDD(J)/3.*(U(
     *J)*(AK(J)-U(J)*U(J)/6.)-U(J+2)*(AK(J+2)-U(J+2)*U(J
     *+2)/6.))
      GO TO 30
23    IF(J-149)24,24,22
24    PD1(J)=(-3.*PSPI(J)+4.*PSPI(J+1)-PSPI(J+2))/(0.02)
      PD1(J+2)=( PSPI(J)-4.*PSPI(J+1)+3.*PSPI(J+2))/(0.0
     * 2)
      PDD(J)=(PSPI(J)-2.*PSPI(J+1)+PSPI(J+2))/0.0001
      SUM1=(PD1(J)*AK(J)-PD1(J+2)*AK(J+2))-PDD(J)/3.*(U(
     * J)*(AK(J)-U(J)*U
     A(J)/6.)-U(J+2)*(AK(J+2)-U(J+2)*U(J+2)/6.))
30    SUM=SUM+SUM1
      IF(K-51)41,41,42
41    X=X+0.1
      SUM2(K)=SUM
      GO TO 40
42    IF(K-151)43,43,41
43    X=X+0.01
      SUM2(K)=SUM
```

```
40    CONTINUE
      X=-5.
      DO 50 K=1,51
      SUM3(K)=SUM2(K)-SUM2(51)
      G1=(X**2)*(A**2)/(2.*R)
      G2=2.*EC*A*SUM3(K)
      HSPI(K)=HO+G1-G2
50    X=X+0.1
      X=0.
      DO 60 K=51,151
      SUM3(K)=SUM2(K)-SUM2(51)
      G1=(X**2)*(A**2)/(2.*R)
      G2=2.*EC*A*SUM3(K)
      HSPI(K)=HO+G1-G2
60    X=X+0.01
      X=1.
      DO 70 K=151,191
      SUM3(K)=SUM2(K)-SUM2(51)
      G1=(X**2)*(A**2)/(2.*R)
      G2=2.*EC*A*SUM3(K)
      HSPI(K)=HO+G1-G2
70    X=X+0.1
      RETURN
      END
```

```
      SUBROUTINE CHEDIP(PDIP,IJ)
      IMPLICIT REAL*8(A-H,O-Z)
      DIMENSION PDIP(191),PTDIP(191)
      IF(IJ-1)10,10,20
   10 DO 15 I=1,191
   15 PTDIP(I)=PDIP(I)
      RETURN
   20 EPS=1.0E-02
      SUM=0.
      DO 30 I=103,150
      A1=DABS((PTDIP(I)-PDIP(I))/PDIP(I))
      IF(SUM-A1)36,30,30
   36 SUM=A1
   30 CONTINUE
      IF(SUM-EPS)40,40,41
   41 IF(IJ-5)42,43,43
   43 WRITE(6,44)IJ
   44 FORMAT(T5,'NO CONVERGENCE IN',I2,'ITERATIONS')
      GO TO 42
   40 WRITE(6,45)IJ
   45 FORMAT(T5,'CONVERGED IN ',I2,'ITERATIONS')
      IJ=5
   42 DO 50 I=1,191
   50 PTDIP(I)=PDIP(I)
      RETURN
      END
```

```
      SUBROUTINE DIPCAL(HO,VS,PS,HSPI,PSPI,U,A,D,LL,PDIP
     * )
      IMPLICIT REAL*8(A-H,O-Z)
      DIMENSION HSPI(191),PSPI(191),D(101),Z(101), VAL(1
     *01),H(101),PDIP(191)
      VAL(1)=0.
      ROO=D(51)
       UB=6.*VS*U*1.45E-05/(PS*A*2000.)
      HOND=HO/A
      RO=1.
      J=153-LL
      H(1)=D(51)*HO/A
      DO 10 I=2,LL
      H(I)=HSPI(J)/A
      RO=1.0D00+(0.009*PSPI(J))/(1.+0.026*PSPI(J))
      VAL(I)=UB*(H(I)-HOND*ROO/RO)/(H(I)**3)
10    J=J+1
      NDIM=LL
      E=0.01
      CALL DQSF(E,VAL,Z,NDIM)
      DO 50 I=1,LL
      Z(I)=Z(I)+1.
      WRITE(6,20)Z(I)
20    FORMAT(T10,E15.8)
50    CONTINUE
      J=153-LL
      DO 30 I=2,LL
      A1=1./(1.-Z(I))
      IF(A1)60,60,70
70    A2=DLOG(A1)
      PDIP(J)=A2*PS
      WRITE(6,40)A2,J,PDIP(J)
40    FORMAT(T10,F15.8,T35,I3,T55,F15.8)
      GO TO 30
60    WRITE(6,61)LL
61    FORMAT(T10,'NECESSARY TO MOVE SPIKE TO THE RIGHT.V
     * ALUE OF LL',I3)
      STOP
30    J=J+1
      J=153-LL
       DO 80 I=J,150
80    PSPI(I)=PDIP(I)
      PSPI(151)=0.
      J=152
      PDIP(J-LL)=PSPI(J-LL)
      RETURN
      END
```

```
      SUBROUTINE DPOLRT(XCOF,COF,M,ROOTR,ROOTI,IER)
      IMPLICIT REAL*8(A-H,O-Z)
      DIMENSION XCOF(1),COF(1),ROOTR(1),ROOTI(1)
      IFIT=0
      N=M
      IER=0
      IF(XCOF(N+1))10,25,10
 10     IF(N)15,15,32
C
C     SET ERROR CODE TO 1
C
 15     IER=1
 20   RETURN
C     SET ERROR CODE TO 4
 25   IER=4
      GO TO 20
C
C      SET ERROR CODE TO 2
C
 30    IER=2
      GO TO 20
 32   IF(N-36) 35,35,30
 35    NX=M
      NXX=N+1
      N2=1
      KJ1=N+1
      DO 40 L=1,KJ1
      MT=KJ1-L+1
 40   COF(MT)=XCOF(L)
C
C     SET INITIAL VALUES
C
 45     XO=0.00500101
      YO=0.01000101
C
C     ZERO INITIAL COUNTER
C
      IN=0
 50     X=XO
C
C     INCREMENT INITIAL VALUES AND COUNTER
      XO=-10.0*YO
      YO=-10.0*X
C
C     SET X AND Y TO CURRENT VALUE
C
      X=XO
      Y=YO
      IN=IN+1
      GO TO 59
```

```
 55     IFIT=1
        XPR=X
        YPR=Y
C
C       EVALUATE POLYNOMIAL AND DERIVATIVES
 59     ICT=0
 60     UX=0.0
        UY=0.0
        V=0.0
        YT=0.0
        XT=1.0
        U=COF(N+1)
        IF(U)65,130,65
 65     DO 70 I=1,N
        L=N-I+1
        TEMP=COF(L)
        XT2=X*XT-Y*YT
        YT2=X*YT+Y*XT
        U=U+TEMP*XT2
        V=V+TEMP*YT2
        FI=I
        UX=UX+FI*XT*TEMP
        UY=UY-FI*YT*TEMP
        XT=XT2
 70     YT=YT2
        SUMSQ=UX*UX+UY*UY
        IF(SUMSQ)75,110,75
 75     DX=(V*UY-U*UX)/SUMSQ
        X=X+DX
        DY=-(U*UY+V*UX)/SUMSQ
        Y=Y+DY
 78     IF(DABS(DY)+DABS(DX)-1.0D-05)100,80,80
C
C       STEP ITERATION COUNTER
C
 80     ICT=ICT+1
        IF(ICT-500)60,85,85
 85     IF(IFIT)100,90,100
 90     IF(IN-5)50,95,95
C
C       SET ERROR CODE TO 3
 95     IER=3
        GO TO 20
 100    DO 105 L=1,NXX
        MT=KJ1-L+1
        TEMP=XCOF(MT)
        XCOF(MT)=COF(L)
 105       COF(L)=TEMP
        ITEMP=N
        N=NX
```

```
      NX=ITEMP
      IF(IFIT)120,55,120
110     IF(IFIT)115,50,115
115     X=XPR
      Y=YPR
120     IFIT=0
122   IF(DABS(Y)-1.0D-4*DABS(X))135,125,125
125     ALPHA=X+X
      SUMSQ=X*X+Y*Y
      N=N-2
      GO TO 140
130     X=0.0
      NX=NX-1
       NXX=NXX-1
135     Y=0.0
       SUMSQ=0.0
      ALPHA=X
       N=N-1
140     COF(2)=COF(2)+ALPHA*COF(1)
145     DO 150 L=2,N
150    COF(L+1)=COF(L+1)+ALPHA*COF(L)-SUMSQ*COF(L-1)
155     ROOTI(N2)=Y
      ROOTR(N2)=X
      N2=N2+1
      IF(SUMSQ)160,165,160
160   Y=-Y
      SUMSQ=0.0
      GO TO 155
165   IF(N)20,20,45
      END
```

```
      SUBROUTINE RRK2(FUN,H,XI,YI,J,JJ,VEC)
      IMPLICIT REAL*8(A-H,O-Z)
      DIMENSION VEC(41)
      VEC(1)=0.
      H2=H/2.
      Y=YI
      X=XI
        DO 2 I=1,JJ
      DO 1 J2=1,J
      T1=H*FUN(X,Y)
      T2=H*FUN(X+H2,Y+T1/2.)
      T3=H*FUN(X+H2,Y+T2/2.)
      T4=H*FUN(X+H,Y+T3)
      Y=Y+(T1+2.*T2+2.*T3+T4)/6.
    1 X=X+H
    2 VEC(I+1)=Y
      RETURN
      END
```

```
FUNCTION FUN(X,Y)
IMPLICIT REAL*8(A-H,O-Z)
COMMON R,A,HO,ETAO,PS,PMAX,U
A1=DSQRT(DABS(X**2-1.))
HB=(A*A/R)*(DABS(X*A1)-DLOG(DABS(DABS(X)+A1)))/2.
H=HB+HO
PO=PMAX/PS
ROO=1.+((.003*PS*PO)/(1.+.0067*PS*PO))
HND=H/A
HBND=HB/A
HOND=HO/A
RO=1.+((.003*PS*Y)/(1.+.0067*PS*Y))
UB=6.*ETAO*U*1.45E-05/(PS*A*2000.)
FUN=UB*DEXP(Y)*(HND-HCND*ROO/RO)/(HND**3)
RETURN
END
```

```
      SUBROUTINE ECAL(R,EC,HO,A,PD,HT ,KC,KD,KE,HD,L)
      IMPLICIT REAL*8(A-H,O-Z)
      DIMENSION E(101),U(101),AK(101),PD1(101),PDD(101),
     *SUM2(101),SUM3(101),HT(101),HTT(101),PD(101),HD(10
     *1)
      WRITE(6,1)R,EC,HO,A,KC,KD,KE,L
1     FORMAT(4F15.8,4I4)
      DO 10 J=L,KC
      E(J)=(J-1)*0.1 -5.
10    CONTINUE
      X=-5.
      DO 40 K=L,KD
      SUM=0.
      DO 20 J=L,KE,2
      U(J)=E(J)-X
      U(J+2)=E(J+2)-X
      A1=DABS(U(J))
      A2=1.0E-03
      IF(A1-A2)15,15,16
15    AK(J)=0.
      GO TO 17
16    AK(J)=0.5*U(J)*U(J)*(DLOG(DABS(U(J)))-1.5)
17    M=J+2
      A1=DABS(U(M))
      IF(A1-A2)18,18,19
 18   AK(M)=0.
      GO TO 21
19    AK(M)=0.5*U(M)*U(M)*(DLOG(DABS(U(M)))-1.5)
21    PD1(J)=(-3.*PD(J)+4.*PD(J+1)-PD(J+2))/(0.2)
      PD1(J+2)=(PD(J)-4.*PD(J+1)+3.*PD(J+2))/(0.2)
       PDD(J)=(PD(J)-2.*PD(J+1)+PD(J+2))/0.01
      SUM1=(PD1(J)*AK(J)-PD1(J+2)*AK(J+2))-PDD(J)/3.*(U(
     *J)*(AK(J)-U(J)*U(J)/6.)-U(J+2)*(AK(J+2)-U(J+2)*U(J
     **+2)/6.))
20    SUM=SUM+SUM1
      IF(KE.EQ.99)GO TO 22
      A1= DABS(E(KC)-X)
      IF(A1-A2)22,22,23
22    ADD=0.
      GO TO 24
23    ADD=PD(KC)*(E(KC)-X)*(DLOG(DABS(E(KC)-X))-1.)
24    SUM=SUM+ADD
      IF(L-1)25,25,26
25      SUBTRA =0.
      GO TO 27
 26   A1=DABS(E(L)-X)
      IF (A1-A2)28,28,29
 28     SUBTRA =0.
      GO TO 27
 29   SUBTRA =PD(L)*(E(L)-X)*(DLOG(DABS(E(L)-X))-1.)
```

```
 27   SUM=SUM-SUBTRA
      X=X+0.1
      IF(K.EQ.51)SUMX=SUM
      SUM2(K)=SUM
40    CONTINUE
      X=-5.
      DO 50 K=1,KD
      SUM3(K)=SUM2(K)-SUM2(51)
      G1=(X**2)*(A**2)/(2.*R)
      G2=2.*EC*A*SUM3(K)
      HT(K)=HO+G1-G2
      X=X+0.1
50    CONTINUE
      RETURN
      END
```

```
      SUBROUTINE CLSHIF(HT,A,R,H0)
      IMPLICIT REAL*8(A-H,O-Z)
      DIMENSION HT(101)
      C=(HT(49)-HT(50))*R/(0.1*A)
      CONST=H0-HT(50)+(HT(49)-HT(50))
      X=-5.
      DO 195 I=1,101
      HT(I)=HT(I)-C*X*A/R+CONST
  195 X=X+0.1
      RETURN
      END
```

```
      SUBROUTINE HELMAT(HT,EC,R,AA)
      IMPLICIT REAL*8(A-H,O-Z)
      DIMENSION HT(101),DELPD(10,1),A(10,10),HCH(10,1),B
     * (10),R(10,1)
C
C     THE MATRIX FOR STRAIN IN REGION B DUE TO DELTAP IS
     *  SET
C
      HH=0.1D00
      B(1)=28./90.*DLOG(10.*HH)*HH
      B(2)=32.*4.*DLOG(9.*HH)*HH/90.
      B(3)=12.*4.*DLOG(8.*HH)*HH/90.
      B(4)=32.*4.*DLOG(7.*HH)*HH/90.
      B(5)=2.*7.*4.*DLOG(6.*HH)*HH/90.
      B(6)=HH*32.*4.*DLOG(5.*HH)/90.
      B(7)=HH*12.*4.*DLOG(4.*HH)/90.
      B(8)=HH*32.*4.*DLOG(3.*HH)/90.
      B(9)=HH*7.*4.*DLOG(2.*HH)/90.+HH*0.5*DLOG(2.*HH)
      B(10)=HH*0.5*DLOG(HH)
      A(1,1)=HH*(DLOG(HH)-1.)-B(1)
      A(2,1)=-B(1)
      A(3,1)=0.5*HH*DLOG(2.*HH)-B(1)
      A(4,1)=0.333333*HH*DLOG(3.*HH)-B(1)
      A(5,1)=0.375*HH*DLOG(4.*HH)-B(1)
      K1=5
      K2=4
      K3=3
       K4=2
      K5=1
      DO 10 I=6,10
      A(I,1)=7.*4.*DLOG(K1*HH)*HH/90.-B(1)
      A(I,2)=32.*4.*DLOG(K2*HH)*HH/90.-B(2)
       A(I,3)=12.*4.*DLOG(K3*HH)*HH/90.-B(3)
      A(I,4)=32.*4.*DLOG(K4*HH)*HH/90.-B(4)
      A(I,5)=7.*4.*DLOG(K5*HH)*HH/90.-B(5)
      K1=K1+1
      K2=K2+1
      K3=K3+1
      K4=K4+1
 10   K5=K5+1
      A(7,5)=A(7,5)+0.5*HH*DLOG(2.*HH)
      A(8,5)=A(8,5)+0.3333*HH*DLOG(3.*HH)
      A(9,5)=A(9,5)+0.375*HH*DLOG(4.*HH)
      A(10,5)=A(10,5)+28.*DLOG(5.*HH)/90.
      K=2
      DO 15 I=1,5
      A(I,K)=7.*4.*DLOG(HH)*HH/90.-B(K)
      A(I,K+1)=32.*4.*HH*DLOG(2.*HH)/90.-B(K+1)
      A(I,K+2)=12.*4.*DLOG(3.*HH)*HH/90.-B(K+2)
      A(I,K+3)=32.*4.*DLOG(4.*HH)*HH/90.-B(K+3)
      A(I,K+4)=7.*4.*DLOG(5.*HH)*HH/90.-B(K+4)
 15   K=K+1
```

```
      A(1,6)=A(1,6)+28.*DLOG(5.*HH)*HH/90.
      A(2,7)=A(2,7)+28.*DLOG(5.*HH)*HH/90.
      A(3,8)=A(3,8)+0.375*HH*DLOG(5.*HH)
      A(4,9)=A(4,9)+0.33333*HH*DLOG(5.*HH)
      A(5,10)=A(5,10)+0.5*HH*DLOG(5.*HH)
      DO 16 I=2,10
   16 A(I,I)=2.*HH*DLOG(HH)-HH-B(I)
C
C     REST OF THE ELEMENTS ARE LISTED INDIVIDUALLY
      A(3,2)=0.5*HH*DLOG(HH)-B(2)
      A(4,2)=1.33333*HH*DLOG(2.*HH)-B(2)
      A(5,2)=9.*HH*DLOG(3.*HH)/8.-B(2)
      A(4,3)=0.33333*HH*DLOG(HH)-B(3)
       A(5,3)=9.*HH*DLOG(2.*HH)/8.-B(3)
      A(5,4)=0.375*HH*DLOG(HH)-B(4)
      A(7,6)=0.5*HH*DLOG(HH)-B(6)
      A(8,6)=1.3333*HH*DLOG(2.*HH)-B(6)
      A(9,6)=9.*HH*DLOG(3.*HH)/8.-B(6)
      A(10,6)=HH*32.*4.*DLOG(4.*HH)/90.-B(6)
      A(1,7)=32.*4.*HH*DLOG(6.*HH)/90.-B(7)
       A(6,7)=7.*4.*HH*DLOG(HH)/90.-B(7)
      A(8,7)=0.3333*HH*DLOG(HH)-B(7)
      A(9,7)=9.*HH*DLOG(2.*HH)/8.-B(7)
      A(10,7)=12.*4.*HH*DLOG(3.*HH)/90.-B(7)
      A(1,8)=12.*4.*HH*DLOG(7.*HH)/90.-B(8)
      A(2,8)=32.*4.*HH*DLOG(6.*HH)/90.-B(8)
      A(6,8)=32.*4.*HH*DLOG(2.*HH)/90.-B(8)
      A(7,8)=0.375*HH*DLOG(HH)-B(8)
      A(9,8)=0.375*HH*DLOG(HH)-B(8)
      A(10,8)=32.*4.*HH*DLOG(2.*HH)/90.-B(8)
      A(1,9)=32.*4.*HH*DLOG(8.*HH)/90.-B(9)
      A(2,9)=12.*4.*HH*DLOG(7.*HH)/90.-B(9)
      A(3,9)=9.*HH*DLOG(6.*HH)/8.-B(9)
        A(6,9)=12.*HH*4.*DLOG(3.*HH)/90.-B(9)
      A(7,9)=9.*HH*DLOG(2.*HH)/8.-B(9)
      A(8,9)=HH*DLOG(HH)/3.-B(9)
      A(10,9)=7.*4.*HH*DLOG(HH)/90. -B(9)
      A(1,10)=HH*7.*4.*DLOG(9.*HH)/90.+HH*0.5*DLOG(9.*HH
     * )-B(10)
      A(2,10)=32.*4.*HH*DLOG(8.*HH)/90.-B(10)
      A(3,10)=9.*HH*DLOG(7.*HH)/8.-B(10)
      A(4,10)=4.*HH*DLOG(6.*HH)/3.-B(10)
      A(6,10)=32.*4.*HH*DLOG(4.*HH)/90.-B(10)
      A(7,10)=9.*HH*DLOG(3.*HH)/8.-B(10)
      A(8,10)=4.*HH*DLOG(2.*HH)/3.-B(10)
      A(9,10)=0.5*HH*DLOG(HH)-B(10)
      DO 20 I=1,10
      WRITE(6,19)(A(I,J),J=1,10)
   19 FORMAT(10F12.8)
   20 CONTINUE
      K=41
```

```
      DO 25 I=1,10
      R(I,1)=HT(K)/(2.*AA*EC)
      WRITE(6,100)R(I,1), HT(K),AA,EC
100   FORMAT(4F15.8)
 25   K=K+1
      M=10
      N=1
      EPS=1.0E-03
      CALL DGELG(R,A,M,N,EPS,IER)
      WRITE(6,19)( R(I,1),I=1,10)
      RETURN
      END
```

```
      SUBROUTINE ECAL1(HTT,HT,PD,EC,A)
      IMPLICIT REAL*8(A-H,P-Z)
      DIMENSION HTT(101),HT(101),PD(101),E(101),U(101),A
     *K(101),C(9,9),D(9,1),G(101)
      DO 6 I=41,51
      WRITE(6,5)HTT(I),HT(I)
5     FORMAT(T10,2E15.8)
6     CONTINUE
      WRITE(6,7)EC,A
7     FORMAT(T10,2F15.8)
      DO 10 J=1,101
      E(J)=(J-1)*0.1 -5.
10    CONTINUE
      X=-1.1D00
      DO 40 K=1,9
      X=X+0.1D00
      DO 20 J=41,51,2
      U(J)=E(J)-X
      U(J+2)=E(J+2)-X
      A1=DABS(U(J))
      A2=1.0E-03
      IF(A1-A2)15,15,16
15    AK(J)=0.
      GO TO 17
16    AK(J)=0.5*U(J)*U(J)*(DLOG(DABS(U(J)))-1.5)
17    M=J+2
      A1=DABS(U(M))
      IF(A1-A2)18,18,19
 18   AK(M)=0.
      GO TO 21
19    AK(M)=0.5*U(M)*U(M)*(DLOG(DABS(U(M)))-1.5)
21     G(J)=U(J)*(AK(J)-U(J)*U(J)/6.)-U(J+2)*(AK(J+2)-U(
     * J+2)*U(J+2)/6.)
      G(J)=G(J)/3.
20    CONTINUE
      G(51)=G(49)
      DO 30 I=41,51,2
      AK(I)=AK(I)-AK(51)
30    G(I)=G(I)-G(51)
      C1=4.*AK(41)/0.2+4.*AK(43)/0.2+2.*G(41)/0.01
      C2=-AK(41)/0.2-3.*AK(43)/0.2-G(41)/0.01
      C3=-3.*AK(43)/0.2-AK(45)/0.2-G(43)/0.01
      C4=4.*AK(43)/0.2+4.*AK(45)/0.2+2.*G(43)/0.01
      C5=-AK(43)/0.2-3.*AK(45)/0.2-G(43)/0.01
      C6=-3.*AK(45)/0.2-AK(47)/0.2-G(45)/0.01
      C7=4.*AK(45)/0.2+4.*AK(47)/0.2+2.*G(45)/0.01
      C8=-AK(45)/0.2-3.*AK(47)/0.2-G(45)/0.01
      C9=-3.*AK(47)/0.2-AK(49)/0.2-G(47)/0.01
      D1=4.*AK(47)/0.2+4.*AK(49)/0.2+2.*G(47)/0.01
      D2=-AK(47)/0.2-3.*AK(49)/0.2-G(47)/0.01
      D3=-3.*AK(49)/0.2-AK(51)/0.2-G(49)/0.01
```

```
      D4=4.*AK(49)/0.2+4.*AK(51)/0.2+2.*G(49)/0.01
      C(K,1)=C1
      C(K,2)=C2+C3
      C(K,3)=C4
      C(K,4)=C5+C6
      C(K,5) =C7
      C(K,6)=C8+C9
      C(K,7)=D1
      C(K,8)=D2+D3
      C(K,9)=D4
40    CONTINUE
      J=41
      DO 100 I=1,9
      D(I,1)=(HTT(J)-HT(J))/(2.*EC*A)
      WRITE(6,99)D(I,1)
99    FORMAT(T10,E15.8)
100     J=J+1
      OPS=1.0E-03
      M=9
      N=1
      CALL DGELG(D,C,M,N,OPS,IER)
      WRITE(6,90)(D(I,1),I=1,9)
90    FORMAT(T5,9E12.5)
      J=42
      DO 150 I=1,9
      PD(J)=PD(J)-D(I,1)
150   J=J+1
      RETURN
      END
```

```
      SUBROUTINE THERMA(P,H,TLC1,TLC2)
C     THERMAL SOLUTION
      IMPLICIT REAL*8(A-H,K-Z)
      DIMENSION P(200),H(200),A1(200),B1(200),C1(200),D1
     *(200),T(200),P1(200),Q1(200),G1(200),DPX(200),DMU1
     *(200),YMUBA1(200),DMUE(200),DMUEP(200),TLC1(200),T
     *LC2(200),VL(200),QQ(200),OMEGAN(200),DMINT(200),TT
     *(200),PP(200),DDPX(200),DMUEP2(200),ROB(200),UU(20
     *0),DUY(200),TAU(200),FTRAC(200),FTRACS(200),DFTRAC
     A(200),DITRAC(200)
C
C
      WRITE(6,9)(P(I),I=1,121)
      WRITE(6,9)(H(I),I=1,121)
 9    FORMAT(121F10.7)
      HO=.453D-04
      L=1.2837D-02
      VIS=0.58D-05
      VLS=VIS
      W=0.32
      EPS2=0.
C      NONDIMENSIONALISE PRESSURE AND H
C
C
      DO 2 I=1,121
      P(I)=P(I)*L/(2.*W)
 2    H(I)=H(I)/HO
      WRITE(6,9)(P(I),I=1,121)
      WRITE(6,9)(H(I),I=1,121)
      HH=0.05
      JDIM=21
      CALL DDET3(HH,P,DPX,JDIM,IER)
      J=1
      DO 3 I=21,121
      PP(J)=P(I)
 3    J=J+1
      HH=0.005
      JDIM=101
      CALL DDET3(HH,PP,DDPX,JDIM,IER)
      DO 4 J=1,101
 4    DPX(J+20)=DDPX(J)
      WRITE(6,9)(DPX(I),I=1,121)
C
C       VALUES OF THE PHYSICAL CONSTANTS ARE READ IN
C
      READ(5,11)KS,KL,CPS,CPL,DS,DL
 11   FORMAT(6F10.7)
C
C     CALCULATE VELOCITIES
C
```

```
      DO 999 IJMK=1,2
      READ (5,12)ROLVEL,SLIP
 12    FORMAT(2F10.5)
      U1=ROLVEL*(1.-SLIP)/(2.-SLIP)
      U2=ROLVEL-U1
      WRITE(6,110)KS,KL,CPS,CPL,DS,DL,ROLVEL,SLIP,U2,U1
 110  FORMAT(10E13.4/////)
C
C      CALCULATE REYNOLDS,PRANDTL,ECKERT NUMBERS
      REY=DS*ROLVEL*L/(VIS*32.2*12.)
      REYM=REY*HO*HO/(L*L)
      PRANL=CPL*VLS/KL*43200.*32.2*12.
      ECKT=(ROLVEL**2)/(CPL*570.*32.2*12.*12.*778.)
      M=W*2000./(CPL*DL*570.*0.5*L*778.*12.)
      WRITE(6,111)REY,REYM,PRANL,ECKT,M
 111  FORMAT(5E13.5///)
      DO 15 I=1,153
 15   T(I)=1.0
      JJ=102
      J1=1
C
C     TEMPERATURE CALCULATION IN FLUID STREAM BEGINS
C
      DO 70 JJJ=11,121
      WRITE(6,170)JJJ
 170  FORMAT(50X,'STATION',I3)
      ITER=1
      HR1=KS*HO/KL
      RS1=L*DS*CPS*U1*HR1*HR1*43200./(L*L*KS)
      RS2=RS1*U2/U1
      WRITE(6,112)HR1,RS1,RS2
 112  FORMAT(3E13.5////)
      IF(JJJ-22)20,21,21
 20   DXB=0.05
      GO TO 22
 21    DXB=0.005
 22   DYB1=0.05
      DYB2=0.05
      DYB=0.1
      DO 57 III=1,50
      DO 25 J1=1,19
      A1(J1)=3.*RS1+4.*DXB/(DYB1**2)
      B1(J1)=-2.*DXB/(DYB1**2)
      D1(J1)=B1(J1)
      C1(J1)=RS1*(T(JJ+J1-50)*4.-T(JJ+J1-101))
      IF(J1.EQ.1)C1(J1)=C1(J1)-D1(J1)
 25   CONTINUE
C
C     BOUNDARY CONDITION
      A1(20)=(1.+      DYB/DYB1)
```

```
      B1(20)=-1.
      D1(20)=-      DYB/DYB1
      C1(20)=0.
C     ENERGY EQUATION FOR LUBRICANT
      CALL CALMU(JJJ,P,T,VL,DMU1,YMUBA1,DMUE,DMUEP,TLC1,
     *TLC2,W,L,DMUEP2,U1,U2)
      CALL BEEJAY(PRANL,REYM,DXB,DYB,H,HO,M,L,EPS2,JJJ,W
     *,DPX,YMUBA1,DMU1,DMUE,DMUEP,QQ,VLS,RQLVEL,U1,U2,VL
     *,OMEGAN,DMINT,P,ECKT,ROB,UU,DUY,TAU,T)
      DO 30 J1=21,29
      A1(J1)=QQ(J1-19)
      B1(J1)=-DXB*2.   /(DYB*DYB*H(JJJ)*H(JJJ))
      D1(J1)=B1(J1)
      C1(J1)=OMEGAN(J1-19)*VL(J1-19)+DMINT(J1-19)*T(J1+5
     *2)*4.-DMINT(J1-19)*T(J1+1)
 30   CONTINUE
C     BOUNDARY CONDITION BETWEEN LUBRICANT AND SOLID2
      A1(30)=1.+DYB/DYB2
      D1(30)=-1.
      B1(30)=-DYB/DYB2
      C1(30)=0.
C
C     ENERGY EQUATION FOR SOLID 2
      DO 35 J1=31,49
      A1(J1)=3.*RS2+4.*DXB/(DYB2**2)
      B1(J1)=-2.*DXB/(DYB2**2)
      D1(J1)=B1(J1)
 35   C1(J1)=RS2*(T(JJ+J1-50)*4.-T(JJ+J1-101))
      C1(49)=C1(49)-B1(49)
C
C     TRIDIAGONAL MATRIX SOLUTION BEGINS
      P1(1)=A1(1)
      Q1(1)=B1(1)/P1(1)
      G1(1)=C1(1)/P1(1)
      DO 40 J1=2,49
      P1(J1)=A1(J1)-D1(J1)*Q1(J1-1)
      Q1(J1)=B1(J1)/P1(J1)
 40   G1(J1)=(C1(J1)-D1(J1)*G1(J1-1))/P1(J1)
      DO 41 I=1,153
 41    TT(I)=T(I)
      JJ=102
      J2=49
      J21=J2+1
      T(J21+JJ)=G1(J2)
      DO 45 J1=1,48
      J2=J2-1
      J21=J2+1
 45     T(J21+JJ)=G1(J2)-Q1(J2)*T(J21+1+JJ)
C
C
```

```
C     CHECK FOR CONVERGENCE
C
      EPS=0.01
      ERMAX=0.
      DO 55 I=1,153
      QQQ=DABS((T(I)-TT(I))/TT(I))
 55   IF(QQQ.GT.ERMAX)ERMAX=QQQ
      IF(ERMAX.GT.EPS)GO TO 65
      GO TO 69
C
C     CONVERGENCE PARAMETERS ARE PUT IN
C
 65   DO 56 I=1,153
 56   T(I)=0.5*TT(I)+(1.-0.5)*T(I)
 57   ITER=ITER+1
 69   WRITE(6,171)ITER
 171  FORMAT(50X,'CONVERGED IN',I3,'ITERATIONS')
      WRITE(6,173)(T(I),I=123,133)
 173  FORMAT(10X,'LUBRICANT TEMPERATURES ARE',11F8.5//)
      WRITE(6,174)(T(I),I=103,123)
 174  FORMAT(10X,'LOWER SOLID TEMPERATURES ARE',21F8.5//
     * )
      WRITE(6,175)(T(I),I=133,153)
 175  FORMAT(10X,'TOP   SOLID TEMPERATURES ARE',21F8.5//
     * )
      WRITE(6,201)JJJ
 201  FORMAT(10X,'FOR STATION',I3,':',T40,'VELOCITY',T60
     *,'DU/DY',T90,'SHEAR STRESS',T105,'DENSITY',T120,'V
     *ISCOSITY')
      DO 202 I=1,11
      WRITE(6,203)I,UU(I),DUY(I),TAU(I),ROB(I),VL(I)
 203  FORMAT(T5,I2,T40,F10.5,T60,F10.5,T90,F12.5,T105,E1
     * 0.4,T120,E12.4)
 202  CONTINUE
      WRITE(6,205)DMUE(JJJ),DMUEP(JJJ),DMUEP2(JJJ),TLC1(
     * JJJ) ,TLC2(JJJ)
 205   FORMAT(5E12.5)
      FTRAC(JJJ)=TAU(11)/H(JJJ)
      DO 172 I= 1,102
 172   T(I)=T(I+51)
 70   CONTINUE
      DO 176 I=11,121
      FTRAC(I-10)=FTRAC(I)
 176    CONTINUE
      HH=0.05
      JDIM=11
      CALL DQSF(HH,FTRAC,FTRACS,JDIM)
      AX=FTRACS(11)
      DO 300 JKS=21,121
 300  DFTRAC(JKS-20)=FTRAC(JKS)
      JDIM=101
      HH=0.005
      CALL DQSF(HH,DFTRAC,DITRAC,JDIM)
      AY=DITRAC(101)
```

```
      WRITE(6,450)AX,AY
  450 FORMAT(2E12.4)
      FT=(AX+AY)*L*ROLVEL*VIS/(W*2000.*HO)
      SVEL=U2-U1
      WRITE(6,301)SVEL,FT
  301 FORMAT(10X,'FOR A SLIP VELOCITY OF ',F10.5,'FRICTI
     *ONAL TRACTION IS ',F10.5//)
      WRITE(6,451) (DITRAC(I),I=1,101)
  451 FORMAT(101E10.4)
  999 CONTINUE
      STOP
      END
```

```
      SUBROUTINE BEEJAY(PRANL,REYM,DXB,DYB,H,HO,M,L,EPS2
     *,JJJ,W,DPX,YMUBA1,DMU1,DMUE,DMUEP,QQ,VLS,ROLVEL,U1
     *,U2,VL,OMEGAN,DMINT,P,ECKT,ROB,UU,DUY,TAU,T)
      IMPLICIT REAL*8(A-H,K-Z)
      DIMENSION H(200),DPX(200),YMUBA1(200),DMU1(200),DM
UE(200),DMUEP(200),QQ(200),VL(200),OMEGAN(200),DMINT(200
     *),DUY(200),UU(200),P(200),ROB(200),TAU(200),T(200)
      AA1=2.*DXB/((DYB**2)*(H(JJJ)**2))
      AA2=W*(H(JJJ)**2)*(HO**2)*2000./(VLS*ROLVEL*L*0.5*
     * L)
      AA3=U1/ROLVEL
      UU(1)=AA3
      UU(11)=U2/ROLVEL
      AA10=P(JJJ)*W/(0.5*L)
      YY=0.1D00
      DO 10 I=2,10
      AA4=AA2*DPX(JJJ)*YMUBA1(I)
      AA5=(U2-U1)/ROLVEL*(DMUE(JJJ))*DMU1(I)
      AA6=AA2/2.*DPX(JJJ)*DMUE(JJJ)/DMUEP(JJJ)*DMU1(I)
      UU(I)=AA4+AA5-AA6+AA3
      AA7=YY-DMUE(JJJ)/(2.*DMUEP(JJJ))
      DUY(I)=AA2*DPX(JJJ)*AA7/VL(I)+(U2-U1)/ROLVEL*DMUE(
     * JJJ)/VL(I)
      YY=YY+0.1D00
10    CONTINUE
      J=123
      DO 30 I=1,11
      ROB(I)=1.+0.009*AA10/(1.+0.026*AA10)-0.00035*570.*
     * (T(J)-1.)
30    J=J+1
      J=123
      DO 15 I=2,10
      EPS2=0.00035*570.*(T(J)-1.)
      J=J+1
      QQ(I)=2.*AA1+3.*PRANL*REYM*ROB(I)*UU(I)-2.*DXB*HO*
     * HO*M*EPS2*UU(I)*
     ADPX(JJJ)*PRANL/(L*L)
      OMEGAN(I)=2.*DXB*PRANL*ECKT*DUY(I)*DUY(I)/(H(JJJ)*
     * *2)
      DMINT(I)=PRANL*REYM*ROB(I)*UU(I)
15    CONTINUE
      AA7=-DMUE(JJJ)/(2.*DMUEP(JJJ))
      DUY(1 )=AA2*DPX(JJJ)*AA7/VL(1 )+(U2-U1)/ROLVEL*DMU
     * E(JJJ)/VL(1 )
      DUY(1 )=AA2*DPX(JJJ)*AA7/VL(1 )+(U2-U1)/ROLVEL
      DUY(11)=AA2*DPX(JJJ)*AA7/VL(11)+(U2-U1)/ROLVEL*DMU
     * E(JJJ)/VL(11)
      DO 40 I=1,11
40    TAU(I)=VL(I)*DUY(I)
      RETURN
      END
```

```
      SUBROUTINE CALMU(JJJ,P,T,VL,DMU1,YMUBA1,DMUE,DMUEP
     *,TLC1,TLC2,W,L,DMUEP2,U1,U2)
      IMPLICIT REAL*8(A-H,K-Z)
      DIMENSION P(200),T(200),VL(200),DMU1(200),DMU(200)
     *,DMUE(200),YMUBA(200),YMUBA1(200),YMUBA2(200),YMUB
     *A3(200),TLC1(200),TLC2(200),DMUEP(200),DMUEP2(200)
      ALPHA=-0.214*2.*W/L
      BETA=8300.
      GAMA=350.*2.*W/L
      A1=ALPHA*P(JJJ)
      A2=BETA/570.
      J=123
      DO 10 I=1,11
      A3=BETA/(T(J)*570.)
      A4=GAMA*P(JJJ)/(T(J)*570.)
      VL(I)=DEXP(A1+A3-A2+A4)
      DMU(I)=1./VL(I)
      J=J+1
   10 CONTINUE
      HH=0.1D00
      JDIM=11
      CALL DQSF(HH,DMU,DMU1,JDIM)
      DMUE(JJJ)=1./DMU1(11)
      YY=0.
      DO 15 I=1,11
      YMUBA(I)=YY/VL(I)
      YMUBA2(I)=YY*YY/VL(I)
   15 YY=YY+0.1D00
      CALL DQSF(HH,YMUBA,YMUBA1,JDIM)
      CALL DQSF(HH,YMUBA2,YMUBA3,JDIM)
      DMUEP(JJJ)=1./(2.*YMUBA1(11))
      DMUEP2(JJJ)=1./(3.*YMUBA3(11))
      VARAD=DMUE(JJJ)/(3.*DMUEP2(JJJ))
      SRINU=DMUE(JJJ)/(2.*DMUEP(JJJ))
      SRINI=SRINU**2
      TLC1(JJJ)=12.*(VARAD-SRINI)
      TLC2(JJJ)=1.+(U2-U1)/(U2+U1)*(1.-DMUE(JJJ)/DMUEP(J
     * JJ))
      RETURN
      END

 STOP      0
08:47.35 10.484 RC=0
```